DEVELOPMENT OF SEAWATER-FRESHWATER INTERFACE IN HETEROGENEOUS COASTAL AQUIFERS

A Dissertation
Presented to
The Academic Faculty

by

Saubhagya Singh Rathore

In Partial Fulfillment
of the Requirements for the Degree
Doctor of Philosophy in the
School of Civil and Environmental Engineering

Georgia Institute of Technology
May 2020

DEVELOPMENT OF SEAWATER-FRESHWATER INTERFACE IN HETEROGENEOUS COASTAL AQUIFERS

Approved by:

Dr. Jian Luo, Advisor
School of Civil and Environmental Engineering
Georgia Institute of Technology

Dr. Marc Stieglitz
Arctic Natural Sciences
National Science Foundation

Dr. Aris Georgakakos, Co-advisor
School of Civil and Environmental Engineering
Georgia Institute of Technology

Dr.Yi Deng
School of Earth and Atmospheric Sciences
Georgia Institute of Technology

Dr. Jingfeng Wang
School of Civil and Environmental Engineering
Georgia Institute of Technology

Date Approved: January 17, 2020

To my parents—Manohar Singh Rathore and Indra Kanwar Rathore

ACKNOWLEDGMENTS

I would like to express my deepest gratitude to my supervisor, Dr. Jian Luo, for continuously supporting me and providing invaluable guidance throughout my Ph.D. journey. He was always available for me—be it for discussion about my research or guidance for my career. I will always be indebted to him.

I am also extremely grateful to Dr. Aris Georgakakos for being my co-advisor. He always encouraged me to continuously improve and strive for the best. His support and guidance played a key role in the completion of this thesis.

I would also like to extend my sincerest gratitude to my committee members: Dr. Jingfeng Wang, Dr. Marc Stieglitz, and Dr.Yi Deng for their constructive criticism, valuable feedback and suggestions that were extremely helpful to complete this thesis.

I gratefully acknowledge the members of the Water Resource Engineering group, especially my labmates, Yue Zhao and Yuening Tang for their help and feedback on my research. I would also like to acknowledge the contributions of our collaborator, Dr. Chunhui Lu, at Hohai Univesity.

Finally, I would like to thank from the bottom of my heart my parents, Manohar Singh Rathore and Indra Kanwar Rathore, my brother, Pradyuman Singh Rathore and other family members for their continuous love and support. I would also like to thank my friends for always being there during challenging times.

TABLE OF CONTENTS

ACKNOWLEDGMENTS **iv**

LIST OF TABLES **viii**

LIST OF FIGURES **ix**

LIST OF SYMBOLS AND ABBREVIATIONS **xiii**

SUMMARY **xvii**

CHAPTER 1. Introduction **1**
1.1 Seawater-freshwater Interface and Groundwater Discharge **1**
1.2 Research Motivation, Objectives, and Approach **5**
1.2.1 Research Motivation 5
1.2.2 Specific Objectives 6
1.2.3 Approaches 6
1.3 Organization of Thesis **7**

CHAPTER 2. Literature Review **8**
2.1 Seawater Intrusion **8**
2.1.1 SWI Field Measurements 9
2.1.2 SWI Prediction 11
2.2 Submarine Groundwater Discharge **17**
2.2.1 SGD Measurements 18
2.2.2 SGD Predictions 19
2.3 Heterogeneity Effects **19**
2.4 Transient SWI **23**

CHAPTER 3. A New Parameter Accounting for Stratification Effects On Seawater Intrusion **26**
3.1 Introduction **26**
3.2 Conceptual Model **28**
3.3 Theory **31**
3.3.1 Steady-state Solution for a Flux-controlled System 31
3.3.2 Steady-state Solution for a Head-controlled System 33
3.3.3 Effective Parameters 35
3.3.4 Continuously-varying Hydraulic Conductivity 37
3.4 Results and Discussion **38**
3.4.1 Effective Parameters 38
3.4.2 Effects of Stratification in a Head-controlled Multiple-layer System 41
3.4.3 Implication on Preferential Flow Paths 48
3.4.4 Sensitivity of Qx and xt to the decay coefficient of exponentially decaying K51
3.5 Summary and Conclusions **53**

CHAPTER 4. Explicit Analytical Interface Profile in StraTIfied Coastal Aquifers 55
4.1 Introduction 55
4.2 Conceptual Model 57
4.3 Theory 60
4.3.1 Confined Aquifer 60
4.3.2 Unconfined Aquifer 64
4.4 Comparison with Numerical Results 68
4.5 Discussion 72
4.5.1 The Proposed Equation in the Context of the Existing Comprehensive Discharge Potential Theory (Strack and Ausk, 2015; Strack et al., 2016) 72
4.5.2 Interface Profile in Layer-configurations with Different Hydraulic-conductivity Contrasts 73
4.5.3 Implications of the Dependence of the Interface on the Local Transmissivity Parameters 77
4.6 Conclusion 80

CHAPTER 5. A Semi-Analytical Method to Fast Delineate Seawater-Freshwater Interface in 2D Heterogeneous Coastal Aquifers 82
5.1 Introduction 82
5.2 Conceptual Model 86
5.3 Semi-Analytical Method 88
5.4 Comparison with Variable-density Flow Simulation 92
5.4.1 Base Case 94
5.4.2 Cases with Different Heterogeneity Parameters 96
5.5 Effect of 2D Heterogeneity on Seawater Intrusion 99
5.6 Summary and Conclusion 102

CHAPTER 6. Stochastic Analysis of Seawater Intrusion 103
6.1 Introduction 103
6.2 Randomly Stratified Aquifers 105
6.2.1 Model Conceptualization 105
6.2.2 Solutions in Random Stratification 108
6.2.3 Validation 109
6.2.4 Discussion 114
6.3 2D Heterogeneous Aquifer 118
6.3.1 Quantification and Sensitivity Analysis of Uncertainty 118
6.3.2 Stochastic Upscaling 123
6.4 Conclusion 127

CHAPTER 7. Transient Seawater Intrusion 129
7.1 Introduction 129
7.2 Transient Seawater Intrusion in Homogeneous Aquifers 133
7.2.1 Theoretical Derivation of the Explicit Timescale Solution 133
7.2.2 Comparison with Numerical Results 141
7.2.3 Analysis and Discussion 149

7.2.4 Effects of Inland-Boundary Condition and Aquifer Parameters on the Timescale 157
7.2.5 Sensitivity of Timescales 159
7.3 Numerical and Analytical Analysis of Transient SWI in Stratified Aquifers 163
7.3.1 Conceptual Model: 163
7.3.2 Numerical Analysis: 164
7.3.3 Response Timescale Indicator 173
7.4 Summary and Conclusion 179

CHAPTER 8. Conclusions and Future Work Recommendations 182
8.1 Conclusions 182
8.2 Implications 184
8.3 Limitations 185
8.4 Recommendations for Future Work 185
8.4.1 Developing a Semi-analytical Technique to Compute the Seawater-freshwater Interface in 3D 185
8.4.2 Inverse Modeling of the Conductivity from Field Salinity Measurements 186
8.4.3 Modeling the Effects of Heterogeneity on Solute Transport into Estuary Ecosystems 188
8.4.4 Effects of Heterogeneity on Dense Contaminants 190
8.4.5 Estimation of the Salinity Fluxes at the Coastal Boundary 192
8.4.6 Integrated Modeling of Water and Solute exchanges between Groundwater, River, Sea and Human Activities in Coastal Areas 194

Appendix A: Computing the integration constant for a general ith layer 196

Appendix B: Solution of the freshwater flux in a stratified unconfined aquifer 198

Appendix C: Proof for the mathematical sameness of our solution for the interface profile and Strack and Ausk (2015) 200

Appendix D: Moments of yc and T 203
D1. $K(y)$ as a continuous variable 203
D2. $K(y)$ set of discrete variables 207

Appendix E: Moments of xt in a flux-controlled system 208

Appendix F: Moments of Qx and xt in a head-controlled system 209

Appendix G: Solution for transient freshwater discharge into the sea in a flux boundary case by Bear (1972) 212

Appendix H: Simplification of the timescale expression 215

References 216

LIST OF TABLES

Table 1	Commonly Used SWI Codes (adapted from Werner et al. (2011))	15
Table 2	Effective Parameters for Different Cases	40
Table 3	Layer Names, Thickness, and Hydraulic Conductivity Values	42
Table 4	Aquifer Parameters Used in the Numerical Experiment with a Preferential Flow Path	49
Table 5	Aquifer Layer Properties for Comparison with Numerical Results	70
Table 6	Aquifer Parameters Used in the Numerical Simulation of the Three-layer Case	78
Table 7	Parameters Used to Assess the Performance of the Proposed Methodology	93
Table 8	Aquifer Parameters for Validation using Monte-Carlo Simulation	112
Table 9	Aquifer Parameters for the Specified-head Boundary Case	143
Table 10	Inland Boundary Head Values (m) for the Specified-head Boundary Case	144
Table 11	Aquifer Parameters for the Specified-flux Boundary Case	146
Table 12	Inland Boundary Flux Values (m^2/d) in the Specified-flux Boundary Case	147
Table 13	Aquifer Systems with Different Parameters and Respective R_T Values Estimated Using Numerical Simulations	156
Table 14	Timescales in 5 Special Stratified Cases in the Increasing Order	167
Table 15	Characteristic Timescale for Each Layer and RTI for the Aquifer for Five Special Cases	178

LIST OF FIGURES

Figure 1	Critical processes associated with seawater intrusion in coastal aquifers	3
Figure 2	Conceptual model of the 2D stratified confined aquifer	30
Figure 3	Comparison of Velocity Fields: (a) Homogeneous Case, y_c = 12.50 cm, (b) stratified case S1, y_c = 12.50 cm and, (c) stratified case S2, y_c = 12.50 cm; the redline represents the 50% isochlor	43
Figure 4	Seawater-freshwater interfaces for 13 cases with fairly spaced y_c values, including the two bounding cases, and the homogenous case. E1 and E2 represent the cases with a monotonically descending and ascending order of hydraulic conductivities from bottom	45
Figure 5	Theoretical and numerical – (a) discharge values; and (b) toe-positions, for 13 stratified cases presented in Figure 4	47
Figure 6	Seawater-freshwater interface in a preferential flow path setting with – (a) different hydraulic conductivity contrasts; (b) different positions of the preferential flow layer	50
Figure 7	Variation of: (a) Q_x and (b) x_t with respect to decay coefficient λ	52
Figure 8	Conceptual models for a stratified - (a) confined aquifer and (b) unconfined aquifer	59
Figure 9	Comparison of numerical and analytical results (Line-Analytical, Colormap-Numerical)	71
Figure 10	Interface profiles in aquifer configurations with different hydraulic conductivity contrast with a: a) given-flux boundary; b) given-head boundary	76
Figure 11	Interface profile for two layer-placements showing if only the lower two layers are rearranged, the interface profile will be changed only in the lower two layers	79
Figure 12	Conceptual model for the 2D heterogeneous confined aquifer depicting relevant parameters	87

Figure 13 Conceptual model depicting K grid, series of elevations, ζ_m's, with relevant parameters involved in the computation of the interface profile in 2D heterogeneous aquifers 91

Figure 14 (a) Maps of logarithmic hydraulic conductivities representing four realizations generated from base-case parameters; (b) Comparison of variable density flow simulation (heat map) and semi-analytical interface profile (black line) for four realizations of base-case hydraulic conductivity fields 95

Figure 15 (a) Heat maps of logarithmic conductivity fields generated using combinations of four different values of each l_x and σ_{lnK}^2 as mentioned in Table 1; (b) Comparison of variable density flow simulation (map) and semi-analytical interface profile (black line) for four different values of each l_x and σ_{lnK}^2 as mentioned in Table 7 97

Figure 16 Comparison of toe positions from the proposed semi-analytical method and numerical simulations (toe of the 50% isochlor) 98

Figure 17 Comparison of SWI in the modified and original hydraulic conductivity fields demonstrating the insignificance of the region under the transition zone and landward of the toe position 101

Figure 18 Conceptual model for stratified coastal aquifer with y_c as one of the random parameters 107

Figure 19 Histogram represents the distribution of toe-positions in the flux-controlled system, and discharges and toe-positions in the head-controlled system for 50 K field realizations; Red lines represent analytical mean (solid) and 95% confidence intervals (dashed) 113

Figure 20 Sensitivity of mean and confidence intervals (CI) of TCE (blue), and toe position in a head-controlled system (orange) to a) the ratio of variance to mean squared b) normalized correlation length 116

Figure 21 Sensitivity to the normalized correlation length of K of the variance of the discharge rate in a head-controlled case (blue), the variance of the toe position in a flux-controlled case (orange) 117

Figure 22 Semi-analytical interface profiles for 50 realizations out of total 500 realizations for each combination of four different values of each l_x and σ_{lnK}^2 as mentioned in Table 7; Ensemble mean and 5th and 95th percentile in red lines; Interface profile in the aquifer homogenized using the geometric mean 120

Figure 23 Histograms of the x coordinate of the interface (semi-analytical) at different interface elevations for 500 realizations of the base case (σ_{lnK}^2= 1, l_x= 10 m) 121

Figure 24 Variation of ensemble mean and variance (500 realizations) of the toe-position (semi-analytical) with respect to σ_{lnK}^2 and l_x 122

Figure 25 Variation of K_{eff} corresponding to the mean toe position with respect to σ_{lnK}^2 and l_x 125

Figure 26 Distribution of K_{eff} for each case of the heterogeneity parameter 126

Figure 27 Conceptual model for the (a) specified-flux boundary case, modified from Bear (1972); (b) specified-head boundary case 136

Figure 28 Comparison of analytical and numerical results for (a) SWI and (b) SWR timescales for the specified-head boundary case 145

Figure 29 Comparison of analytical and numerical results for (a) SWI and (b) SWR timescales for the specified-flux boundary case; lnT vs lnQ'_{fL} for different Q_{fL}^0 148

Figure 30 Schematic representation of the freshwater flux at the inland boundary, freshwater and seawater fluxes at the coastal boundary in the specified-flux boundary case 151

Figure 31 Non-dimensional toe displacements vs corresponding non-dimensional net seawater flux (also representing the rate of the seawater wedge movement) in response to an abrupt change in the freshwater flux at the inland boundary (0.6 m^2/d to 0.3 m^2/d for SWI and 0.3 m^2/d to 0.6 m^2/d for SWR) 153

Figure 32 Comparison of the temporal asymmetry index, R_T obtained analytically and numerically for different ratios of higher to lower inland boundary fluxes (Q_H/Q_L) 154

Figure 33 Logarithmic τ vs logarithmic β obtained analytically and numerically for the specified-flux boundary case 158

Figure 34 Variation of the toe-response timescale with (a) hydraulic conductivity; (b) cubic depth; and (c) porosity, for SWI and SWR in the specified-flux boundary case 160

Figure 35 Sensitivity of the SWI and SWR timescales to different aquifer parameters and boundary conditions; Lines- Analytical Eq. (12), Points - Numerical (Lu and Werner, 2013) 161

Figure 36	Conceptual model for the confined stratified aquifer for transient analysis	165
Figure 37	Initial (solid) and final (dashed) interfaces for five special cases – Homogeneous, S1 S2, E1, E2	170
Figure 38	Interfaces and velocity vectors right after the abrupt boundary change during SWI in (a) E1, (b) Homogeneous, (c) S1, (d) S2, and (e) E2	171
Figure 39	Individual layer responses characterized by the movement of the center of the interface section in the layer for (a) E1, (b) Homogeneous, (c) S1, (d) S2, and (e) E2	172
Figure 40	Using salinity values for inverse modeling to estimate hydraulic conductivity field	187
Figure 41	Influence of seawater wedge on the solute pathways near the coastal boundary	189
Figure 42	Spreading of a dense contaminant in a heterogeneous aquifer	191
Figure 43	Velocity vectors depicting recirculating seawater	193
Figure 44	Key processes in the coastal areas	195

LIST OF SYMBOLS AND ABBREVIATIONS

L	Length of the aquifer [L]
H_s	Coastal head/Sea level [L]
x_t	Toe position [L]
h_f	Constant freshwater head at the inland boundary [L]
Q_x	Constant freshwater flux at the coastal boundary [L]
b_i	Thickness of the i^{th} layer [L]
y_i	Elevation of the center of the i^{th} layer [L]
K_i	Hydraulic conductivity of the i^{th} layer [L/T]
d_i	Base elevation of the i^{th} layer [L]
B	Total thickness of the aquifer [L]
T	Total transmissivity of the aquifer [L^2/T]
Φ	Comprehensive discharge potential [L^3/T]
Φ_0	Comprehensive discharge potential at the coastal boundary [L^3/T]
C_m	Discharge potential continuity coefficient for m^{th} layer [L^3/T]
ϕ_t	Piezometric head at the toe [L]
y_c	Elevation of the centroid of the transmissivity field (TCE) [L]
α	Density ratio [-]
B_{eff}	Effective aquifer depth for homogenization [L]
K_{eff}	Effective hydraulic conductivity for homogenization [L/T]
Δh	Corrected difference in head between inland and coastal boundary [L]
K_T	Hydraulic conductivity at the top of the aquifer for continuously varying field [L/T]
λ	Exponential decay coefficient for continuously varying field [L^{-1}]

Pe	Peclet number [-]
n	Effective porosity [-]
α_L	Longitudinal dispersivity [L]
α_T	Transverse dispersivity [L]
C_s	Salinity of seawater [M/L^3]
ζ	Elevation of the interface [L]
h	Freshwater head above the sea level [L]
T_ζ	Local transmissivity—transmissivity of the flow domain above the interface [L^2/T]
$y_{c\zeta}$	Centroid elevation of the local transmissivity field [L]
ρ_s	Density of the seawater [M/L^3]
ρ_f	Density of the freshwater [M/L^3]
Δ_x, Δ_y	Grid size on x and y direction, respectively, for semi-analytical method [L, L]
N_r, N_c	Number of rows and columns, respectively, for semi-analytical method [-, -]
l_x, l_y	Correlation lengths in x and y direction, respectively, for random field [L, L]
$\mu_{\ln K}$	Mean of lognormal conductivity field [-]
$\sigma^2_{\ln K}$	Variance of lognormal conductivity field [-]
μ_T	Mean of transmissivity for random conductivity field [L^2/T]
σ^2_T	Variance of transmissivity for random conductivity field [L^4/T^2]
μ_{y_c}	Mean of TCE for random conductivity field [L]
$\sigma^2_{y_c}$	Variance of TCE for random conductivity field [L^2]
μ_{x_t}	Mean of toe position for random conductivity field [L^2/T]
$\sigma^2_{x_t}$	Variance of toe position for random conductivity field [L^2/T]
μ_{Q_x}	Mean of discharge for random conductivity field [L^2/T]

$\sigma_{Q_x}^2$	Variance of discharge for random conductivity field [L^4/T^2]
$\rho_z(h)$	Correlation function for lognormal field in a randomly stratified aquifer [-]
μ_K	Mean of hydraulic conductivity [L/T]
σ_K^2	Variance of hydraulic conductivity [L/T]
$\rho_K(h)$	Correlation function for K in a randomly stratified aquifer [-]
e_K	Statistical efficiency of K [-]
Q_{fL}^0	Initial freshwater flux at inland boundary [L^2/T]
Q_{f0}^0	Initial freshwater outflow into the sea at the coastal boundary [L^2/T]
Q_{fL}'	Final freshwater flux at inland boundary [L^2/T]
$Q_{f0}(t)$	Transient freshwater outflow into the sea [L^2/T]
h_{fL}'	Final boundary head [L]
h_{fL}^0	Initial boundary head [L]
$\eta\ (x,t)$	Transient interface profile [L]
$X(t)$	Transient toe position [L]
ε	Density ratio $(1/\alpha)$ [-]
T_{SWI}	Seawater intrusion timescale in response to abrupt boundary change [T]
T_{SWR}	Seawater retreat timescale in response to abrupt boundary change [T]
R_T	Temporal asymmetry index defined as ratio fo intrusion to retreat timescale [-]
σ	Ratio of higher to lower boundary value (could be flux or head difference) [-]
Q_H, Q_L	Higher and lower inland boundary flux, respectively [L^2/T]
h_H, h_L	Higher and lower boundary head, respectively [L]
τ	Dimensionless timescale [T]
β	Ratio of final to initial inland boundary [-]

RTI	Response timescale indicator for the aquifer [T]
V_{si}	Volume of seawater in i^{th} layer [L^3]
τ_i	RTI of i^{th} layer [T]
T_{Ui}	Transmissivity of the layer above i^{th} layer [L^2/T]

SUMMARY

Freshwater-seawater interface is one of the most important regions in coastal aquifer systems, delineating the subsurface into zones with distinct fluid density and biogeochemical properties. The growth and decay of the interface control the subsurface flow field and water and chemical exchange processes between groundwater and ocean environments such as seawater intrusion (SWI) and submarine groundwater discharge (SGD). Although there are extensive studies regarding seawater intrusion and submarine groundwater discharge, there remain huge knowledge gaps in understanding the impacts of formation heterogeneity, making it challenging to accurately estimate the seawater intrusion extent and submarine groundwater discharge rates, upscale effective aquifer parameters and quantify uncertainties. In this study, we aim to develop a series of analytical and numerical solutions to quantify seawater intrusion and groundwater discharge and identify key governing parameters encompassing the effects of formation heterogeneity. Using the obtained new insights and tools, we aim to achieve fast delineation of the freshwater-seawater interface, improved control of SWI, understanding the impact of the preferential flow path, new aquifer homogenization and upscaling approaches, fast ensemble computations for uncertainty analysis, and recommendations for optimization of aquifer characterization.

We, for the first time, identified a single parameter—Transmissivity Centroid Elevation (TCE)—encompassing the effects of the spatial distribution of hydraulic conductivities. Higher values of TCE, i.e., higher conductivity zones lying in the upper part of the aquifer, represent a greater proportion of discharge in the upper aquifer and result in

greater SWI extent and SGD. Based on the TCE concept, we derived compact analytical solutions for SWI and SGD in stratified aquifers. To homogenize stratified aquifers, we then derived effective hydraulic conductivity as a function of TCE which represents layer placement. For uncertain conductivity fields modeled as random stratification, we derived explicit analytical solutions for the moments of toe-position and discharge to quantify uncertainties. We found that the elevation of the preferential flow layer has a significantly more dominant effect than hydraulic conductivity contrast. To delineate the seawater-freshwater interface profile separating zone of distinct salinity, we extended the TCE concept to the local transmissivity parameters premised on the insight that the extent of SWI only depends on the transmissivity field above the interface represented by local TCE and local transmissivity.

Leveraging the effectiveness of local-transmissivity parameters in estimating SWI, we developed a semi-analytical technique to compute the seawater-freshwater interface in aquifers with hydraulic conductivity varying along two dimensions. The semi-analytical technique is able to compute the interface with great accuracy when compared with numerical solutions of coupled variable-density flow which is time-consuming and computationally expensive. This rapid computation of the interface allowed us to perform a comprehensive stochastic and sensitivity analysis of SWI in a 2D heterogeneous case. We found that the near-coast near-top region of the aquifer controls the SWI extent, and aquifer characterization efforts should be concentrated mainly in this region. Recommendations on future work are made to analyze the effect of heterogeneity on the transience of SWI.

CHAPTER 1. INTRODUCTION

Groundwater constitutes 30 percent of the freshwater on the earth (National Groundwater Association, 2019). Given that most of the world's freshwater (about 69 percent) is locked away in glaciers and ice caps, groundwater becomes a vital source of freshwater supporting drinking water, agricultural and industrial demands. In the US, nearly 38 percent of the population relies on groundwater for drinking as reported by the National Groundwater Association (2019). Groundwater becomes much more critical in highly populated coastal areas as nearly 40 percent of the world's population living within 100 km of the coast is dependent on groundwater for various needs. Unfortunately, coastal groundwater resources are facing a multitude of threats in the form of lowering water-table, increasing pollution, and salinization. These threats are direct or indirect results of various manmade and natural factors which include but not limited to excessive extraction of groundwater, droughts, sea-level rise, and nutrient loading through freshwater discharge.

1.1 Seawater-freshwater Interface and Groundwater Discharge

Coastal groundwater flow involves complex processes arising from the difference in the densities of seawater and freshwater, which are miscible resulting in variable-density flow in porous media. Heavier seawater slides under the freshwater forming a seawater wedge which is contained near the coast by the pressure field due to seaward freshwater flow. The seawater and freshwater are separated by a transition zone or mixing zone, in which water density varies from that of freshwater to seawater. Drop in the pressure or lowering in the seaward freshwater flow due to over-extraction of groundwater, droughts, impaired infiltration disturbs seawater-freshwater equilibrium resulting in the advancement

of the transition zone inland. This phenomenon, known as seawater intrusion (SWI), has become a widespread problem in coastal aquifers around the globe.

SWI has serious impacts on the coastal environment and ecology. Broadly, there are three critical processes or regions of our interest (Figure 1):

1) The seawater-freshwater transition zone marks a rapid change in the biogeochemical conditions, hence delineating the shape and location of this zone is critical not only for managing SWI but also for modeling the fate of chemicals and microorganisms in coastal subsurface ecosystems.
2) The density-driven flow dynamics resulting from the seawater-freshwater interaction has a significant impact on the subsurface-freshwater discharge into the sea, popularly referred to as submarine groundwater discharge (SGD). SGD has a substantial contribution to the transport of chemicals from land into the marine environment. Excessive nutrient loading through SGD resulting from heavy urbanization and extensive use of chemical fertilizers in agriculture poses a great threat to delicate estuary and near-shore ecosystems.
3) The seawater wedge is characterized by continuous circulation of the saline water in and out of the sea into the aquifer. Chemicals and microorganisms entering the aquifer undergo biogeochemical processing under a range of residence times, resulting in a wide-ranging output into the sea.

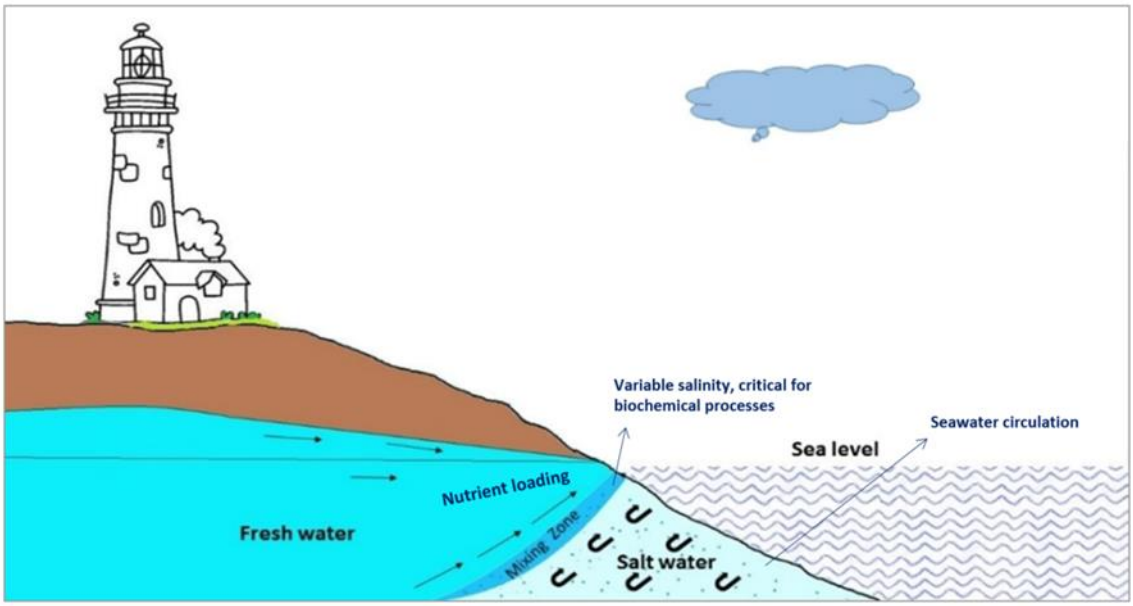

Figure 1 – Critical processes associated with seawater intrusion in coastal aquifers

In order to mitigate threats to coastal environmental and groundwater resources, it is vital to understand the subsurface flow dynamics governing SWI and SGD, and the effects of hydrogeological conditions on them. Heterogeneity in the form of spatial variation of hydrogeological properties, which is inherent in subsurface formations, has a strong influence on groundwater flow dynamics. Heterogeneous formations result in distinct discharge patterns, and shape and location of the seawater-freshwater interface compared with the homogenous case, hence, it becomes crucial to identify the parameters representing the effects of heterogeneity on SWI and SGD (Lu et al., 2013a). It is practically impossible to exactly characterize the hydrogeological properties of the subsurface, in which the parameters of interest like hydraulic conductivity are often modeled as a random field resulting in uncertainties in the analysis which need to be quantified and managed. For the purpose of large-scale modeling of field cases, it is desirable to obtain upscaled effective parameters that can represent the heterogeneity

effects through a homogenized domain. Achieving these modeling and analysis objectives for coastal aquifers is very challenging because of the combined complexities of variable-density subsurface flow and aquifer heterogeneity.

Characterization of the seawater-freshwater mixing zone (also known as transition zone and zone of diffusion/dispersion) developed due to interaction between freshwater and seawater is critical for the management of coastal aquifers facing the threat of SWI. To date, there is no exact solution available for the mixing zone shape and location due to non-linearities in the governing partial differential equations (PDE). Broadly, there are two approaches used to characterize the mixing zone. First, the mixing zone is approximated by an interface separating seawater and freshwater (also referred to as the interface flow) for which analytical solutions based on the potential theory can be derived. Such analytical solutions require minimal computation efforts and conveniently provide many useful insights into both steady-state and transient SWI. Second, the mixing zone is computed by numerically solving coupled nonlinear PDEs governing variable-density flow and transport (also referred to as dispersive flow). This approach provides a better representation of more complex systems field conditions like heterogeneity, tidal oscillations, beach slope, etc., however, it is computationally intensive and time-consuming. This approach becomes unviable if we want to solve a large number of cases for stochastic analysis or inverse modeling.

In this thesis, we aim to understand mechanisms through which heterogeneity in the hydraulic conductivity affects the SWI and SGD. We sought to identify key governing parameters encompassing the effects of heterogeneity which will be used to achieve various scientific and modeling objectives as discussed above. In this study, our focus is

limited to the extent of SWI and SGD hence we adopt the interface approximation ignoring the mixing in the transition zone. The insights about the heterogeneity effects on the extent of SWI and SGD in the interface flow are expected to be transferable to the dispersive flow. The main goal of this thesis is to advance our scientific understanding of the effects of aquifer heterogeneity on coastal groundwater flow dynamics and develop a series of analytical and numerical solutions to aid scientific, engineering and water-resource management decision making.

1.2 Research Motivation, Objectives, and Approach

1.2.1 Research Motivation

Coastal aquifers and near coast ecosystems in many regions around the world are under threat from salinization and contamination. In order to protect and remediate coastal ecosystems, it is critical to understand and predict the key phenomena, including SWI which causes salinization and SGD which controls chemical loading into the ocean through the subsurface flow. The groundwater flow dynamics underlying these phenomena are strongly impacted by spatial variation of hydraulic properties of the flow domain, of which hydraulic conductivity heterogeneity is the most important. Understanding and quantifying the effects of hydraulic-conductivity heterogeneity (referred henceforth as heterogeneity for the sake of brevity) is highly desired as most of the aquifers in the field are inherently heterogeneous. Analytical approach to study coastal groundwater flow dynamics though requires adoptions of some approximations for arriving at simple solutions, offers extremely useful insights about the underlying mechanisms and key parameters in addition to providing first-order prediction tools. Detailed analytical analysis of heterogeneity

effects on coastal aquifer is not available because of challenges involved in modeling variable-density flow which is governed by nonlinear PDEs. We aim to develop a new analytical modeling framework to understand and quantify heterogeneity effects on SWI and SGD. This framework will define new parameters accounting for the heterogeneity effects yielding a series of analytical and semi-analytical solutions for SWI and SGD in different heterogeneity settings. Such parameters are also expected to help us conveniently quantify uncertainties in SWI and SGD due to uncertainties in hydraulic conductivity fields, and also provide the foundation for upscaling effective parameters in both deterministic and stochastic framework.

1.2.2 Specific Objectives

Specific objectives of this research include:

(i) Developing elegant analytical and semi-analytical solutions for steady seawater-freshwater interface and submarine groundwater discharge in different heterogeneity settings

(ii) Quantifying uncertainties in SWI extent and SGD due to heterogeneous hydraulic conductivities

(iii) Developing effective parameters for deterministic and stochastic upscaling of coastal aquifers

(iv) Quantifying the timescale of transient seawater intrusion and analyzing the effects of stratification on the transience

1.2.3 Approaches

This study is primarily theoretical in nature offering a series of new analytical and semi-analytical solutions and discussing critical insights obtained from the analyses. Numerical methods are employed frequently to validate analytical solutions, providing complementary analysis and visualizing key quantifies like velocity distribution, mixing, etc. To quantify uncertainties, explicit analytical solutions for statistical moments are developed for the stratified case, and Monte Carlo simulations are used for 2D heterogeneous cases.

1.3 Organization of Thesis

This thesis has 8 chapters. This chapter provides a brief introduction to the research problem, objectives and approaches. Chapter 2 provides a comprehensive review of the literature relevant to this research. Chapter 3 introduces a new concept of Transmissivity Centroid Elevation (TCE) and defines new parameters to account for the effects of stratification on SWI and SGD. This study is published as Rathore et al. (2018b). Chapter 4 extends the TCE concept to local transmissivity parameters and developed an explicit analytical solution for the seawater-freshwater interface in stratified aquifers. This study is published as Rathore et al. (2019). Chapter 5 extends the application of the TCE concept to 2D heterogeneous aquifers and presents a semi-analytical technique for fast delineation of the interface profile in a 2D heterogeneous aquifer. This study is under review. Chapter 6 presents a stochastic analysis of SWI and SGD in stratified and 2D heterogeneous cases. This study is under review. Chapter 7 investigates the transience of SWI in both homogeneous and stratified aquifers. The timescale analysis in homogeneous aquifers is published as Rathore et al. (2018a). Chapter 8 summarizes the conclusions, limitations, implications and future work recommendations.

CHAPTER 2. LITERATURE REVIEW

This chapter provides a comprehensive summary of the scientific literature for the following topics: (i) seawater intrusion, (ii) submarine groundwater discharge, (iii) heterogeneity effects, and (v) transient SWI.

2.1 Seawater Intrusion

Seawater intrusion is the incursion of the saline water from the sea into the freshwater aquifers. The seawater being heavier slides under the freshwater resulting in the wedge-shaped volume of seawater continuously circulating between the aquifer and sea (Figure 1). Seawater intrusion has become a serious threat to coastal groundwater resources around the globe (Kinzelbach et al., 2003; Post, 2005). The salinity as low as 1% in the groundwater is enough to fail the secondary drinking-water standards (250 mg/L chloride concentration (WHO, 2011)). Once salinized, the remediation process for the aquifer is difficult and costly. The main causes of seawater intrusion are excessive groundwater extraction, land-use change, low freshwater flow induced by drought, and sea-level rise (Werner et al., 2011).

The transition from the seawater to freshwater is characterized by a mixing zone (also known as transition zone and zone of diffusion/dispersion), which marks the extent of seawater intrusion and rapid transition in biogeochemical conditions. Prevention of seawater intrusion by optimizing coastal freshwater pumping is a common approach that requires the estimation of the extent of SWI (Cheng et al., 2000; Park and Aral, 2004). Such estimations are also required for the prediction of upconing where intruded saline

water rise vertically thus shrinking the size of freshwater flow domain (Bower et al., 1999; Eeman et al., 2011; Reilly and Goodman, 1987; Saeed et al., 2002; Wirojanagud and Charbeneau, 1985). The location of the mixing zone also has a significant impact on biogeochemical processes and coastal morphology development. Numerous studies have focused on carbonate dissolution in carbonate aquifers leading to cave formations (Back et al., 1979; Smart et al., 1988; Wigley and Plummer, 1976), difference in cation exchange in freshwater an seawater (Appelo and Willemsen, 1987; Faye et al., 2005; Giménez-Forcada, 2010; Valocchi et al., 1981), sulfate reduction in the intruded seawater compared to seawater (Berner, 1980; Gomis-Yagües et al., 2000; Grassi and Cortecci, 2005). Hence, it is critical to estimate the location, thickness and shape of this zone for the coastal water security and preventing environmental degradation of coastal systems.

2.1.1 SWI Field Measurements

In the field, to manage the coastal aquifers facing the threat of SWI, the temporal measurements and monitoring of the location of the mixing zone is essential. Accurate delineation of the extent of SWI is challenging because of the lack of direct access and scarcity of salinity measurements. Werner (2010), Barlow and Reichard (2010) and Custodio (2010) presented an overview of the monitoring and assessment of SWI in Australia, North America, and Europe, respectively. Assessing SWI in the field requires a combination of multiple techniques like head measurements, geophysical methods, environmental tracers, as any techniques by itself fail to provide a clear picture.

Head measurement is difficult in coastal aquifers because of the strong influence of the density-differences on the head values. Post et al. (2007) provided an overview of head measurements in coastal aquifers.

Geophysical methods like direct current (DC) methods and electromagnetic (EM) methods leveraging the large electrical resistivity contrast between seawater and freshwater have been found effective in mapping the salinity distributions in the groundwater. Resistivity methods have been deployed at various locations like Hawaiian Islands (Swartz, 1937), Europe (Flathe, 1955; Van Dam and Meulenkamp, 1967), Israel (Ginsberg and Levanton, 1976), and Florida (Fretwell and Stewart, 1981). Over the past couple of decades, electrical resistivity tomography (ERT), a method for 2D and 3D visualization of resistivity distributions in the subsurface (Werner et al., 2013) has become popular in coastal hydrogeology, and it has been used in many field studies (e.g., Day-Lewis et al., 2006; Henderson et al., 2010; Manheim et al., 2004). Recently, using permanent networks of electrodes for time-lapse resistivity imaging has become popular because of the effectiveness of these techniques in detecting small salinity changes (De Franco et al., 2009; Ogilvy et al., 2009; Poulsen et al., 2010). EM methods have also been found to be successful in mapping the groundwater salinity variations (Goldman et al., 1991; Stewart, 1982). The ability of the EM methods to make measurements remotely has been leveraged recently by using airborne measurement systems, which makes the mapping of the subsurface resistivity over large areas cost-effective (Paine, 2003). These systems become even more useful for study areas that are inaccessible through ground transportation systems, like Everglades in Florida (Fitterman and Deszcz-Pan, 1998). A detailed review of the helicopter-borne EM methods can be found in Siemon et al. (2009).

Chemical tracers have been used to characterize the seawater intrusion based on the ages of saltwater from different sources including salinity (Vengosh et al., 1999; Werner and Gallagher, 2006). Isotope based characterization is particularly helpful in the region with multiple phases of seawater inundations to distinguish salinity from different events based on isotope aging (Darling et al., 1997; Petalas and Diamantis, 1999). Since the focus of this thesis is mainly physical processes of SWI, we do not provide a detailed review of literature pertaining to the chemical techniques.

2.1.2 SWI Prediction

The flow dynamics in coastal aquifers are heavily influenced by the density-difference between seawater and freshwater. These density-driven flow dynamics are governed by advection, dispersion, and convection (Henry, 1964; Smith, 2004b). These processes control the extent of seawater intrusion and the mixing in the transition zone. To date, there is no exact solution available for the mixing zone shape and location due to non-linearities in the governing partial differential equations (PDE). Broadly, there are two types of mathematical models used to characterize the mixing zone. First is a system of coupled non-linear PDEs governing variable-density flow and transport (also referred to as dispersive flow) (Diersch, 1998; Henry, 1964). The variable density models resolve salinity distribution which is essential for studying mixing and reactive transport. These coupled non-linear PDEs cannot be solved analytically and require numerical techniques which are summarized in the next section. Numerical computations of variable-density flow solutions enable a better representation of more complex systems field conditions like heterogeneity, tidal oscillations, beach slope, etc., however, it is computationally intensive and time-consuming. This approach becomes unviable if we wish to solve a large number of cases

for stochastic analysis or inverse modeling. The second approach involves approximating the mixing zone by an interface separating seawater and freshwater (also referred to as the interface flow), thus seawater and freshwater are assumed to be immiscible. With this simplified approach, it is possible to derive analytical solutions based on potential theories (Bakker, 2006; Bear and Dagan, 1964; Collins and Gelhar, 1971; Dagan and Zeitoun, 1998; Huppert and Woods, 2006; Kacimov, 2002; Kacimov and Obnosov, 2001; Kacimov and Sherif, 2006; Naji et al., 1998; Öztürk, 1970; Strack, 1976). Such analytical solutions require minimal computation effort and conveniently provide many useful insights into both steady state-state and transient SWI.

In this study, our aim is to advance the theoretical understanding and the modeling capabilities of the effects of heterogeneity on seawater intrusion. Our focus is mainly on the extent SWI, hence we adopt the interface approximation approach to derive elegant analytical and semi-analytical solutions for heterogeneous coastal aquifers that are not available to date. We sought to identify key governing parameters encompassing the effects of heterogeneity which will be used to achieve various scientific and modeling objectives, and provide the foundation for the studies focused on mixing and reactive transport in heterogeneous aquifers. In the next two subsections, we provide a brief overview of the existing numerical and analytical solutions for SWI.

2.1.2.1 Numerical Modeling

Numerical codes solving system of variable-density flow equations has become indispensable tool for solving complex real-world SWI problems and developing future projections at local and regional scales. With the betterment of our understanding of

physical and biogeochemical processes coupled with advancements in computational techniques and power, numerical codes have become popular in simulating coastal aquifers. Compared to the flow solutions, the solute transport solution requires much finer spatial and temporal discretization. Additionally, for variable-density flow, the coupling of flow and transport equation through the density-salinity relation results in an extra level of iteration which increases the computation time significantly. The common methods used to solve coupled PDEs are the finite difference and finite element methods which are susceptible to numerical dispersions.

One of the most popular SWI code is SEAWAT (Guo and Langevin, 2002), a finite difference based computer program designed to simulate three-dimensional variable-density flow. SEAWAT uses MODFLOW to solve groundwater flow and MT3D to solve transport, coupling them together through the VDF package. SUTRA (Voss and Provost, 2002) is another popular program which is a more general-purpose program—a hybrid of finite element and finite difference—with the capabilities of solving variable-density flow for both saturated and unsaturated domains. Werner et al. (2011) provided a comprehensive list of popular codes, their associated numerical techniques and field studies in which these programs were applied, which is adapted in Table 1.

Programs for numerical solutions need to be tested against the analytical solutions of simplified standard variable-density flow problems for benchmarking. There are many benchmark problems proposed in the literature, among which Henry (Henry, 1964) and Elder (Elder, 1967) problems are the most popular ones. Various modifications have been proposed in the Henry problem to increase the density effects in the flow (e.g., Abarca et al., 2007a; Abarca et al., 2007b; Simpson and Clement, 2003; Simpson and Clement,

2004). The Elder problem, another popular benchmark problem presents a free convention of the heavier saltwater into freshwater (Elder, 1967; Voss and Souza, 1987). Other commonly used problems include HYDROCOIN salt dome problem (Konikow et al., 1997), salt lake problem (Simmons et al., 1999), salt pool problem (Johannsen et al., 2002; Oswald and Kinzelbach, 2004), and rotating fluids problem (Bakker et al., 2004a). Benchmarking problems have their own limitations as they are often oversimplified and do not reflect well the real field conditions.

Table 1 - Commonly used SWI codes (adapted from Werner et al. (2011))

SWI Code	Numerical Technique	Field applications
FEFLOW	Finite Element	Gossel et al. (2010); Watson et al. (2010); Yechieli et al. (2010)
FEMWATER	Finite Element	Carneiro et al. (2010); Datta et al. (2009)
HYDROGEOSPHRE	Finite Element	Graf and Therrien (2005); Thompson (2007)
MARUN	Finite Element	Abdollahi-Nasab et al. (2010); Boufadel (2000); Boufadel et al. (2011); Li and Boufadel (2011)
MOCDENS3D	Finite Difference	Bakker et al. (2004b); Giambastiani et al. (2007); Vandenbohede and Lebbe (2006); Vandenbohede et al. (2010); Vandenbohede et al. (2008a); Vandenbohede et al. (2008b); Vandenbohede et al. (2008c)
MODHMS	Finite Difference	Werner and Gallagher (2006)
SEAWAT	Finite Difference	Cherubini and Pastore (2011); El-Bihery (2009); Kourakos and Mantoglou (2009); Lin et al. (2009); Mao et al. (2006); Vandenbohede and Lebbe (2011)
SUTRA	Finite Element/Difference	Nishikawa et al. (2009); Pool and Carrera (2010)
SWI	Finite Difference	Bakker et al. (2004b)

2.1.2.2 Seawater-freshwater Interface

This thesis is focused on the analysis of the heterogeneity effects on SWI and SGD using the interface flow assumption, therefore, we limit the literature review to the analytical solutions for the interface flow. Although the analytical solution for the variable density flow for Henry problem (Henry, 1964) is available, it has a very limited utility in providing insights transferable to real aquifers which are mostly heterogeneous. With the interface approximations, we can study transient SWI and SWI in heterogeneous aquifers analytically. The interface-flow solutions satisfy the continuity and flow across the interface. The slope of the interface is a function of the density difference, freshwater discharge and hydraulic "local" hydraulic conductivity (Bear, 1972). The interface flow solution under steady-state condition is simplified significantly with the Dupuit approximation (e.g., Dupuit, 1863) of no resistance to vertical flow. Thus, the head values under Dupuit approximation is are only a function of horizontal coordinates, in other words, the equipotential lines are vertical. The Dupuit interface is solved using the Ghyben–Herzberg (Badon Ghyben, 1888) formula (e.g., Bear, 1972; Strack, 1989).

To obtain exact solutions for the steady-interface flow in homogeneous aquifers, many studies adopted the hodograph method in combination with conformal mapping (for e.g., Bakker, 2000; Bear, 1972; Kacimov, 2002; Kacimov and Obnosov, 2001; Kacimov and Sherif, 2006; Strack, 1989; Verruijt, 1970). Pool and Carrera (2011) proposed an empirical modification to the saltwater density to correct the overestimation of SWI due to interface approximation. The potential theory solution by (Strack, 1989; Strack, 1976) is a very powerful tool to estimate the interface profile as the potential is a function of only horizontal coordinate and have a unique relationship with the interface location (with

Dupuit approximation). Strack's potential theory solutions are valid for piecewise homogeneous aquifers. These solutions' applicability in a 3D setting makes them a popular choice for evaluating critical pumping rates and optimizing groundwater withdrawals from coastal aquifers.

The extent of SWI is often characterized by the point of intersection of the seawater-freshwater interface and the aquifer bottom, referred to as toe position. Toe-position has been used as the key indicator in studies for many studies like maximum pumping from a well avoiding SWI (Strack and Ausk, 2015), the timescale of SWI (Chang and Clement, 2012; Watson et al., 2010).

Attempts have also been made to solve the moving interface. Bear and Dagan (1964); Bear et al. (1985) used the method of successive steady-state to simulated the movement of the interface in response to an abrupt boundary change. Bakker (1998) presented a comprehensive potential based method to resolve the instantaneous velocity field for a moving seawater wedge.

2.2 Submarine Groundwater Discharge

Submarine groundwater discharge (SGD) here refers to the fresh groundwater flow into the sea at the coastal boundary. SGD, which is coupled with seawater intrusion process, is now widely recognized as the major source of chemical inputs into marine environment, negatively affecting the ecosystem (Burnett et al., 2006; Burnett et al., 2003; Church, 1996; Li et al., 1999; Moore, 2010; Robinson et al., 2018; Simmons Jr, 1992). SGD is interconnected with SWI through the constituent relationship between the location and shape of the seawater-freshwater interface and the seaward freshwater discharge,

where lower SGD corresponds to the higher extent of SWI and vice versa (Bear, 2013; Strack, 1976; Werner et al., 2012). This interdependence of SWI and SGD is also studied in the field (Dimova et al., 2011; Shibuo et al., 2006), numerical modeling (Kaleris, 2006) and laboratory (Chang and Clement, 2012; Chang and Clement, 2013; Goswami and Clement, 2007). The groundwater discharge flows above the seawater wedge, hence the location and shape of the interface control the pathway of groundwater flow, strongly influencing the geochemical process that nutrients go through near and across the interface (in the mixing zone) (Kaleris et al., 2002; Price et al., 2006).

2.2.1 SGD Measurements

Estimating the SGD is critical to understanding and modeling the oceanic chemical balance and hydrothermal cycle. For the field investigations, many methods have been proposed in the literature to estimate the contribution of the SGD to the freshwater and nutrient discharge into the ocean environment. The direct measurement techniques include usage of devices like seepage meters (e.g., Krupa et al., 1998; Paulsen et al., 2001; Sholkovitz et al., 2003; Taniguchi and Fukuo, 1993) and piezometers (Barwell and Lee, 1981). However, in most cases, direct measurements are impractical because of the vast extent over which SGD occurs. For indirect measurement of SGD, geochemical tracer techniques using natural radium isotopes and ^{222}Rn have been used widely in recent years (Burnett, 1996; Cable et al., 1996; Charette et al., 2001; Corbett et al., 2000; Crotwell and Moore, 2003; Krest and Harvey, 2003; Moore, 1996; Moore and Shaw, 1998; Moore and Wilson, 2005). Geophysical tracers like groundwater temperatures have also been used to estimate groundwater discharge rates (Boyle and Saleem, 1979; Bredehoeft and Papaopulos, 1965; Moore et al., 2002; Silliman and Booth, 1993).

2.2.2 SGD Predictions

Numerical modeling has been used to investigate ad quantify SGD (Michael, 2005; Oberdorfer, 2003; Shishaye, 2015; Thompson et al., 2007). For understanding the effects of different aquifer parameters on SGD and obtaining first-order prediction capabilities, various analytical solutions have been proposed for different hydrogeological settings. Strack (1976) proposed the single potential theory which provided the relation between groundwater head and freshwater flux in both confined and unconfined homogeneous aquifers. Based on a single potential theory, Lu et al. (2015) provided correction for the coastal head to facilitate estimation of SGD directly using classical Darcy's law for single density, single layer aquifer. Strack and Ausk (2015) extended the single potential theory to layered aquifers as comprehensive discharge potential theory and provided a method to exactly compute vertically integrated discharge using the comprehensive discharge potential. However, a series form of potential theory solution does not provide us capabilities for uncertainty analysis and homogenization because of a large number of terms representing layers' properties. There is a need for compact parameters that can represent the effects of hydraulic conductivity values and their spatial distribution efficiently, thus providing us elegant solutions and insights about the key mechanisms in heterogeneous coastal aquifers.

2.3 Heterogeneity Effects

Hydrogeological systems are inherently heterogeneous with spatial variations of hydrogeological properties strongly influencing flow and contaminant transport dynamics. Heterogeneous aquifers are found to have distinct mixing zone characteristics, seawater-

freshwater interface and groundwater discharge compared to homogenous aquifers (Lu et al., 2013a; Simmons et al., 2001; Strack and Ausk, 2015). Heterogeneity due to the spatial variation of hydraulic conductivity cannot be exactly characterized by the sub-surface flow domain. Heterogeneity manifests at many scales and in many forms. Small scale heterogeneity which is often modeled as random fields found to influence mixing zone thickness due to macrodispersion (Abarca, 2006; Kerrou and Renard, 2010). Abarca (2006) through numerical simulations found that heterogeneity results in a smaller extent of SWI and wider mixing zone. Contrary to Abarca's results for the 2D model, Kerrou and Renard (2010) showed that for a 3D case, with the increase in the degree of heterogeneity, the extent of SWI increases. Hence, hydraulic conductivity is modeled as random fields, and the analysis of dependent flow and transport variables is performed in a stochastic framework to quantify resulting uncertainties. Abarca (2006) analyzed SWI in multiple 2D heterogeneous field realizations while Kerrou and Renard (2010) analyzed a single 3D realization, hence a more comprehensive study is required for making general conclusions. Pool et al. (2015) analyzed the combined effect of heterogeneity and tidal oscillations using three-dimensional Monte Carlo realizations and numerically solving variable flow and transport for each realization. Since the numerical simulation of SWI in heterogeneous is time-consuming, the number of realizations in their analyses was limited to 50. They confirmed the reduction of the extent of SWI and the widening of the mixing zone due to heterogeneity and found it to be linearly proportional to the product of correlation length and variance of the log-permeability field.

It is almost impractical to characterize the small-scale heterogeneities deterministically, hence, they are often modeled as random fields. Dagan and Zeitoun

(1998) represented heterogeneity as random stratification (1D random field) and provided closed-form solutions for the statistical moments of the interface profile in a vertical slice of an aquifer with a constant flux boundary. They found that the variance of the toe-positions is dependent on variance and correlation length of the randomly stratified field, however, they did not comment on the type of relation. A similar stochastic analysis for a 2D heterogeneous case is missing.

Horizontal layering or stratification is a form of heterogeneity common in sedimentary coastal aquifers (Dagan and Zeitoun, 1998). Examples of field investigations dealing with stratified coastal aquifer include Floridan Aquifer System (Sacks and Tihansky, 1996), coastal aquifers in Long Island, New York (McClymonds and Franke, 1972), Savannah, Georgia (Collins and Gelhar, 1971), and Israel (Dafny et al., 2010). Through numerical and experimental investigations, Lu et al. (2013a) studied the effect of stratification on the mixing zone. They found that different layer placements resulted in significantly different toe-position and the shape of the mixing zone, which implied that the upscaled parameters for single density flow cannot be used in the variable-density flow. In their laboratory and numerical experiments, the case with a low permeability layer on the top of the higher permeability layer showed a widening of the mixing zone in the low permeability layer. This widening of the mixing zone was explained through refraction and separation of the streamlines (Lu et al., 2013a). Numerical modeling has been extensively used to study many field cases of stratified aquifers, for e.g., Xia et al. (2010), Guo et al. (2010), Kim et al. (2006), and Oki et al. (1998).

In order to understand the mechanisms controlling heterogeneity and identify key parameters, analytical solutions are crucial. For a specific case of stratification wherein, a

homogeneous system divided into two layers by a semi-pervious layer, Collins and Gelhar (1971) and Mualem and Bear (1974) derived analytical solutions to predict the interface shape. Rumer and Shiau (1968) derived approximate interface solutions for anisotropic deep coastal aquifers. However, their solution was proved erroneous by Strack (2016) for not satisfying flow continuity. Recently, Strack and Ausk (2015) presented a comprehensive discharge potential for stratified coastal aquifer which can solve for the interface profile in 3D. This is an extension of their single potential theory (Strack, 1976). This discharge potential theory as then extended to more general cases like perched aquifers (Strack, 2017). Although the potential theory solutions provide a convenient tool for quick delineation of the interface, it is not possible to make general conclusions from the series form potential theory solutions. There is a need to identify concise set of parameters controlling the heterogeneity effects to understand the key mechanisms, homogenization and upscaling, and stochastic analysis.

Upscaling is essentially reproducing the independent variable of interest by replacing fine-scale hydraulic conductivity values (high resolution) by a coarser grid block. Upscaling in groundwater flow models in heterogeneous aquifers is desired for two main reasons: to reduce the computation burden, and to deal with the differences in the scales of measurement and discretization of the model. There is a vast literature available on theories and approaches for upscaling mainly focused on single-phase, single-density flow through heterogeneous porous media. A review of upscaling literature can be found in Wen and Gómez-Hernández (1996), Sanchez-Vila et al. (2006), Renard and de Marsily (1997), Farmer (2002), and Cushman et al. (2002). The variable-density flow involved in SWI is governed by non-linear PDEs making their numerical modeling computationally

demanding. With the added complication of the formation heterogeneity, upscaled parameterization is highly desired to make numerical solutions for field applications practical. Most of the upscaling studies for SWI focused on mixing to obtain macrodispersion parameters in heterogeneous coastal aquifers. Held et al. (2005) applied the homogenization theory to arrive at the effective hydraulic conductivity and dispersivity in 2D isotropic and anisotropic heterogeneous conductivity fields. Their scale of considered heterogeneity was very small compared to the scale of SWI (distance of toe from the coastal boundary) or the aquifer domain, which enabled them to derive geometric mean of the conductivity field as the effective conductivity in an intrinsic sense. However, for the extent of SWI and SGD, which are key dependent variables for coastal aquifer, there have not been sufficient efforts for deriving or estimating effective parameters. Especially, for the cases in which the scale of heterogeneity is comparable to the extent of SWI.

2.4 Transient SWI

Understanding and predicting the transience of SWI is essential for the effective management of coastal aquifers. There have been several studies exploring the transience of SWI in homogeneous aquifers. Watson et al. (2010) used numerical modeling to study the transience of SWI driven by sea-level rise in an unconfined aquifer. They defined the SWI timescale as the time taken by the interface toe to transition from one steady-state to another. Watson et al. (2010) also revealed the counter-intuitive phenomena of temporal disparity between seawater intrusion and seawater retreat (SWR, i.e., movement of the interface towards the sea). Chang and Clement (2012) confirmed the temporal disparity between SWI and SWR through laboratory and numerical experiments simulating aquifer

systems with fixed flux as the inland boundary. They found that the interface takes smaller time to recede towards the sea than time to intrude into the aquifer in response to the same magnitude of change in the boundary condition. Chang and Clement (2012) explained this disparity through the difference in flow fields during SWI and SWR, where SWI exhibits opposing flow fields with a distinct stagnation point at the aquifer bottom, while the SWR case exhibits a well-aligned unidirectional flow field. Lu and Werner (2013) analyzed the time scale of SWI and SWR identified simple log-linear relationships between boundary values and timescales using a series of numerical simulations and linear regression. They studied the sensitivity of regression coefficients of different aquifer parameters. However, their empirical relationships between timescales and boundary values fail to reveal physical relationships between timescales and effective parameters. Finding such empirical relationships between timescales and aquifer parameters is susceptible to high computational efforts.

For transient SWI, because of lack of field studies and limitations of time-consuming numerical simulations, analytical solutions prove to be an attractive alternative to understand underlying hydrodynamic processes and identifying key parameters, in addition to providing a first-order prediction tool. Bear developed a method of successive steady-state to simulate the moving interface in response to an abrupt change in the inland flux boundary (Bear, 1972; Bear and Dagan, 1964; Bear et al., 1985). Vappicha and Nagaraja (1976) also derived an analytical solution for the transient interface. Kiro et al. (2008) derived analytical solutions for the timescale of the water table and transition zone response to aa sea-level drop. These studies highlight the importance of analytical solutions for transient SWI. There is a need for an explicit analytical solution for the timescale for the

cases with constant head and constant flux as inland boundaries. Such a solution will enable us to understand the key mechanisms and explain important phenomena like temporal asymmetry between SWI and SWR.

CHAPTER 3. A NEW PARAMETER ACCOUNTING FOR STRATIFICATION EFFECTS ON SEAWATER INTRUSION

3.1 Introduction

Geological systems are inherently heterogeneous with spatial variations of hydraulic properties that control the groundwater flow and solute transport. In coastal aquifer systems, heterogeneity is often assumed to be in horizontal layering or stratification, in agreement with many field investigations of sedimentary aquifers (Dagan and Zeitoun, 1998). Examples of such stratified coastal aquifers include the Floridan Aquifer System (Sacks and Tihansky, 1996), coastal aquifers in Long Island, New York (McClymonds and Franke, 1972), Savannah, Georgia (Collins and Gelhar, 1971), and Israel (Dafny et al., 2010), among others. Stratification strongly influences groundwater flow dynamics in coastal aquifers, resulting in both distinct discharge patterns and freshwater-seawater interface behavior compared with the homogeneous case, and a better understanding of such systems is important to remedy seawater intrusion (SWI) and control solute inputs into the sea through submarine groundwater discharge.

Attempts to understand and predict the effects of stratification on the interface flow have been undertaken through numerical, experimental and analytical methods (Dagan and Zeitoun, 1998; Lu et al., 2013a; Mualem and Bear, 1974; Rumer and Shiau, 1968; Strack, 2017; Strack and Ausk, 2015). Recently, Lu et al. (2013a) conducted both laboratory experiments and numerical simulations for a three-layer aquifer and demonstrated that the toe position and shape of the mixing zone vary significantly in stratified aquifers with the

same hydraulic conductivities but different layer placement. This result implies that upscaled effective parameters for single-density flow in stratified aquifers may not be valid for the interface flow. Shi et al. (2018) assessed the impact of sea-level rise on the SWI in stratified aquifers.

Several analytical solutions have been derived to approximate steady-state interfaces in stratified aquifers. For example, Collins and Gelhar (1971) and Mualem and Bear (1974) derived analytical solutions to predict interface shape in a homogeneous system divided into two layers by a semi-pervious layer. Rumer and Shiau (1968) provided approximate solutions for deep coastal aquifers under anisotropic conditions. However, their approach of layer transformation in a stratified aquifer was proven to be erroneous by Strack (2016). A recent study by Strack and Ausk (2015) extended the single potential theory (Strack, 1976) to three-dimensional flow in horizontally stratified aquifers by integrating vertically the discharge throughout the aquifer. Strack (2017) extended discharge potential theory to more general conditions like perched aquifers. They noted the effects of aquifer stratification on the discharge and toe position by relating them to the discharge potential. Toller and Strack (2019) investigated SWI in aquifers with hydraulic conductivity varying in the vertical direction. Modeling heterogeneity using a continuous function is common in modeling hydraulic conductivity of rocks, which decreases with depth due to increasing overburden on microfractures. Although, despite that the analytical solution derived in Strack and Ausk (2015) and Strack (2017) provides a convenient tool for calculating the interface position and discharge, a series form of the solution limits the analysis of the aquifer stratification effect, and the general physical understanding of seawater intrusion and freshwater discharge in a stratified coastal aquifer is still not available.

The present study aims to reveal the aquifer-stratification effects on seawater intrusion by expressing previous analytical solutions (Strack and Ausk, 2015) in a simple form for both flux-controlled and head-controlled systems. The new expression of the analytical solution reduces stratification effect terms into a couple of terms with simple physical meanings and delineates the effects of layer arrangement and hydraulic conductivity magnitudes. The proposed formulation allows us to provide simple explanations and more generalized conclusions about the effects of aquifer stratification on the interface toe and discharge rate. It also allows us to analyze special cases of heterogeneity, such as the preferential flow path and symmetric aquifers. Based on our formulation, we also provide effective parameters for the stratified coastal aquifer to reproduce the toe position and discharge rate, which have not been given in previous homogenization studies. We also analyze the case exponentially decaying hydraulic conductivity with depth and provide analytical solutions for the toe-position and groundwater discharge. We then assess the sensitivity of the derived solutions to key parameters.

3.2 Conceptual Model

We consider a typical two-dimensional confined stratified aquifer with layers of different hydraulic conductivities, bounded by a horizontal impermeable top and bottom layer, and vertical inland and coastal boundary, as shown in Figure 2. For simplicity, the system is assumed to be in a steady state with seawater and freshwater separated by an interface.

The regional groundwater flow is considered perpendicular to the coastline in the far-field. Therefore, there are two zones in the aquifer: an interface-flow zone consisting of both freshwater and saltwater (Zone 1) and a zone without interface consisting of only freshwater (Zone 2). The origin is located at the point where the aquifer base meets the coastline. The x axis is along the top of the underlying impervious layer pointing towards inland, and y axis along the vertical coastline pointing upwards. L $[L]$, H_s $[L]$ and x_t $[L]$ represent the distance of the known inland boundary from the coastal boundary, seawater head at the coastal boundary, and interface toe position, respectively. Figure 2 depicts the case with an inland boundary as a constant head h_f $[L]$ (referred henceforth as "head-controlled system"), and we also analyze the case with the inland boundary as a constant flux Q_x $[L^2/T]$ (referred he tonceforth as "flux-controlled system"). The Dupuit-Forchheimer approximation (Dupuit, 1863; Forchheimer, 1886) of horizontal flow is adopted, which implies that the piezometric head and potential are constant at any vertical cross-section in the aquifer. The layers are numbered from 1 to N bottom-up where N is the total number of layers. b_i $[L]$, y_i $[L]$ and K_i $[L/T]$ represent respectively the thickness, the elevation of the center and hydraulic conductivity of the ith layer (note that "elevation" in this paper means elevation relative to the aquifer base unless mentioned otherwise). d_i $[L]$ represents the base elevation with respect to the sea level for the ith layer. $T_i = b_i K_i$ is the transmissivity of each layer. B $[L]$ and T $[L^2/T]$ are the total aquifer thickness and transmissivity, respectively:

$$B = \sum_{i=1}^{N} b_i \, , T = \sum_{i=1}^{N} T_i \tag{1}$$

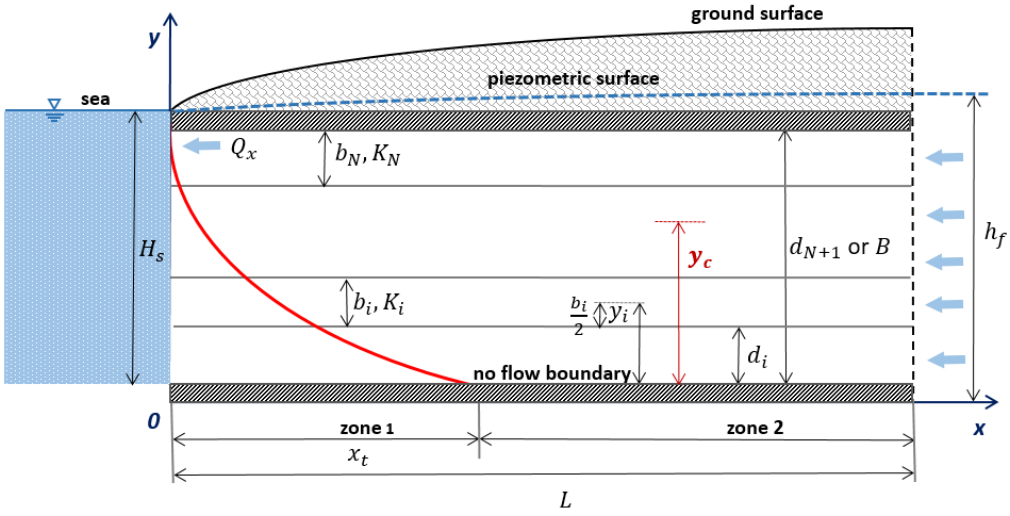

Figure 2 - Conceptual model of the 2D stratified confined aquifer

3.3 Theory

3.3.1 Steady-state Solution for a Flux-controlled System

The comprehensive potential Φ $[L^3/T]$ (referred to henceforth as "potential") at the boundary, $x = 0$, can be evaluated as follows (Strack and Ausk, 2015):

$$\Phi_0 = \frac{1}{\alpha} T H_s - \frac{1}{\alpha} \sum_{i=1}^{N} T_i y_i - \frac{1}{2} K_N d_{N+1}^2 \quad (2)$$

Strack and Ausk (2015), using the Dupuit-Forchheimer approximation, provided the relation between the potential and head at any cross-section as follows:

$$\Phi(\phi) = (\sum_{j=m+1}^{N} K_j H_j + K_m d_{m+1})\, \phi - \frac{1}{2} K_N d_{N+1}^2 + C_m \quad (3)$$

where m represents the stratum containing the interface, ϕ $[L]$ represents the piezometric head above the sea level, and C_m $[L^3/T]$ is a constant introduced to maintain the continuity of the potential across the strata boundaries,

$$C_m = \frac{1}{2\alpha} (\sum_{j=2}^{m} (K_j - K_{j-1}) d_j^2 + K_1 H_s^2) \quad (4)$$

For the interface toe, $m = 1$ and $C_1 = \frac{1}{2\alpha} K_1 H_s^2$.

The piezometric head (above the sea level) at the toe, ϕ_t $[L]$, can be obtained from the Ghyben-Herzberg equation (Badon Ghyben, 1888):

$$\phi_t = \frac{H_s}{\alpha} \quad (5)$$

By substituting ϕ_t and C_1 in Eq. (2), we get Φ_t as:

$$\Phi_t = \frac{1}{\alpha} T H_s - \frac{1}{2} K_N d_{N+1}^2 \tag{6}$$

Using the definition of the comprehensive potential, the magnitude of the discharge can be expressed as:

$$Q_x = \frac{\Phi_t - \Phi_0}{x_t - 0} \tag{7}$$

Rearranging the Eq. (9) and substituting Φ_0 and Φ_t from Eqs. (2) and (6), respectively, we get x_t as:

$$x_t = \frac{\frac{1}{\alpha}\sum_{i=1}^{N} T_i y_i}{\alpha Q_x} \tag{8}$$

We rewrite the above equation after dividing and multiplying with T:

$$x_t = y_c \frac{T}{\alpha Q_x} \tag{9}$$

where

$$y_c = \frac{\sum_{i=1}^{N} T_i y_i}{T} \tag{10}$$

y_c $[L]$ represents the elevation of the centroid of the transmissivity field relative to the aquifer base (referred henceforth as "transmissivity centroid elevation (TCE)" for the sake of brevity), which essentially accounts for effects of aquifer stratification. For a given total

transmissivity, different layer arrangements result in different TCE values, and as per Eq. (9), the toe position is linearly correlated to the TCE in a flux-controlled system. Thus, theoretically, by artificially lowering the TCE in a coastal aquifer, SWI can be reduced. This explains the approach suggested by Strack et al. (2016) for reducing SWI by reducing the hydraulic conductivity in the upper part of the aquifer by using a precipitate, which essentially lowers the TCE.

3.3.2 Steady-state Solution for a Head-controlled System

In a head-controlled system, we derive the equations for both the discharge rate and toe position. Assuming that the piezometric head h_f is known at a certain location in Zone 2, at a distance *L* from the coast, we can apply the single density groundwater flow equation for the confined stratified aquifer between the toe and known head location:

$$Q_x = T\left(\frac{h_f - h_t}{L - x_t}\right) \tag{11}$$

Substituting h_t as $H_s\left(1 + \frac{1}{\alpha}\right)$ and x_t from Eq. (9), we get:

$$Q_x = \frac{T}{L}\left(h_f - H_s\left(1 + \frac{1}{\alpha}\right) + \frac{y_c}{\alpha}\right) \tag{12}$$

Eq. (12) presents the solution to directly obtain freshwater discharge based on the coastal and inland boundary heads. It clearly shows that one cannot simply apply Darcy's law between the inland and coastal freshwater heads to evaluate the discharge rate. In fact, we can treat the terms $H_s(1 + 1/\alpha) - y_c/\alpha$ as a corrected coastal head h_s^*, hence,

facilitating the direct application of Darcy's law between the inland and coastal boundary to get the discharge as $Q_x = T\left(h_f - h_s^*\right)/L$.

We can also obtain the toe position as a function of boundary heads by substituting Q_x from Eq. (9) into Eq. (12):

$$x_t = L\frac{\frac{y_c}{\alpha}}{h_f - H_s\left(1+\frac{1}{\alpha}\right)+\frac{y_c}{\alpha}} \tag{13}$$

Therefore, from Eqs. (9), (12) and (13) we can make a remarkable conclusion that the effects of stratification on the discharge and toe positions can be exactly represented by the TCE. T represents the effects of magnitudes of the layer transmissivities and y_c accounts for the effects of the spatial distribution of these magnitudes. This allows us to elegantly analyze seawater intrusion in stratified aquifers with any number of layers.

Another conspicuous observation from Eq. (13) is that even in heterogeneous aquifers the toe position is independent of the total transmissivity in a head-controlled system. This entails that, for given boundary conditions, it is possible to estimate the upper bound of the extent of the seawater intrusion without actually characterizing the hydraulic conductivity distribution, where the upper limit of toe position, x_t^{max}, calculated from the upper limit of y_c i.e. the aquifer depth B, is given as:

$$x_t^{max} = L\frac{\frac{B}{\alpha}}{h_f - H_s\left(1+\frac{1}{\alpha}\right)+\frac{B}{\alpha}} \tag{14}$$

Note that y_c approaches to the center elevation of the top layer (y_N) if $K$of the top layer is significantly large compared to those of other layers. Furthermore, if the top layer is very thin, y_c essentially approaches to B, but can never be exactly equal to B.

In the case of a single-layer aquifer, the TCE is located at $B/2$. For a head-controlled aquifer system, the toe position and discharge can be given as:

$$x_t = L\frac{\frac{B}{2\alpha}}{h_f - H_s\left(1+\frac{1}{\alpha}\right)+\frac{B}{2\alpha}} \tag{15}$$

$$Q_x = \frac{T}{L}\left(h_f - H_s\left(1+\frac{1}{\alpha}\right)+\frac{B}{2\alpha}\right) \tag{16}$$

which are consistent with the solutions provided by Lu et al. (2015) for homogeneous aquifers. Accordingly, in flux-controlled homogeneous aquifers, the toe position is given as:

$$x_t = \frac{B}{2}\frac{T}{\alpha Q_x} \tag{17}$$

3.3.3 Effective Parameters

Eqs. (9), (12) and (13) show that unlike stratified single-density flows, the arithmetic mean of the hydraulic conductivities or the total transmissivity cannot be used as effective parameters for homogenization since the TCE is an additional parameter apart from T determining the toe position and discharge rate in stratified interface flows. If the thickness of the homogenized aquifer is equal to twice the TCE of the original stratified aquifer, we get the same y_c in both stratified and homogeneous cases. Thus, after

performing the domain transformation of changing the aquifer thickness to twice the TCE, i.e., $B_{eff} = 2y_c$, the arithmetic mean of the hydraulic conductivity can be used as the effective parameter, $K_{eff} = T/B_{eff}$, in the stratified interface flow, similar to stratified single-density flow. Such a domain transformation has been used previously to solve the flows in an anisotropic aquifer (Cihan et al., 2014). The proposed effective parameters are applicable to both head- and flux-controlled systems to reproduce both the discharge rate and toe position.

If we have just one variable of interest, e.g., x_t or Q_x, we can avoid domain transformation by defining effective hydraulic conductivity, K_{eff}, in terms of T and y_c. To reproduce the toe position in a flux-controlled system, the effective hydraulic conductivity is obtained by equating the toe position solution for the stratified case, Eq. (9), and the homogeneous case, Eq. (17):

$$K_{eff} = \frac{2Ty_c}{B^2} \tag{18}$$

To reproduce the discharge rate in a head-controlled system, the proposed equivalent hydraulic conductivity is obtained by equating the discharge-rate solution for the stratified, Eq. (12), and the homogeneous, Eq. (16), case:

$$K_{eff} = \frac{T}{B}\left(\frac{\Delta h + y_c/\alpha}{\Delta h + B/2\alpha}\right) \tag{19}$$

where $\Delta h = h_f - h_s^*$. Eq. (13) indicates that the toe position in a head-controlled system is only controlled by the TCE, and independent of the hydraulic conductivity magnitudes.

Therefore, the only way to get the same toe position in a homogenized aquifer as in a stratified aquifer is to use domain transformation, $B_{eff} = 2y_c$, as discussed above.

In a special case where the TCE coincides with the half-thickness of the aquifer, such as layers with an asymmetric distribution of transmissivity, we can just use $K_{eff} = T/B$ to reproduce both the discharge rate and the toe position.

3.3.4 Continuously-varying Hydraulic Conductivity

A coastal aquifer with exponentially decaying hydraulic conductivity ($K(z)$), another deterministic case of heterogeneity, can also be conveniently analyzed using TCE based solutions for Q_x and x_t. $K(z)$ in such cases is often modeled as exponentially decaying because of increasing overburden (Toller and Strack, 2019):

$$K(z) = K_T e^{-\lambda z} \tag{20}$$

where K_T $[L/T]$ is the hydraulic conductivity measured at the top of the aquifer, λ $[L^{-1}]$ is the exponential decay coefficient, and z $[L]$ is the depth measured from the top of the aquifer ($z = B - y$). Total transmissivity $T = \int_0^B K(z)dz$ for the considered $K(z)$ is obtained as:

$$T = K_T \frac{1-e^{-\lambda B}}{\lambda} \tag{21}$$

y_c by definition is evaluated as:

$$y_c = B - \frac{\int_0^B zK(z)dz}{\int_0^B K(z)dz} \tag{22}$$

Using the $K(z)$ model described, y_c is obtained as:

$$y_c = \frac{B}{1-e^{-\lambda B}} - \frac{1}{\lambda} \tag{23}$$

Note that y_c is independent of K_T. Inputting T and y_c from above into derived TCE based toe position and discharge solutions for a head-controlled case, we get:

$$Q_x = \frac{K_T(1-e^{-\lambda B})}{L\lambda}\left(h_f - H_s\left(1+\frac{1}{\alpha}\right) + \frac{1}{\alpha}\left(\frac{B}{1-e^{-\lambda B}} - \frac{1}{\lambda}\right)\right) \tag{24}$$

$$x_t = L\frac{\frac{1}{\alpha}\left(\frac{B}{1-e^{-\lambda B}} - \frac{1}{\lambda}\right)}{h_f - H_s\left(1+\frac{1}{\alpha}\right) + \frac{1}{\alpha}\left(\frac{B}{1-e^{-\lambda B}} - \frac{1}{\lambda}\right)} \tag{25}$$

3.4 Results and Discussion

3.4.1 Effective Parameters

To analyze the goodness of effective parameters proposed in section 3.3.3, we consider a stratified version of the experimental problem described in Goswami and Clement (2007), which is under the confined condition with following parameter values: B = 25 cm, L = 53 cm, H_s = 25.5 cm, longitudinal dispersivity α_L = 0.1 cm and transverse dispersivity $\alpha_T = \alpha_L/10$. Five layer stratification is considered with the thickness of each layer as 5 cm and hydraulic conductivities from the bottom to top as 130 cm/min, 100 cm/min, 70 cm/min, 50 cm/min and 20 cm/min, respectively. The resulting total transmissivity and TCE are 1850 cm^2/min and 8.85 cm, respectively. All the numerical

simulations are performed using SEAWAT, a MODFLOW/MT3DMS-based computer program designed to simulate three-dimensional variable-density flow (Langevin et al., 2003). The spatial discretization is determined according to the criteria based on the Grid Peclet number [-] (Voss and Souza, 1987).

$$Pe = \frac{\nu\,\Delta x}{D_m + \alpha_L \nu} \approx \frac{\Delta x}{\alpha_L} \leq 4 \tag{26}$$

where ν [L/T] is the average pore velocity, Δx [L] is the grid spacing, D_m [L^2/T] is the molecular diffusion coefficient, and α_L [L] is the longitudinal dispersion coefficient.

To reproduce x_t and homogenize a flux-controlled stratified with a constant discharge rate of 20 cm^2/min, effective K_{eff} calculated from Eq. (18) is used. To reproduce Q_x and homogenize a head-controlled stratified case with a constant head of 26.5 cm, effective K_{eff} calculated from Eq. (19) is used. To reproduce x_t, and homogenize the mentioned head-controlled case, $B_{eff} = 2y_c$ is used. The results summarized in Table 2 shows the goodness of the proposed effective parameters.

Table 2 - Effective Parameters for Different Cases

Case	Variable of interest	Effective parameter	Variable value	
			Stratified aquifer	Homogenized aquifer
Flux-controlled	x_t	K_{eff} = 52.39 cm/min	16.11 cm	15.91 cm
Head-controlled	Q_x	K_{eff} = 64.00 cm/min	20.38 cm^2/min	20.38 cm^2/min
Head-controlled	x_t	B_{eff} = 17.70 cm	16.11 cm	16.59 cm

3.4.2 Effects of Stratification in a Head-controlled Multiple-layer System

To analyze the effects of layer arrangement and to identify bounding cases, we consider the problem described in the previous section. There are a total of 120 possible cases of the layer placement, and associated y_c values for the five-layer coastal aquifer.

In a head-controlled system, when the TCE is half the aquifer thickness ($y_c = B/2$), the discharge and toe position in the stratified case are the same as those in a homogenized case for a given total transmissivity. For the considered stratified aquifer with the layer properties described in Table 3, there are two such layer arrangements, [L1 L5 L4 L3 L2] and [L2 L3 L4 L5 L1], referred as S1 and S2, respectively, in which y_c is to equal 12.5 cm ($B/2$). Figure 3 shows numerically simulated velocity fields and seawater-freshwater interfaces in S1, S2 and the homogeneous case. Despite different velocity fields, the resulting discharge values and toe positions in stratified cases S1 and S2 are almost the same as in the homogeneous case with K equal to 74 cm/min, because of the same TCE.

Table 3 - Layer Names, Thickness, and Hydraulic Conductivity Values

Layers	L1	L2	L3	L4	L5
H (cm)	5	5	5	5	5
K (cm/min)	20	50	70	100	130

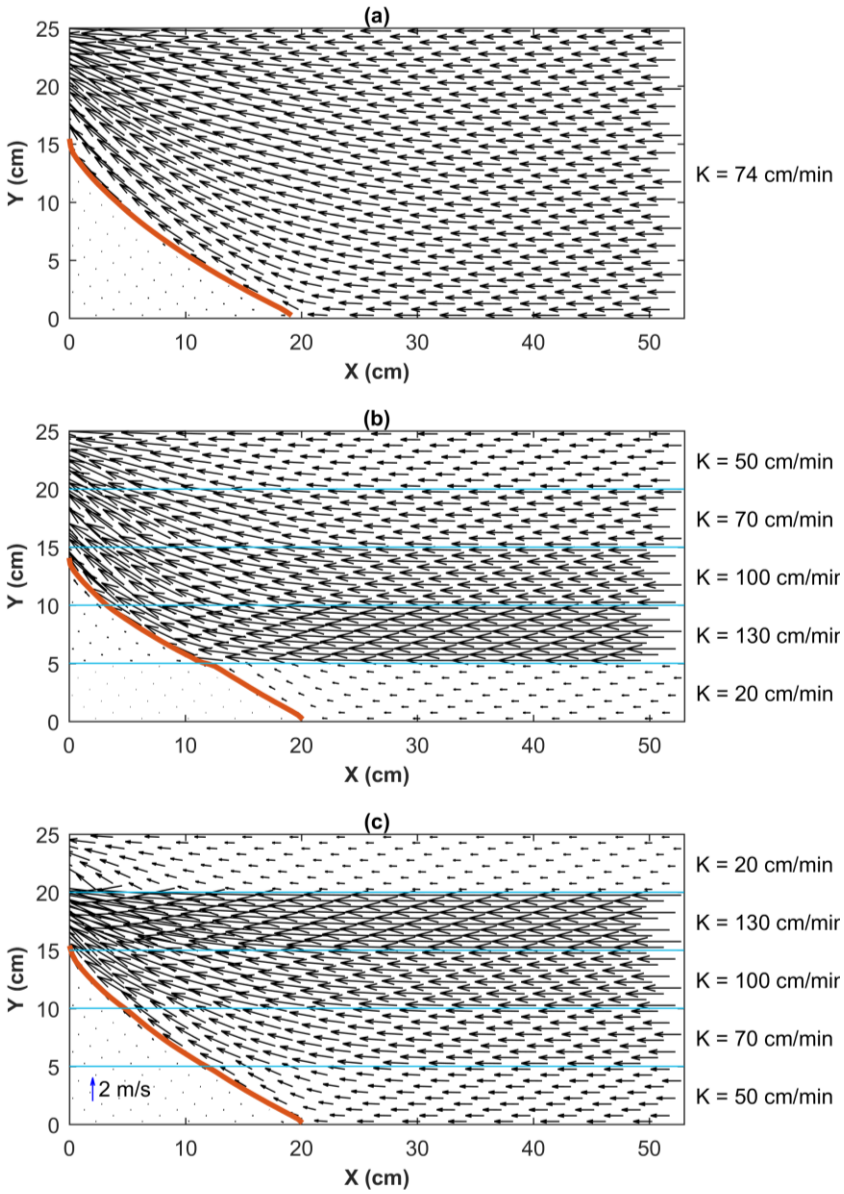

Figure 3 - Comparison of velocity fields: (a) homogeneous case, y_c = 12.50 cm, (b) stratified case S1, y_c = 12.50 cm and, (c) stratified case S2, y_c = 12.50 cm; the redline represents the 50% isochlor

When the TCE in the stratified case is higher than $B/2$, we get a greater discharge and a longer toe length (distance between the interface toe and the coastal boundary) compared to the homogenous case, and vice-versa. The discharge and toe position values in 120 scenarios with different layer arrangements are bounded by two extreme cases in which the TCE is lowest and highest, which occur when the layers are arranged in a descending and ascending order of the hydraulic conductivity, from bottom to top, respectively. This results conveniently explain the observation in Lu et al. (2013a).

Figure 4 shows the interfaces in the homogeneous case and selected 13 cases having layer arrangements with fairly spaced y_c including the two bounding cases, out of possible 120 layer arrangements. We refer to cases with the lowest and highest y_c value as E1 and E2, respectively.

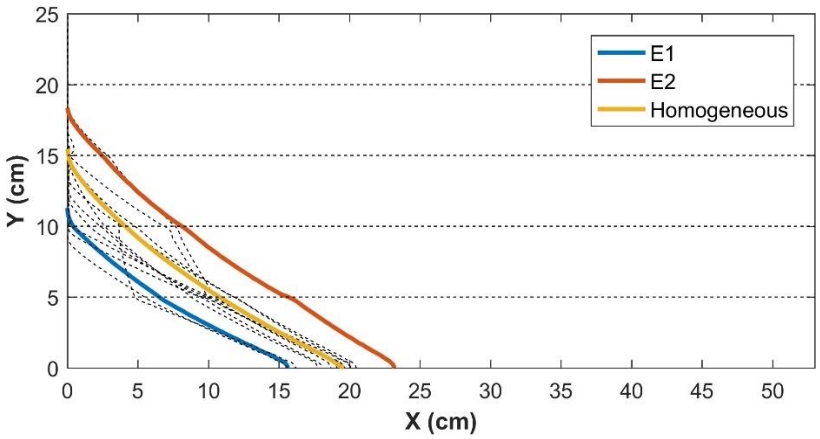

Figure 4 - Seawater-freshwater interfaces for 13 cases with fairly spaced y_c values, including the two bounding cases, and the homogenous case. E1 and E2 represent the cases with a monotonically descending and ascending order of hydraulic conductivities from bottom

In Figure 5(a), Q_x is plotted against y_c for all the cases in Figure 4, ascertaining the linear relation between the Q_x and y_c with 2 bounding cases. A nearly perfect match between numerical and analytical discharge values is because the comprehensive potential (Strack and Ausk, 2015) can be computed accurately along the two vertical parallel planes (in this case, coastal boundary and inland boundary). However, the equation for the toe position is approximate because of the adoption of the Dupuit-Forchheimer approximation. Figure 5(b) shows the toe positions evaluated by numerical models and the analytical solutions with a correction factor (Lu and Werner, 2013; Pool and Carrera, 2011) to avoid the overestimation of the toe-position due to ignoring dispersive effects (interface assumption). The match between analytical and numerical toe-positions (Figure 5(b)) is obtained not as good as discharge but is still accurate enough for practical purposes given the simplicity of the solution.

We also numerically demonstrate the independence of the toe-position to the total transmissivity in a head-controlled stratified aquifer. We double the hydraulic conductivities of all layers for a particular layer arrangement, thus doubling the total transmissivity but keeping the TCE the same. The toe position in the doubled-conductivity case is found to be unchanged, ascertaining that the toe position does not depend on the magnitude of hydraulic conductivity but depends on the spatial distribution of the conductivity values in a head-controlled system.

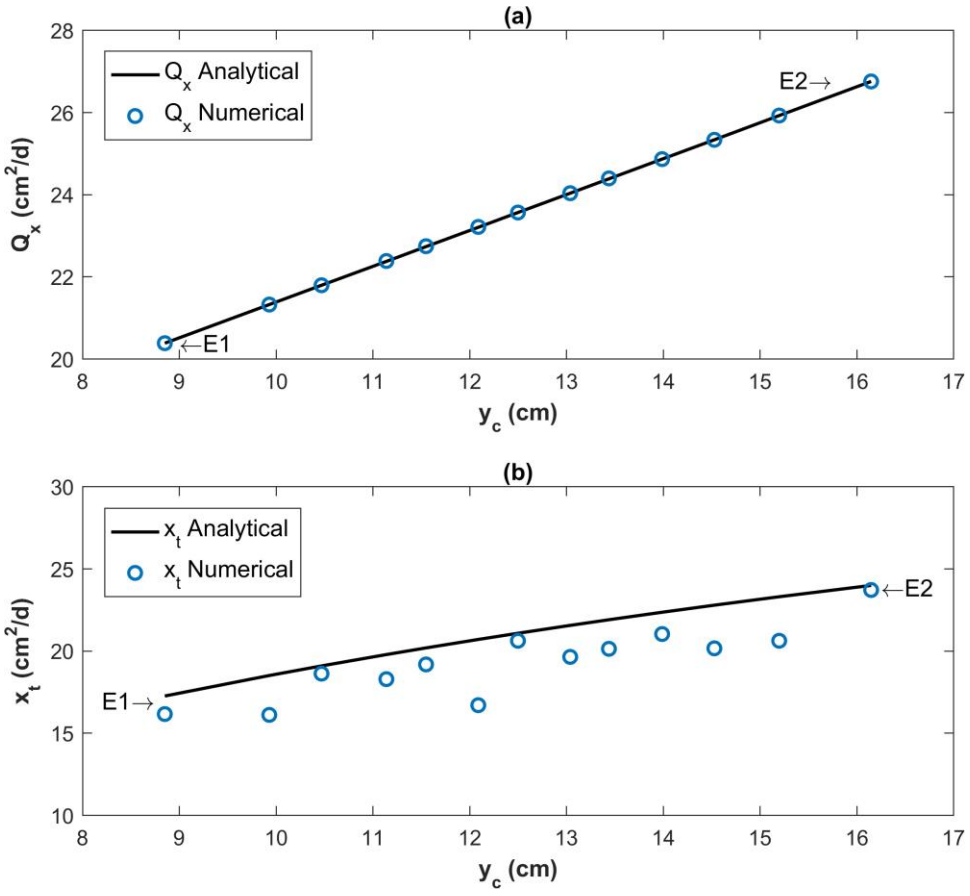

Figure 5 - Theoretical and numerical – (a) discharge values; and (b) toe-positions, for 13 stratified cases presented in Figure 4

3.4.3 Implication on Preferential Flow Paths

An important implication of the stratification effects discussed in the previous section is preferential flow paths in coastal aquifers. If we conceptualize the preferential flow paths as a layer with high hydraulic conductivities (K_H) embedded in a homogeneous aquifer with low hydraulic conductivities (K_L), the elevation or the position of the preferential flow layer determines the centroid of the transmissivity field, thereby controls the interface toe position in a head-controlled coastal aquifer system.

We consider a specific numerical case with field-scale parameters (summarized in Table 4) and a 2 m thick preferential flow layer. Figure 6(a) shows a symmetric system, i.e., the preferential flow layer is at the center of the aquifer, with three cases of hydraulic conductivity contrasts. The interface-toe positions are almost the same in three cases because the TCE does not change with the hydraulic conductivity contrast in a symmetric system. For a non-symmetric system (i.e., the preferential flow layer located at elevations other than the center of the aquifer), the TCE will be close to the center of the preferential flow layer, and it will approach the center with the increasing hydraulic conductivity contrast (Figure 6(b)). That is, the elevation of the fast flow layer is the key, while the influence of the hydraulic conductivity contrast is limited. It should be noted that the groundwater discharge rate changes with the hydraulic conductivity contrast because it is a function of total transmissivity.

Table 4 - Aquifer Parameters Used in the Numerical Experiment with a Preferential Flow Path

Parameters	**Unit**	**Value**
Domain length ($\boldsymbol{L}$)	m	100
Domain thickness ($\boldsymbol{B}$)	m	12
Longitudinal dispersivity ($\boldsymbol{\alpha_L}$)	m	0.1
Transverse dispersivity ($\boldsymbol{\alpha_T}$)	m	0.01
Effective porosity ($\boldsymbol{n}$)	-	0.3
Constant seawater level ($\boldsymbol{H_s}$)	m	12
Constant freshwater level ($\boldsymbol{h_f}$)	m	12.75
Seawater density ($\boldsymbol{\rho_s}$)	kg/m^3	1025
Freshwater density ($\boldsymbol{\rho_f}$)	kg/m^3	1000
Salt concentration in seawater ($\boldsymbol{C_s}$)	kg/m^3	35

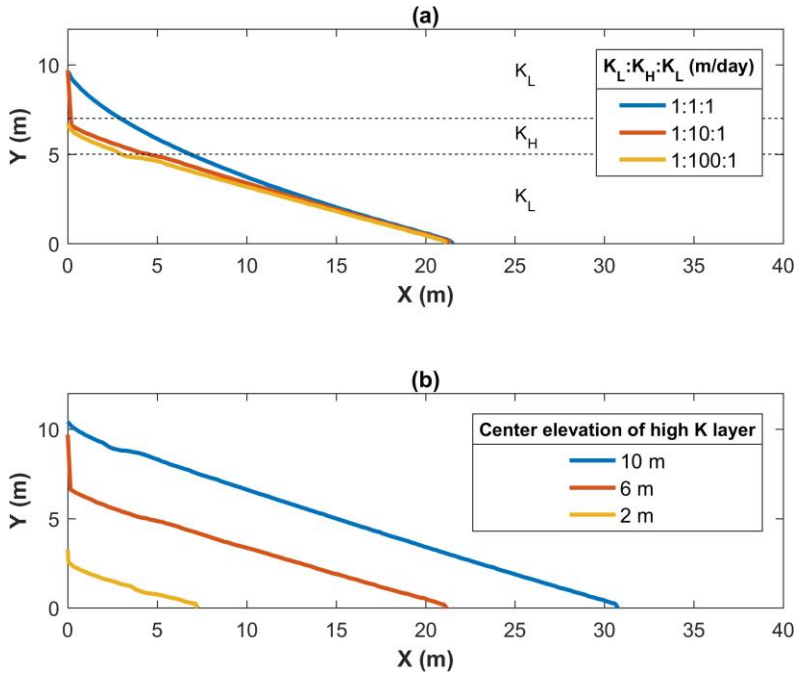

Figure 6 - Seawater-freshwater interface in a preferential flow path setting with – (a) different hydraulic conductivity contrasts; (b) different positions of the preferential flow layer

3.4.4 Sensitivity of Q_x and x_t to the decay coefficient of exponentially decaying K

Hydraulic conductivity decay coefficient λ controls the y_c, thus controls the Q_x and x_t (Eqs. 24) and 25). The relation of Q_x and x_t with λ is plotted in Figure 7(a) and (b), respectively. With the increasing decay coefficient, groundwater flow decreases as a result of a decrease in the total transmissivity. Since, the toe-position is independent of the total transmissivity in head-controlled aquifers, a higher value of the decay coefficient results in a higher extent of seawater intrusion. This is because of the rise in TCE as a result of a steep decrease in K with the depth for higher λ values.

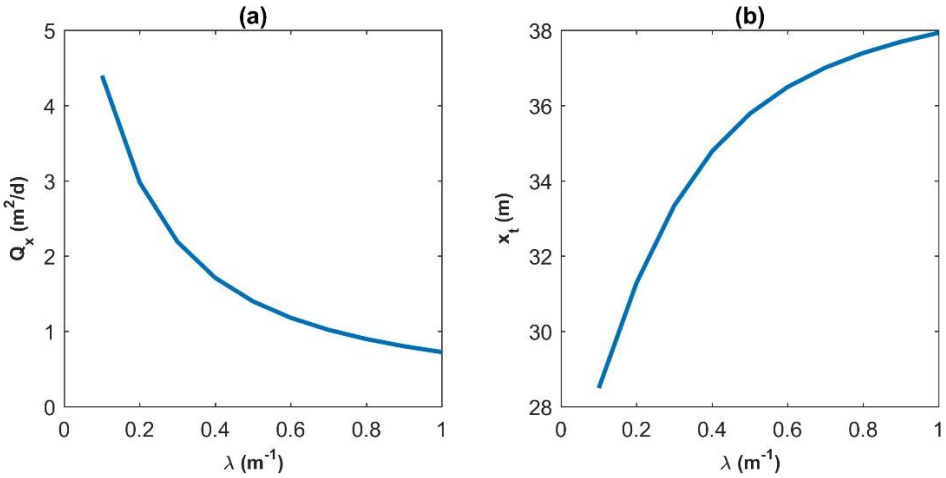

Figure 7 - Variation of: (a) Q_x and (b) x_t with respect to decay coefficient λ

3.5 Summary and Conclusions

We provide analytical solutions based on Strack and Ausk (2015) in a simple form to analyze the effect of aquifer stratification on the groundwater discharge rate and interface toe position in coastal aquifers. Such solutions are verified by numerical simulations. The current analysis is limited to steady, two-dimensional, confined groundwater flow. With the interface approximation, we did not consider the effects of stratification on mixing between freshwater and seawater (Lu et al., 2013a). Major results and conclusions of this study include:

(1) We present analytical solutions for the interface toe position in both flux-controlled and head-controlled systems, as well as the freshwater discharge rate in a head-controlled system, for the first time in terms of the transmissivity centroid elevation (TCE). This provides new insights to explain the effect of stratification observed in previous experimental and numerical studies.

(2) Effective parameters are provided for the first time to homogenize a stratified coastal aquifer by reproducing the groundwater discharge and toe position. The proposed effective parameters are functions of the TCE.

(3) Given the same transmissivity value, different transmissivity centroid elevations, representing different layers of arrangements, result in different discharge rates and toe positions. The higher the centroid elevation (due to high transmissivity layers at high elevations), the greater the discharge rate and the longer the toe position. Thus, given a deterministic transmissivity distribution, the stratified aquifers with ascending and descending transmissivities from aquifer-bottom to -top are two bounding cases for the discharge rate and toe position.

(4) The stratification effects are extended to the conceptualization of a preferential flow layer embedded in low hydraulic conductivity aquifers. We found that the interface toe position is mainly determined by the elevation of the preferential layer but weakly influenced by the hydraulic conductivity contrast.

CHAPTER 4. EXPLICIT ANALYTICAL INTERFACE PROFILE IN STRATIFIED COASTAL AQUIFERS

4.1 Introduction

Delineation of the seawater-freshwater interface is one of the critical tasks for investigating coastal hydrogeological systems. Many studies have assumed the existence of an interface separating freshwater and seawater in coastal aquifers and provided analytical solutions for the interface profile under different hydrogeological settings, including the interface in steady-homogeneous aquifers (Bakker, 2006; Bear, 1972; Strack, 1976) and transient-homogeneous aquifers (Bear, 1972; Bear and Dagan, 1964; Bear et al., 1985; Isaacs and Hunt, 1986; Vappicha and Nagaraja, 1976), and the stochastic solution for steady random hydraulic conductivity fields (Dagan and Zeitoun, 1998; Naji et al., 1998). In coastal areas, heterogeneity often exhibits a pattern of horizontal layering or stratification, as shown in many field investigations of sedimentary aquifers (Dagan and Zeitoun, 1998). Lu et al. (2013a) demonstrated through laboratory experiments and numerical simulations in a three-layer aquifer that the toe position and shape of the mixing zone vary significantly with different layer placements even with the same hydraulic conductivities. Collins and Gelhar (1971) and Mualem and Bear (1974) provided analyses to predict the interface shape in a homogeneous system divided into two layers by a semi-pervious layer. For a more general layered case, Rumer and Shiau (1968) provided the first analytical solution, which, however, was proved to be erroneous by Strack (2016) as it did not satisfy the flow continuity. Recently, Strack and Ausk (2015) provided an analytical solution for the interface profile for three-dimensional flow, using the Dupuit-Forchheimer

approximation based on the comprehensive discharge potential in layered coastal aquifers. Their solution included a series-summation of combinations of layer properties i.e. hydraulic conductivity, elevation, and thickness of each layer. We present a concise equation with new parameters which improves our understanding of the stratification effects on the interface and allows us to make more general conclusions. Strack et al. (2016) proposed an artificial reduction of the hydraulic conductivity by injecting a precipitate in the upper part of the coastal aquifer as a measure to reduce seawater intrusion. Rathore et al. (2018b) explained the effectiveness of this strategy through their Transmissivity Centroid Elevation (TCE) concept and commented that reducing the conductivity of the top part of the aquifer essentially lowers the TCE, thus reducing the SWI. Werner and Simmons (2009) studied the different impacts of sea-level rise on SWI due to two different landward-boundary types, namely constant-head boundary and constant-flux boundary, and suggested that flux is the fundamental parameter controlling SWI, and even in constant-head boundary case, resulting flux would be the key. Chang et al. (2011) and Chang and Clement (2012) confirmed the sensitivity of SWI in response to sea-level rise to the boundary type.

In this study, we derive a more concise equation for the interface profile taking advantage of the restriction to flow in the vertical plane in stratified-coastal aquifers by using Dupuit-Forchheimer approximation at the outset. The proposed new parameters make it convenient to analyze the effects of stratification on the interface profile. We also prove mathematically that the proposed equation represents the same interface solution as obtained from the vertically integrated flow solution by Strack and Ausk (2015). We further provide a new interpretation of the discharge potential at the coast by comparing

our equation with the vertically integrated flow solution (Strack and Ausk, 2015). We study and explain the difference in interface profile in aquifer configurations with hydraulic-conductivity contrasts in two sets of boundary conditions, namely constant-head and constant-flux boundary. We then discuss the implications of the insights obtained from the new parameters on the uncertainties in the estimation of the SWI extent for random K fields.

4.2 Conceptual Model

We consider a stationary interface in a two-dimensional confined and unconfined aquifer with horizontal stratification in the hydraulic conductivity, as shown in Figure 8. The seaward freshwater discharge Q_x $[L^2/T]$ is assumed to be in a vertical plane with no recharge or pumping (uniform flow). In the case of pumping, we need to perform 3D analysis as the vertical slice of the aquifer if not a representative of the flow field which varies along the coastline. However, based on the governing equation (Eq. 27), we can expect a steeper interface on the landward side of the pumping well and gradual slop of the interface on the coastal side. Uniform recharge can be modeled through a linearly increasing discharge in the flow direction in the region of recharge, which will be an additional factor (one factor is decreasing the thickness of freshwater flow domain) causing an increase in steepness of the interface in the flow direction. However, the elegant explicit solution is not possible in either case. We assume a constant head in the vertical plane by adopting Dupuit (Dupuit, 1863) and Forchheimer (Forchheimer, 1886) approximation. The aquifer is underlain by an impermeable layer and bounded by vertical boundaries at the inland and coastal ends. The flow domain can be divided into two zones: an interface zone consisting of both freshwater and seawater (Zone 1) and zone consisting of only freshwater

and no interface (Zone 2). Let the origin be at the point where the aquifer base meets coastline, the x axis along the top of the underlying impervious layer pointing towards inland, and the y axis along the vertical coastline pointing upwards. L $[L]$, H_s $[L]$ and x_t $[L]$ represent the distance of the inland boundary from the coastal boundary, seawater head at the coastal boundary, and interface-toe position, respectively. The inland boundary can be a constant total flux Q_x $[L^2/T]$ (in a flux-controlled system) or constant head h_f $[L]$ (in a head-controlled system). Note that the total boundary flux redistributes in proportion to transmissivities in each layer. The interface profile is described by ζ $[L]$, which represents the y coordinate of the interface as a function of x.

In a confined aquifer, the layers are indexed from 1 to N from bottom to top, where N is the total number of layers. For a particular ith layer, the thickness, center elevation, base elevation, and hydraulic conductivity are represented by b_i $[L]$, y_i $[L]$, d_i $[L]$ and K_i $[L/T]$, respectively. Note that the elevation is with respect to the base of the aquifer unless mentioned otherwise. h $[L]$ is the freshwater head above sea level. B $[L]$ and T $[L^2/T]$ represent the total aquifer thickness and transmissivity, respectively.

In an unconfined aquifer, N is the index for the highest layer below the sea level. It is assumed that the hydraulic conductivity of the part of the aquifer containing the water table is constant (denoted by K_{N+1}), i.e. the water table is contained within a single layer, which is a reasonable assumption given the elevation of the water above the sea level is fairly small relative to the layer thicknesses. For most practical cases, we can expect $K_N = K_{N+1}$. The h $[L]$ is the water-table elevation above the sea level.

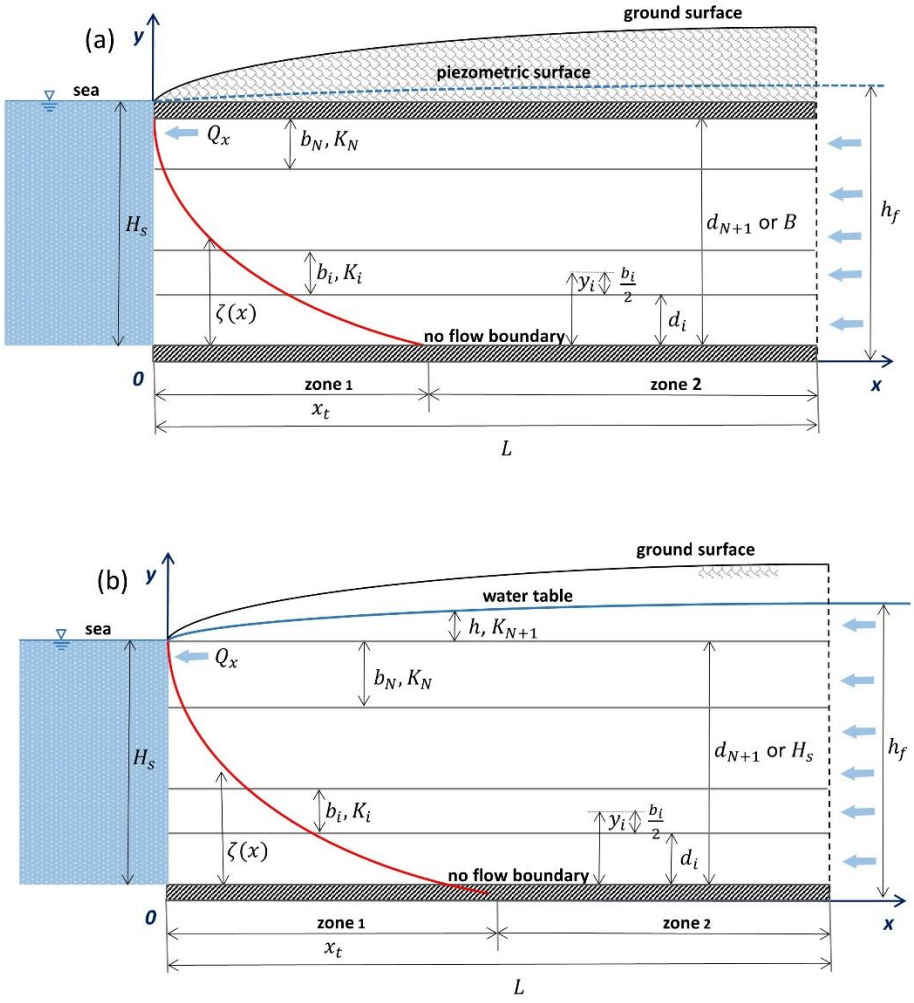

Figure 8 - Conceptual models for a stratified - (a) confined aquifer and (b) unconfined aquifer

4.3 Theory

4.3.1 Confined Aquifer

The freshwater flow rate per unit width of the aquifer at any cross-section can be given by Darcy's law after adopting Dupuit-Forchheimer approximation as:

$$Q_x = -T_\zeta \frac{dh}{dx} \tag{27}$$

T_ζ $[L^2/T]$ is the total transmissivity of the flow domain above the interface. We evaluate h using the Ghyben-Herzberg relation (Badon Ghyben, 1888):

$$h = \frac{H_s - \zeta}{\alpha} \tag{28}$$

where α [.] is the ratio of the freshwater density to the density difference between seawater and freshwater. Differentiating the above equation with respect to x, we get:

$$\frac{dh}{dx} = -\frac{d\zeta}{\alpha dx} \tag{29}$$

Substituting $\frac{dh}{dx}$ from Eq. (29) into (27), we get the discharge as a function of the slope of the interface as:

$$Q_x = \frac{T_\zeta}{\alpha}\frac{d\zeta}{dx} \tag{30}$$

T_ζ, a function of ζ, is given as:

$$T_\zeta = \int_\zeta^B K(y)\,dy = K_m(d_{m+1} - \zeta) + \sum_{m+1}^{N} T_j \tag{31}$$

where m denotes the index of the layer containing the interface at any aquifer cross-section.

After substituting T_ζ in Eq. (30) and rearranging, we get:

$$\frac{d\zeta}{dx} = \frac{Q_x \alpha}{K_m(d_{m+1} - \zeta) + \sum_{m+1}^{N} T_j} \tag{32}$$

It should be noted that the index m in the above equation is also a function of ζ. For a particular i^{th} layer, x can be evaluated by integration:

$$\int dx = \frac{1}{\alpha Q_x} \int \left(K_i(d_{i+1} - \zeta) + \sum_{i+1}^{N} T_j\right) d\zeta \tag{33}$$

which results in:

$$x = \frac{\zeta}{\alpha Q_x}\left[K_i\left(d_{i+1} - \frac{\zeta}{2}\right) + T_{Ui}\right] + C_i \tag{34}$$

where i is the layer index in which ζ lies. T_{Ui} $(=\sum_{i+1}^{N} T_j)$ $[L^2/T]$ represents the total transmissivity of the flow domain above the i^{th} layer. To evaluate C_i, we adopt an assumption which was also used by Bear (1972) to evaluate the interface profile in a homogenous aquifer—the interface meets the top of the aquifer at the coastal boundary, $x = 0, \zeta = B$. We apply this boundary condition in Eq. (34) for the N^{th} layer, to get:

$$C_N = \frac{K_N B^2}{2(-Q_x)\alpha} \tag{35}$$

We find the relation between consecutive $C_i's$ by satisfying the continuity of the interface across the layers. We evaluate x at $\zeta = d_i$ using Eq. (34) in both i^{th} and $(i-1)^{th}$ layers:

$$x = \frac{d_i}{\alpha Q_x}\left[K_i\left(d_{i+1} - \frac{d_i}{2}\right) + T_{Ui}\right] + C_i = \frac{d_i}{\alpha Q_x}\left[K_{i-1}\left(d_i - \frac{d_i}{2}\right) + T_{U(i-1)}\right] + C_{i-1} \tag{36}$$

After rearranging the above equation, we get:

$$C_i - C_{i-1} = \frac{d_i^2}{2\alpha(-Q_x)}(K_i - K_{i-1}) \tag{37}$$

From Eqs. (35) and (37), we derive the equation for a general C_i as (see Appendix A):

$$C_i = \frac{1}{\alpha(-Q_x)}\left(\sum_{i+1}^{N} T_j\, y_j + \frac{K_i d_{i+1}^2}{2}\right) \tag{38}$$

By substituting C_i from the above equation into Eq. (34) and rearranging the equation, we thus obtain the equation for the interface profile in a fully explicit form as:

$$x = \frac{1}{\alpha(-Q_x)}\left[T_{Ui}(y_{ci} - \zeta) + \frac{K_i}{2}(d_{i+1} - \zeta)^2\right] \tag{39}$$

where y_{ci} $[L]$ is the elevation of the centroid of the transmissivity (referred henceforth as "Transmissivity Centroid Elevation" or "TCE") in the flow domain above the i^{th} layer, computed as:

$$y_{ci} = \frac{\sum_{i+1}^{N} T_j y_j}{T_{Ui}} \tag{40}$$

To extend the above solution to the continuously varying hydraulic conductivity field, we conceptualize it by a large number of very thin layers. Thus, the term $\frac{K_i}{2}(d_{i+1}-\zeta)^2$ approaches zero and the term $T_{Ui}(y_{ci}-\zeta)$ can be replaced by $T_\zeta(y_{c\zeta}-\zeta)$, where T_ζ and $y_{c\zeta}$ represents the transmissivity and TCE, respectively, for the aquifer above ζ (freshwater flow domain):

$$x=\frac{1}{\alpha(-Q_x)}\left[T_\zeta(y_{c\zeta}-\zeta)\right] \tag{41}$$

$$T_\zeta=\int_\zeta^B K(y)dy,\ y_{c\zeta}=\frac{\int_\zeta^B K(y)dy}{T_\zeta} \tag{42}$$

Eqs. (39) and (41) reveal the new parameters, namely, local transmissivity (T_ζ) and local TCE ($y_{c\zeta}$) (henceforth collectively referred to as "local transmissivity parameters") governing the horizontal extent of the seawater intrusion. In the case of a homogeneous aquifer with hydraulic conductivity K, T_ζ and $y_{c\zeta}$ can be evaluated as $K(B-\zeta)$ and $(B+\zeta)/2$, respectively, which when substituted in Eq. (41), results in the interface profile as:

$$x=\frac{1}{2\alpha(-Q_x)}(B^2-\zeta^2) \tag{43}$$

which is well known Dupuit parabola (Bear, 1979).

In many SWI studies like the transience of SWI (Chang and Clement, 2012; Lu and Werner, 2013; Rathore et al., 2018a; Watson et al., 2010), we are more concerned about the toe position than the whole interface profile. We get the equation of the toe position by putting $\zeta=0$ in the interface solution (Eqs. 39 and 41).

$$x_t = \frac{Ty_c}{\alpha(-Q_x)} \tag{44}$$

where y_c is the TCE of the whole flow domain computed as:

$$y_c = \frac{\sum_1^N T_j y_j}{T} \tag{45}$$

The toe position (Eq. 44) is exactly the same as that reported by Rathore et al. (2018b) (previous chapter), derived using the comprehensive discharge potential theory (Strack and Ausk, 2015). We derive the interface-profile equation for the head-controlled system by substituting the solution for Q_x given by Rathore et al. (2018b) in terms of the TCE for a stratified interface flow.

$$Q_x = -\frac{T}{L}\left(h_f - h_s^*\right) \tag{46}$$

where h_s^* is the corrected coastal head given as $h_s^* = H_s(1 + 1/\alpha) - y_c/\alpha$, and y_c represents the TCE of the aquifer. Interface solution for the head-controlled system, therefore, is given as:

$$x = \frac{L}{\alpha T(h_f - h_s^*)}\left[T_{Ui}(y_{ci} - \zeta) + \frac{K_i}{2}(d_{i+1} - \zeta)^2\right] \tag{47}$$

4.3.2 Unconfined Aquifer

Using a similar method, we derive an explicit solution for the interface profile in the unconfined coastal aquifer. T_U for the unconfined aquifer is expressed as:

$$T_U = \int_{\zeta}^{H_s+h} K(y)\, dy = K_m(d_{m+1} - \zeta) + \sum_{m+1}^{N} T_j + K_{N+1}h \tag{48}$$

$h\ [L]$ in this case represents the water table elevation above the sea level, which can be approximated using the Ghyben-Herzberg approximation (Badon Ghyben, 1888) as $\frac{H_s-\zeta}{\alpha}$. After substituting T_U in Eq. (30), we get:

$$x\frac{d\zeta}{dx} = \frac{Q_x\alpha}{K_m(d_{m+1}-\zeta)+\sum_{m+1}^{N} T_j+K_{N+1}\frac{H_s-\zeta}{\alpha}} \tag{49}$$

For a particular i^{th} layer x can be evaluated by integration:

$$\int dx = \frac{1}{\alpha Q_x}\int \left(K_i(d_{i+1} - \zeta) + \sum_{i+1}^{N} T_j + K_{N+1}\frac{H_s-\zeta}{\alpha}\right)\, d\zeta \tag{50}$$

resulting in:

$$x = \frac{\zeta}{\alpha Q_x}\left[K_i\left(d_{i+1} - \frac{\zeta}{2}\right) - \frac{K_{N+1}\zeta}{2\alpha} + \frac{K_{N+1}H_s}{\alpha} + T_{Ui}\right] + C_i \tag{51}$$

T_{Ui} in the case of the unconfined aquifer is the total transmissivity of the part of the aquifer between the layer containing the interface and the sea-level; computed as $T_{Ui} = \sum_{i+1}^{N} T_j$. The integration constant C_i for the N^{th} layer can be found using the boundary conditions $\zeta = H_s$ at $x = 0$, yielding:

$$C_N = \frac{H_s^2}{2(-Q_x)\alpha}\left(K_N + \frac{K_{N+1}}{\alpha}\right) \tag{52}$$

To evaluate the general expression for C_i, a relation between the consecutive $C_i's$ is obtained by satisfying the continuity of the interface elevation across the layers; equating x at $\zeta = d_i$ in the interface solution for both i^{th} and $(i-1)^{th}$ layers:

$$x = \frac{d_i}{\alpha Q_x}\left[K_i\left(d_{i+1} - \frac{d_i}{2}\right) - \frac{K_{N+1}d_i}{2\alpha} + \frac{K_{N+1}H_s}{\alpha} + T_{Ui}\right] + C_i = \frac{d_i}{\alpha Q_x}\left[K_{i-1}\left(d_i - \frac{d_i}{2}\right) - \frac{K_{N+1}d_i}{2\alpha} + \frac{K_{N+1}H_s}{\alpha} + T_{Ui-1}\right] + C_{i-1} \tag{53}$$

Rearranging the above equation results in:

$$C_i - C_{i-1} = \frac{d_i^2}{2\alpha(-Q_x)}(K_i - K_{i-1}) \tag{54}$$

Using the relation between C_i, C_{i-1} and C_N, we derive an equation for a general C_i similar to the confined case:

$$C_i = \frac{1}{\alpha(-Q_x)}\left(\sum_{i+1}^{N} T_j\, y_j + \frac{K_i d_{i+1}^2}{2} + \frac{K_{N+1}H_s^2}{2\alpha}\right) \tag{55}$$

We substitute C_i into the interface-profile equation in a fully explicit form:

$$x = \frac{1}{\alpha(-Q_x)}\left[T_{Ui}(y_{ci} - \zeta) + \frac{K_i}{2}(d_{i+1} - \zeta)^2 + \frac{K_{N+1}}{2\alpha}(\zeta - H_s)^2\right] \tag{56}$$

where $y_{ci}\,[L]$ is the TCE for the flow domain between the ith layer and the sea-level computed using the same equation as in the confined case.

Rathore et al. (2018b) discovered that TCE is the key parameter accounting for the stratification effects on SWI in coastal aquifers, and provided solutions for the toe-position

and freshwater discharge in terms of the TCE for the confined aquifers. Using the derived interface profile in Eq. (56) we can easily extend such solutions to the unconfined aquifers which were not provided previously. By putting $\zeta = 0$, we get x_t as:

$$x_t = \frac{T}{(-Q_x)\alpha}\left[y_c + \frac{K_{N+1}H_s^2}{2\alpha T}\right] \tag{57}$$

where y_c is the TCE of the flow domain below sea-level. The solution for the discharge is provided in Eq. (58), and the derivation is provided in Appendix B for the sake of brevity. The first term of the solution is the same as that for the confined aquifer, which here represents the discharge in the aquifer below the sea-level, and the second term represents the discharge in the flow-domain above the sea-level.

$$Q_x = -\frac{T}{L}\left[h_f - H_s\left(1 + \frac{1}{\alpha}\right) + \frac{y_c}{\alpha}\right] - \frac{K_{N+1}}{2L}\left(h_f - H_s\right)^2 \tag{58}$$

It is important to note here that the solutions for the interface profile, toe position and discharge derived for the unconfined aquifer (Eqs. 56-58) can also be presented as general solutions applicable to both confined and unconfined cases. For the impermeable confining bed in confined aquifers, setting the K values of the top layer to zero in Eqs. (56)-(58) results in the solutions for confined cases.

These equations reveal a new approach to analyzing stratification effects in coastal aquifers, with the discovery of the centroid of the transmissivity field and the transmissivity of the region containing freshwater flow (above the seawater wedge) also referred as local transmissivity parameters as key parameters controlling the interface profile. At the interface toe, local TCE is the same as the TCE for the whole depth, which allows us to

directly compute exact freshwater discharge and approximate toe position (Rathore et al., 2018b). TCE based approach provides a better understanding of stratification effects with much fewer parameters for a large number of layers.

In Appendix C, starting from Strack's solution (Strack and Ausk, 2015) for the interface elevation which is based on the potential theory and Dupuit approximation, we arrive at our equation. We thus showed that our concise equation represents the same solution as Strack's but restricted to flow in the vertical plane as opposed to the three-dimensional flow considered by Strack, and not applicable to a vertical coastline with seepage and outflow faces taken into account. To our surprise, the interface elevation in the case with a seepage and outflow face at the coastal boundary as consider by Strack and Ausk, 2015 turns out to be the same in the case where we assume water table, interface coinciding with the coastline.

4.4 Comparison with Numerical Results

In this section, we provide a comparison of our solution with numerically obtained solutions. Pool et al. (2015) investigated the overestimation of the penetration of the seawater front in sharp interface solutions due to implicit static seawater assumption. To extend the solution of a sharp interface to the case with mixing zone, they proposed empirical dispersion factor to be multiplied to density factor, which was later updated by Lu and Werner (2013) as $\alpha' = \alpha/\left[1 - (\alpha_T/B)^{1/4}\right]$, where α, B and α_T are density ratio, aquifer depth and transverse dispersivity, respectively. We adopt the factor by Lu and Werner (2013) for this comparison.

We present a case of ten-layer confined aquifer with 50 m thickness and layer properties as described in Table 5. Seawater head at the coastal boundary is 50 m and the freshwater discharge at the inland boundary is 5 m^3/d. The effective porosity, longitudinal and transverse dispersivities are 0.30, 0.1 and 0.01 respectively Seawater and freshwater densities are 1025 kg/m3 and 1000 kg/m3 respectively. The numerical simulations are performed using SEAWAT, a MODFLOW/MT3DMS-based computer program designed to simulate three-dimensional variable-density flow (Langevin et al., 2003). The spatial discretization is determined according to the criteria based on the Grid Peclet number [-] (Voss and Souza, 1987). Figure 9 shows good agreement between the analytical sharper interface and the numerical mixing zone.

Table 5 - Aquifer layer properties for comparison with numerical results

Layer No. (Bottom to Top)	Layer Thickness (m)	Hydraulic Conductivity (m/d)
1	4	70
2	5	30
3	4	50
4	5	100
5	5	30
6	10	10
7	5	50
8	2	100
9	5	30
10	5	10

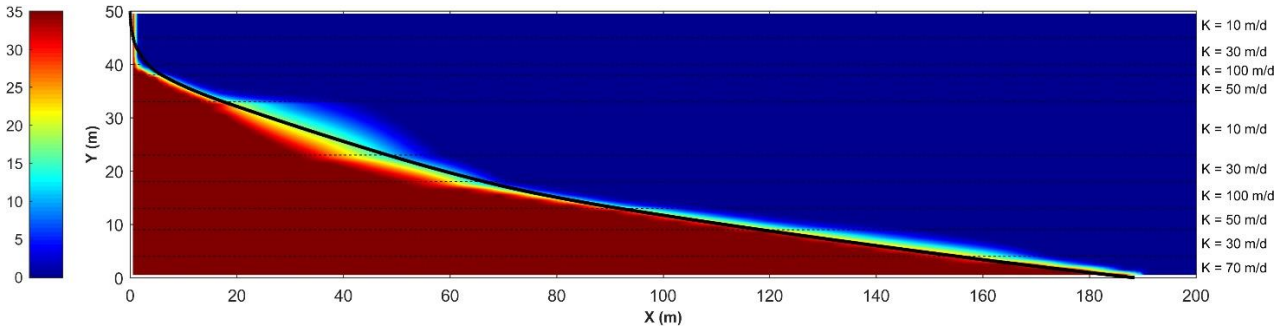

Figure 9 - Comparison of numerical and analytical results (Line-Analytical, Colormap-Numerical)

4.5 Discussion

4.5.1 The Proposed Equation in the Context of the Existing Comprehensive Discharge Potential Theory (Strack and Ausk, 2015; Strack et al., 2016)

Strack's solution (Strack and Ausk, 2015) is more general as it is applicable to three-dimensional vertically integrated flow and allows the inclusion of recharge and pumping as well. Our equation, although with stricter assumptions, allows us to gain some critical insights about stratification effects on the interface profile. In this section, we discuss how the new parameters in the proposed equations correspond to the comprehensive discharge potential for vertically integrated groundwater flow by Strack and Ausk (2015). We will limit our discussion to confined aquifers. Strack's solution for the interface in terms of comprehensive discharge potential is of the form:

$$x = \frac{1}{(-Q_x)}(\Phi - \Phi_0) \tag{59}$$

where, Φ is the comprehensive discharge potential (referred henceforth as "potential) at x, obtained in terms of interface elevation ζ after adopting Dupuit approximation. Φ_0 is the potential at the coastal boundary, which is only a function of aquifer parameters. We rearrange our interface solution Eq. (39393939) into a form similar to Eq. (59) so as to delineate a term independent of ζ:

$$x = \frac{1}{(-Q_x)}\left\{\frac{1}{\alpha}\left[-\zeta \sum_{i+1}^{N} T_j - \sum_{1}^{i} T_j y_j + \frac{K_i}{2}(d_{i+1} - \zeta)^2\right] + \frac{1}{\alpha}\sum_{1}^{N} T_j y_j\right\} \tag{60}$$

Comparing Eqs. (59) and (60), we can identify ζ-dependent terms as Φ, and the terms independent of ζ as Φ_0:

$$\Phi = -\frac{1}{\alpha}\left[\zeta \sum_{i+1}^{N} T_j + \sum_{1}^{i} T_j y_j - \frac{K_i}{2}(d_{i+1} - \zeta)^2\right] \tag{61}$$

$$\Phi_0 = -\frac{1}{\alpha}\sum_{1}^{N} T_j y_j \tag{62}$$

With the assumption of no seepage face $H_s = B$, we verified that the above Φ and Φ_0 are mathematically the same as presented in Strack and Ausk (2015). Therefore, the boundary potential in the comprehensive discharge potential theory essentially represents the first moment of the transmissivity.

4.5.2 Interface Profile in Layer-configurations with Different Hydraulic-conductivity Contrasts

Using the derived interface-profile solutions, we examine the interface in different aquifer configurations of hydraulic-conductivity contrasts between layers for two boundary types, namely, constant-head and constant-flux boundary. Note that for a given aquifer configuration, the interface-profile solution will be identical in the case of a given discharge as boundary or a fixed boundary head resulting in the same discharge. Also, in stratified aquifers with constant-head boundary, the toe-position is independent of the hydraulic-conductivity values and controlled by aquifer TCE (spatial arrangement of conductivities) (Rathore et al., 2018b).

Here, we consider a simple three-layer aquifer, representing an aquifer system with a layer of different hydraulic conductivity embedded in a homogeneous aquifer. The thickness of each layer is equal to 4 m, $H_s = 12$ m, the density of the freshwater is $\rho_f =$ 1000 kg/m^3, and the density of seawater is $\rho_s = 1025$ kg/m^3. For both boundary types, different aquifer configurations corresponding to different hydraulic-conductivity contrasts represented by $\lambda = K_2/K_1$ are solved, where K_2 represents the hydraulic conductivity of the middle layer, and K_1 of the top and bottom layers. K_1 is equal to 10 m/d in all the cases and K_2 is varied to vary λ.

For a given discharge-boundary value $Q_x = 0.4$ m^2/d, five λ values namely, 0.1, 1, 10, 50 and 100 are considered. For a head-boundary value$h_f = 12.5$ m and $L = 100$ m, three λ values namely, 0.01, 1 and 100 are considered. It is important to note that for the considered symmetric aquifers, different K-contrasts result in different total transmissivities but the same TCE which is the centroid elevation of the transmissivity field.

Figure 10(a) shows that in given-flux boundary case, the interface profiles in aquifer configurations with different K-contrasts converge in the top layer of the aquifer and diverge at the bottom resulting in significantly different toe-positions (because of different K_2 or T (Eq. (39)). For a constant flux, higher λ implying higher T results in lower head-gradient in the aquifer (Darcy's law), thus leading to a gentler slope of the interface and longer toe-length. Close to the coastal boundary, all the freshwater flow exit into the sea from the top layer, resulting in the same discharge in the top-layer in all aquifer

configurations. Hence, the same discharge and the same top-layer K leads to the same head-gradients and overlapping interface profiles in the top layer.

For a given-head boundary (Figure 10(b)), the interface profiles in aquifer configurations with different K-contrasts are significantly different in the upper part of the aquifer, however, converge to the same point at the bottom of the aquifer, i.e., the same toe position. It is important to realize that in a for a given-head boundary, the shrinking freshwater-flow domain due to seawater wedge results in a steeper head gradient closer to the coastal boundary to generate higher flow velocities for the flow continuity. This is distinct from the single density flow where the head gradient is uniform throughout the length of the aquifer. In aquifer configurations with higher λ values, there is a higher discharge in the middle layer and eventually in the upper layer as an outflow, resulting in the rapid increase in the interface slope closer to the coast. However, in the lower part of the layer, the freshwater flow rate remains unchanged with changing λs (because of fixed K and boundary heads), thus resulting in the overlapping interface profiles and the same toe position.

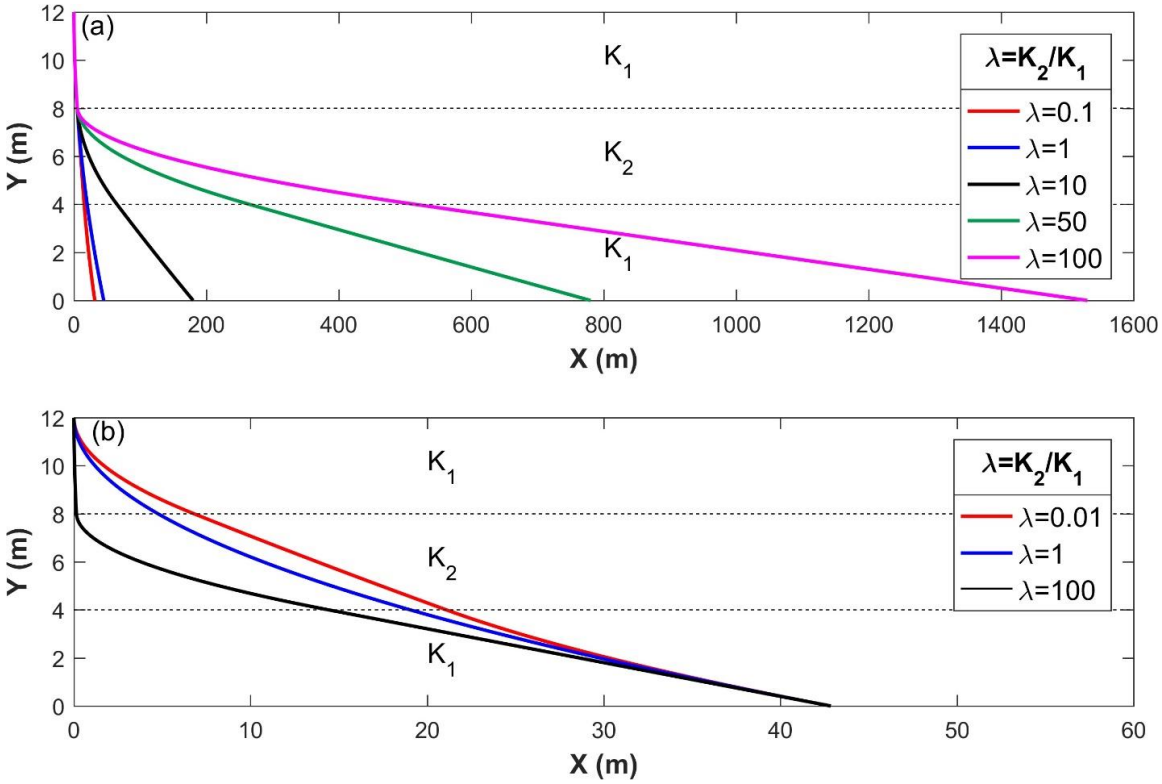

Figure 10 - Interface profiles in aquifer configurations with different hydraulic conductivity contrast with a: a) given-flux boundary; b) given head boundary

4.5.3 Implications of the Dependence of the Interface on the Local Transmissivity Parameters

The proposed equation implies that the extent of SWI at any elevation is governed by the transmissivity field only above the interface-elevation described by parameters—local transmissivity (T_ζ) and local TCE ($y_{c\zeta}$). This result has significant implications on the estimation of the SWI extent in stratified coastal aquifers.

In a stratified coastal aquifer, if the layer arrangement of a certain set of layers in the aquifer is altered, the part of the interface profile above the rearranged layers will remain unaffected and only the profile within and below the rearranged layer will be altered. We demonstrate this through numerical simulation of a simple three-layer case. The hydraulic conductivity of the 20 m thick top layer is assumed to be 50 m/d, and of 15 m thick lower layers as 10 m/d and 100 m/d. Two cases are considered in which placements of lower two layers are switched–Case 1 in which 10 m/d layer is placed above 100 m/d layer, and Case 2 in which 100 m/d layer placed above the 10 m/d layer. Other aquifer parameters are listed in Table 6. As expected due to the dependence of the interface profile on the local transmissivity parameters, interface profiles plotted for both the cases in Figure 11 overlap in the top layer and are separated in the bottom two layers with the interface toe at around 200 m in Case 1 and 275 m in Case 2.

Table 6 - Aquifer parameters used in the numerical simulation of the three-layer case

Parameters	**Unit**	**Value**
Domain length ($\boldsymbol{L}$)	m	500
Longitudinal dispersivity ($\boldsymbol{\alpha_L}$)	m	0.1
Transverse dispersivity ($\boldsymbol{\alpha_T}$)	m	0.01
Effective porosity ($\boldsymbol{n}$)	-	0.3
Constant seawater level ($\boldsymbol{H_s}$)	m	50
Constant inland flux ($\boldsymbol{Q_x}$)	m^3/d	6
Seawater density ($\boldsymbol{\rho_s}$)	kg/m^3	1025
Freshwater density ($\boldsymbol{\rho_f}$)	kg/m^3	1000
Salt concentration in seawater ($\boldsymbol{C_s}$)	kg/m^3	35

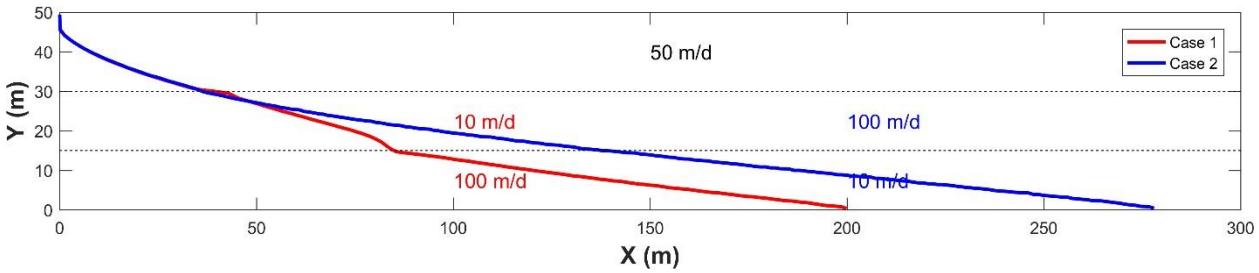

Figure 11 - Interface profile for two layer-placements showing if only the lower two layers are rearranged, the interface profile will be changed only in the lower two layers

We can extend the conclusion from the above analysis to the case of random heterogeneity—the uncertainty in the hydraulic conductivity in a particular stratum of the aquifer will results in the uncertain interface profile in that stratum and the domain below it, however, the profile in the part above the uncertain stratum will still be deterministic. Furthermore, we can also conclude that if the uncertain stratum is placed at the top of the aquifer it will result in the higher variance of the toe-position, and if placed at the bottom of the aquifer, will result in the lower variance of the toe-position. With a more detailed study, these insights could be used to optimize the field-characterization extent to meet the budget constraints and uncertainty requirements.

4.6 Conclusion

By applying the Dupuit-Forchheimer approximation at the outset, we directly derived the explicit analytical solution for the seawater-freshwater interface profile in stratified coastal aquifers. We mathematically showed that the proposed equation represents the solution computed from the vertically integrated groundwater flow solution by Strack and Ausk (2015) for the special case of flow in the vertical plane. We also revealed that the interface elevation will be the same in the cases with two fundamentally different coastal boundaries, namely the boundary with seepage and outflow face, and the one with a coinciding interface, water table, and coastline. The proposed equation is concise compared to the existing solution and provides new parameters governing the interface profile. The interface profile is found to be a function of the elevation of the transmissivity field centroid and the total transmissivity of the freshwater-flow domain above a given point on the interface. We discussed our equation in the context of the comprehensive discharge potential theory and showed that the coastal boundary potential

essentially represents the first moment of the transmissivity. Based on the derived equation, we examined differences in the interface profiles in the aquifer configurations with different hydraulic conductivity contrasts in cases with given-head and given-flux boundaries. We found that with a given-flux boundary, the interface profiles in aquifer configurations with different K-contrasts have different toe-positions, but converge and overlap in the upper part of the aquifer. Conversely, when we consider a given-head boundary, we found interface profiles very different interface profiles in the upper part of the aquifer but the same toe position in aquifer configurations with different K-contrasts. The dependence of interface profile on local transmissivity parameters can potentially help in optimizing the extent of the field characterization for the hydraulic conductivity. The simplicity of our equation makes way for much other theoretical analysis for stratified coastal aquifers. For example, the equation for the interface profile can be integrated to calculate the volume of the intruded seawater and analyze the transience of the seawater intrusion and retreat analytically in stratified aquifers similar to Rathore et al. (2018a) for homogeneous aquifers.

CHAPTER 5. A SEMI-ANALYTICAL METHOD TO FAST DELINEATE SEAWATER-FRESHWATER INTERFACE IN 2D HETEROGENEOUS COASTAL AQUIFERS

5.1 Introduction

Characterization of the seawater-freshwater mixing zone developed in coastal aquifers is critical for the management of coastal aquifers facing the threat of seawater intrusion (SWI). There are two quantitative approaches available to simulate the mixing zone. By approximating the mixing zone as a sharp interface separating seawater and freshwater, analytical solutions based on potential theories can be derived for homogeneous and stratified aquifers (Strack, 1976) (Bakker, 2006; Bear and Dagan, 1964; Collins and Gelhar, 1971; Dagan and Zeitoun, 1998; Huppert and Woods, 2006; Kacimov, 2002; Kacimov and Obnosov, 2001; Kacimov and Sherif, 2006; Naji et al., 1998; Öztürk, 1970; Strack, 1976). Such approximate analytical solutions may not represent field conditions, but require minimal computation effort and conveniently provide many useful insights into understanding interface behavior in both steady-state and transient SWI. By contrast, more complex systems providing a better representation of field conditions like heterogeneity, tidal oscillations, etc., require solving the coupled nonlinear variable-density flow and transport equations (Guo and Langevin, 2002; Voss and Provost, 2002), which is a time consuming and computationally intensive process, especially if we need to solve a large number of cases for uncertainty analysis.

Deterministic analytical solutions for the interface profile have been provided in homogeneous aquifers under steady conditions (Bakker, 2006; Bear, 1972; Strack, 1976) and transient conditions aquifers (Bear, 1972; Bear and Dagan, 1964; Bear et al., 1985; Isaacs and Hunt, 1986; Vappicha and Nagaraja, 1976). Dagan and Zeitoun (1998) and Naji et al. (1998) provided stochastic solutions for steady random hydraulic conductivity fields. Collins and Gelhar (1971) and Mualem and Bear (1974) provided analysis to predict the interface shape in a homogeneous system divided into two layers by a semi-pervious layer. For more general cases of stratified aquifers (heterogeneity only in the vertical direction), Rumer and Shiau (1968) provided the first analytical solution, which, however, was proved to be erroneous by Strack (2016) as it did not satisfy flow continuity. Recently, Strack and Ausk (2015) derived an analytical solution for the interface profile using the vertically integrated groundwater flow solution based on comprehensive discharge potential in stratified coastal aquifers. Rathore et al. (2018b) identified a new parameter, the Transmissivity Centroid Elevation (TCE), governing the interface toe position and groundwater discharge rate in stratified coastal aquifers. (Rathore et al., 2019) further derived a concise equation for the interface profile in stratified coastal aquifers by directly applying the Dupuit-Forchhimer approximation at the outset and found that the interface profile is governed by the local centroid elevation and total transmissivity of the flow-domain above the interface. Toller and Strack (2019) extended the comprehensive discharge potential theory from stratified aquifer (Strack and Ausk, 2015) to vertically varying hydraulic conductivity

Coastal aquifers with two- and three-dimensional heterogeneity have been mostly analyzed using numerical simulations of variable-density flow and transport equations.

Among many SWI simulations codes, SEAWAT (Langevin et al., 2003) and SUTRA (Voss and Provost, 2002) are the most widely used codes. Bear et al. (2001) performed a 3D numerical simulation of the heterogeneous coastal aquifer in Israel. Held et al. (2005) investigated the effect of 2D heterogeneity in the Henry Problem and found using numerical simulations that heterogeneity results in a reduction in the extent of SWI and widening of the mixing zone. They also proposed geometric mean as the effective permeability for the isotropic case, the same as that in the single-density flow. However, Lu et al. (2013a) and Rathore et al. (2018b) showed that unlike single-density flow, the interface flow is significantly affected by the spatial distribution of the heterogeneity, such as layer placement in stratified aquifers. Hence, arithmetic means of the conductivities in the flow domain cannot serve as the effective permeability, and their spatial distribution also needs to be accounted for (Rathore et al., 2018b). Pool et al. (2015) studied the combined effect of heterogeneity and tidal oscillations on three-dimensional SWI. They confirmed the reduction of the extent of SWI and the widening of the mixing zone due to heterogeneity and found it to be linearly proportional to the product of correlation length and variance of the log-permeability field. To quantify the mixing in the heterogeneous medium through a stochastic approach, they used Monte Carlo (MC) simulation based on a series of 50 log-normally distributed random conductivity fields. High computational effort required for solving non-linear variable density equations limited their number of realizations to 50.

Upscaling in groundwater flow models in heterogeneous aquifers is desired for two main reasons: to reduce the computation burden, and to deal with the differences in the scales of measurement and discretization of the model. A review of the literature pertaining

to upscaling can be found in Wen and Gómez-Hernández (1996), Sanchez-Vila et al. (2006), Renard and de Marsily (1997), Farmer (2002), and Cushman et al. (2002). The variable-density flow involved in SWI is governed by non-linear PDEs making their numerical modeling computationally demanding. With the added complication of the formation heterogeneity, upscaled parameterization is highly desired to make numerical solutions for field applications practical. Most of the upscaling studies for SWI focused on mixing to obtain macrodispersion parameters in heterogeneous coastal aquifers (Held et al., 2005; Pool et al., 2015). Held et al. (2005) applied the homogenization theory to arrive at the effective hydraulic conductivity and dispersivity in 2D isotropic and anisotropic heterogeneous conductivity fields. Their scale of considered heterogeneity was very small compared to the scale of SWI (the distance of toe from the coastal boundary) or the aquifer domain, which enabled them to derive geometric mean of the conductivity field as the effective conductivity in an intrinsic sense. However, for the extent of SWI and SGD, which are key dependent variables for coastal aquifer, there have not been sufficient efforts for deriving or estimating effective parameters. Especially, for the cases in which the scale of heterogeneity is comparable to the extent of SWI. For sparse measurements, field is modeled as a random field, hence stochastic effective parameters are derived.

In this chapter, we propose a semi-analytical method to compute the interface profile in 2D heterogeneous aquifers which is significantly faster and requires much lower computational effort compared with the variable-density flow and transport simulations. Our method is based on the insight provided by Rathore et al. (2019), i.e., interface profile is governed by the transmissivity field above the interface (local transmissivity field) characterized by local TCE and transmissivity. We compare the results with variable-

density flow simulations to demonstrate the accuracy of the method and also perform sensitivity analysis with respect to heterogeneity scale (correlation length) and conductivity contrast (log-conductivity variance). With this new method for the rapid computation of the interface profile in a 2D heterogeneous field, we perform stochastic analysis to quantify uncertainties in the SWI extent and groundwater discharge due to random 2D heterogeneity using MC simulations and also perform sensitivity analysis for the uncertainties. We then investigate the possibility of homogenization of a 2D heterogeneous field using an effective hydraulic conductivity.

5.2 Conceptual Model

We consider a 2D slice of a confined aquifer in the vertical plane as shown in Figure 12. The left end is a vertical coastal boundary with sea level as the constant head (H_s $[L]$), and the right end is a vertical inland boundary, which could be constant-flux (Q_x $[L^3/T]$) boundary or constant head (h_f $[L]$) boundary. $K(x,y)[L/T]$ represents the 2D hydraulic conductivity field. Aquifer thickness and length are represented by B $[L]$ and L $[L]$, respectively. The x axis is along the top of the underlying impervious layer pointing towards inland, and y axis along the vertical coastline pointing upwards. At any point x_0 in the aquifer where the interface is at elevation ζ, $T(\zeta)$ represents the total transmissivity of the soil-matrix column above ζ at x_0.

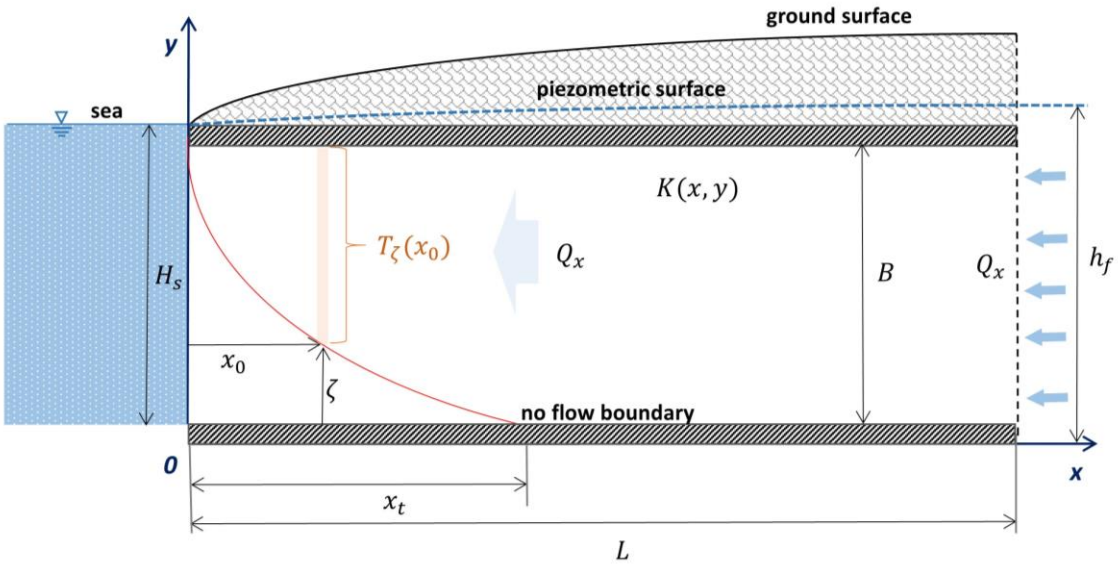

Figure 12 - Conceptual model for the 2D heterogeneous confined aquifer depicting relevant parameters

5.3 Semi-Analytical Method

Previous analytical studies (Rathore et al., 2019; Strack and Ausk, 2015) adopted the Dupuit-Forchheimer approximation to compute an analytical solution for the interface profile in stratified coastal aquifers. Rathore et al. (2019) assumed no seepage face ($x = 0$, $\zeta = B$), a common assumption in many analytical studies (e.g., Bear, 2013; Bear and Dagan, 1964), and revealed that local transmissivity field is the factor governing the interface profile.

$$x = \frac{1}{\alpha(-Q_x)}\left[T_\zeta\left(y_{c\zeta} - \zeta\right)\right] \tag{63}$$

where α is the ratio of the freshwater density to the density difference between seawater and freshwater. T_ζ $[L^2/T]$ is the local transmissivity at a given cross-section, let's say $x = x_0$:

$$T_\zeta(x_0) = \int_\zeta^B K(x_0, y)\, dy \tag{64}$$

In this study also, concerning 2D heterogeneous aquifer, we adopt Dupuit-Forchheimer with no seepage face and use the concept of the local transmissivity field. The freshwater flow rate can be written in terms of the slope of the interface using Darcy's law with Dupuit's assumption of vertical equipotential lines and Ghyben-Herzberg relation (Badon Ghyben, 1888):

$$Q_x = \frac{T_\zeta}{\alpha}\frac{d\zeta}{dx} \tag{65}$$

Using the above equation, we relate the drop in the elevation of the interface, $\Delta\zeta$, and increase in its horizontal extent, Δx:

$$\Delta x = \frac{T_\zeta(x_0)\Delta\zeta}{\alpha Q_x} \tag{66}$$

Using $x = 0, \zeta = B$ as the starting point, we compute x coordinates of the interface profile for different ζ values ranging from B to 0. Note that we can also model ζ as a function of x as $\Delta\zeta = \frac{\alpha Q_x \Delta x}{T_\zeta(x_0)}$, and find ζ for different x values. In stratified aquifers, local transmissivity is just the summation of transmissivity of layers above the interface. In a 2D heterogeneous case, we conceptualize the heterogeneous field as a series of layered aquifers and compute the piecewise interface profile.

To apply the above approach, we model the y-coordinate of the interface as an independent variable and x-coordinate as a dependent. We discretize the thickness of the aquifer to define a series of M elevations, ζ_m $[L]$'s, from $\zeta_1 = B$ to $\zeta_M = 0$, separated by $\Delta\zeta$ $[L]$ distances (represented by horizontal dashed red lines in Figure 13) at which x coordinate of the interface $x(\zeta_m)[L]$ is to be evaluated. Let the T_m $[L^2/T]$ represents the total transmissivity of the column above ζ_m at $x(\zeta_{m-1})$. In Figure 13, we show exaggerated grid by green lines on which K is characterized, with cell sizes in x and y direction as Δ_x $[L]$ and Δ_y $[L]$, respectively. N_r $(= B/\Delta_y)$ $[-]$ and N_c $(= L/\Delta_x)$ $[-]$ represent the total number of rows and columns of the grid, respectively, and a specific cell is referred by (i, j) where i and j are a row and column number, respectively.

The steps involved in the computation are:

1) The interface profile is initialized at the coastal boundary:

$$x_1 = 0 \text{ at } \zeta_1 = B \tag{67}$$

2) Eq. (66) is written in the discretized form to obtain the relation between consecutive x's on the interface for a fixed $\Delta\zeta$:

$$x_m = x_{m-1} + \Delta\zeta \frac{T_m}{\alpha Q} \tag{68}$$

where,

$$T_m = \Delta y \sum_{i=i_0}^{N_r} K_{ij_0} \tag{69}$$

i_0 and j_0 are the row and column number on the K grid containing (x_{m-1}, ζ_{m-1})

3) Using Eq. (68), x-coordinates of the interface profile at all ζ's are evaluated.

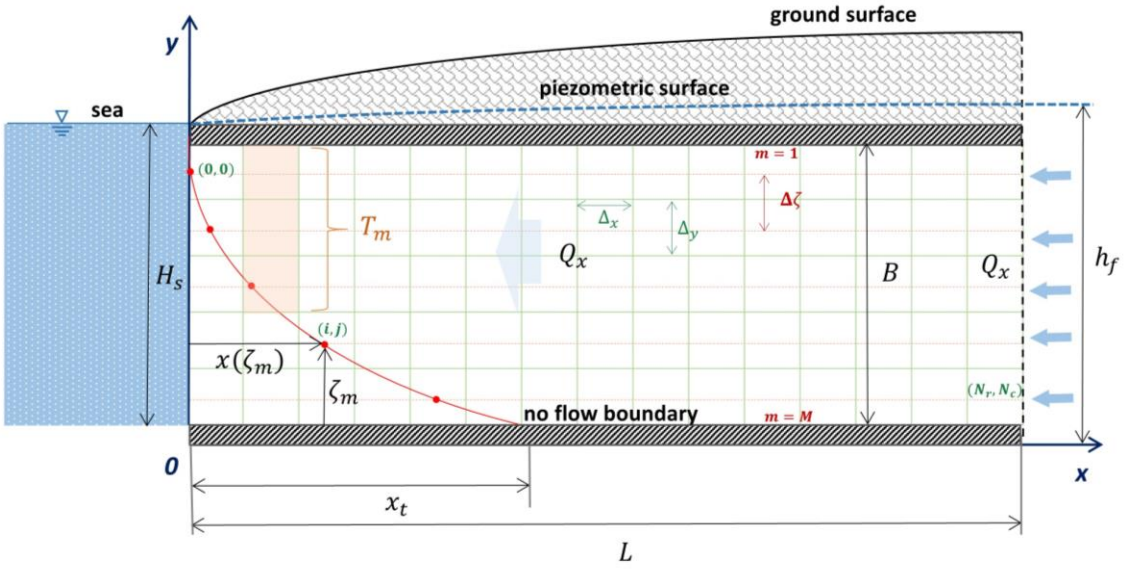

Figure 13 - Conceptual model depicting K grid, series of elevations, ζ_m's, with relevant parameters involved in the computation of the interface profile in 2D heterogeneous aquifers

5.4 Comparison with Variable-density Flow Simulation

We compare our semi-analytical method with the numerical simulation of the variable density flow (referred henceforth as "numerical results" for brevity). Numerical simulations are performed using SEAWAT, a MODFLOW/MT3DMS-based computer program designed to simulate three-dimensional variable-density flow (Langevin et al., 2003). The spatial discretization is determined according to the criteria based on the Grid Peclet number [-] (Voss and Souza, 1987). To simulate 2D heterogeneous hydraulic conductivity, we generate log-normally distributed conductivity fields with a Gaussian correlation function. The lognormal K fields are characterized by their mean ($\mu_{\ln K}$), variance ($\sigma^2_{\ln K}$), and directional correlation lengths (l_x and l_y). We set $\mu_{\ln K}$ to 2.5 for all the cases in this study, which yields the geometric mean of the hydraulic conductivity as 12.18 m/d.

We first compare the semi-analytical interface profile with the numerical salt-concentration fields for multiple realizations of the base case (fixed K field parameters). We then assess the performance of our method over a range of heterogeneity parameters (variance and correlation length). The aquifer parameters and K-field parameters used are summarized in Table 7, and base-case parameters are identified using asterisks.

Table 7 - Parameters Used to Assess the Performance of the Proposed Methodology

Parameter	Value	Description
L (m)	100	Aquifer length
B (m)	12	Aquifer thickness
H_s (m)	12	Sea level
Q_x (m^3/d)	1	Freshwater flow
α_L (m)	0.1	Longitudinal dispersivity
α_T (m)	0.01	Transverse dispersivity
ρ_s (kg/m^3)	1025	Seawater density
ρ_f (kg/m^3)	1000	Freshwater density
$\mu_{\ln K}$	2.5	Mean of lognormal K field
$\sigma^2_{\ln K}$	0.5, 1*, 2, 4	Variance of the lognormal K field
l_x	7, 10*, 12, 16	Correlation length in x direction
l_y	2	Correlation length in y direction

* parameters used in the base case

5.4.1 Base Case

To compare the variable density flow simulations and semi-analytical interface profile, we generate four realizations of K fields from the base-case parameters (Table 7), representing 2D heterogeneous fields. Figure 14(a) shows the maps of the four lognormal K fields.

Figure 14(b) presents the saltwater concentration fields obtained from the numerical simulations of the variable-density flow and interface profiles computed using the semi-analytical method for all four realizations. Results demonstrate that the simple semi-analytical method was able to predict the SWI extent with remarkable accuracy. Since the proposed method does not require solving non-linear equations of coupled variable-density flow, the computation time is fractions of a second compared to several minutes to hours in SEAWAT. There is some mismatch between numerical and semi-analytical results in realization 2 and 3 near the coast which can be attributed to the Dupuit-Forchheimer approximation which breaks down near the coast. However, the toe-position which is the typical indicator of the extent of SWI is accurately predicted in all four cases. It is evident from Figure 14 that despite the same statistics of K in all four cases, the spatial distribution of K has a significant impact on the SWI. We discuss this dependence in detail later in this chapter.

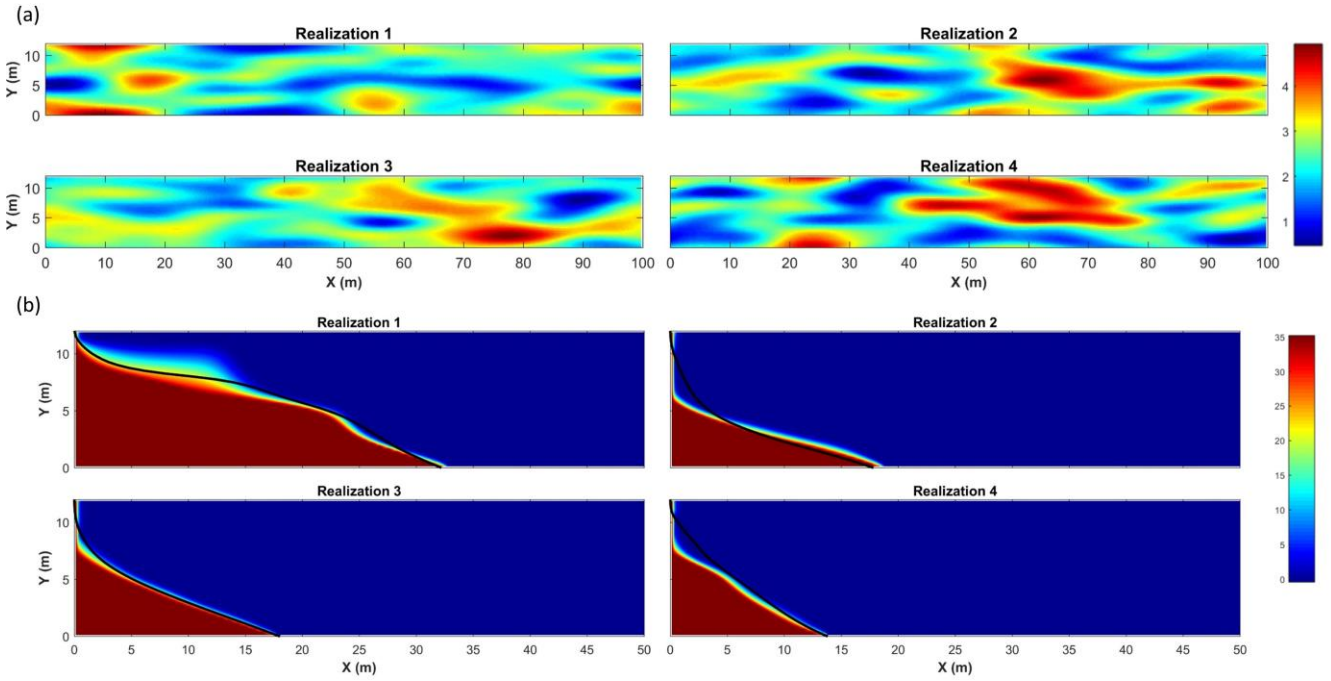

Figure 14 - (a) Maps of logarithmic hydraulic conductivities representing four realizations generated from base-case parameters; (b) Comparison of variable density flow simulation (heat map) and semi-analytical interface profile (black line) for four realization of base-case hydraulic conductivity fields

5.4.2 Cases with Different Heterogeneity Parameters

To ascertain the robustness of the proposed methodology, we compare the numerical and semi-analytical results over a range of degrees and scale of heterogeneity. We consider four values of each l_x and $\sigma^2_{\ln K}$ as shown in Table 7, yielding 16 cases from their combinations. Cases are referred to as ordered pairs of parameters values, ($\sigma^2_{\ln K}$, l_x). Figure 15(a) shows conductivity fields and Figure 15(b) presents the numerical and semi-analytical results. Note that the effect of l_x and $\sigma^2_{\ln K}$ as statistical parameters on SWI needs to be studied in a probabilistic framework, which is covered in the chapter discussing the stochastic part. Figure 15 shows excellent agreement between the semi-analytical interface and the mixing zone in numerical results in almost all cases. In a few cases, namely (2,7), (3,7) and (3,13), where the former number represents the variance and the later correlation length, there is some mismatch near the coast due to breaking of Dupuit-Forchheimer approximation. However, the toe-positions are still accurately predicted. We approximate 50% isochlor of salt concentrations normalized by seawater concentration as the interface in numerical results. Figure 16 compares the toe-positions in semi-analytical and numerical solutions and demonstrates high accuracy in the prediction of the toe-position from the proposed method. Leveraging this ability to rapidly delineate the interface profile, we also performed a stochastic analysis that has not been done before for a 2D heterogeneous case. These stochastic analysis results are presented in the next chapter.

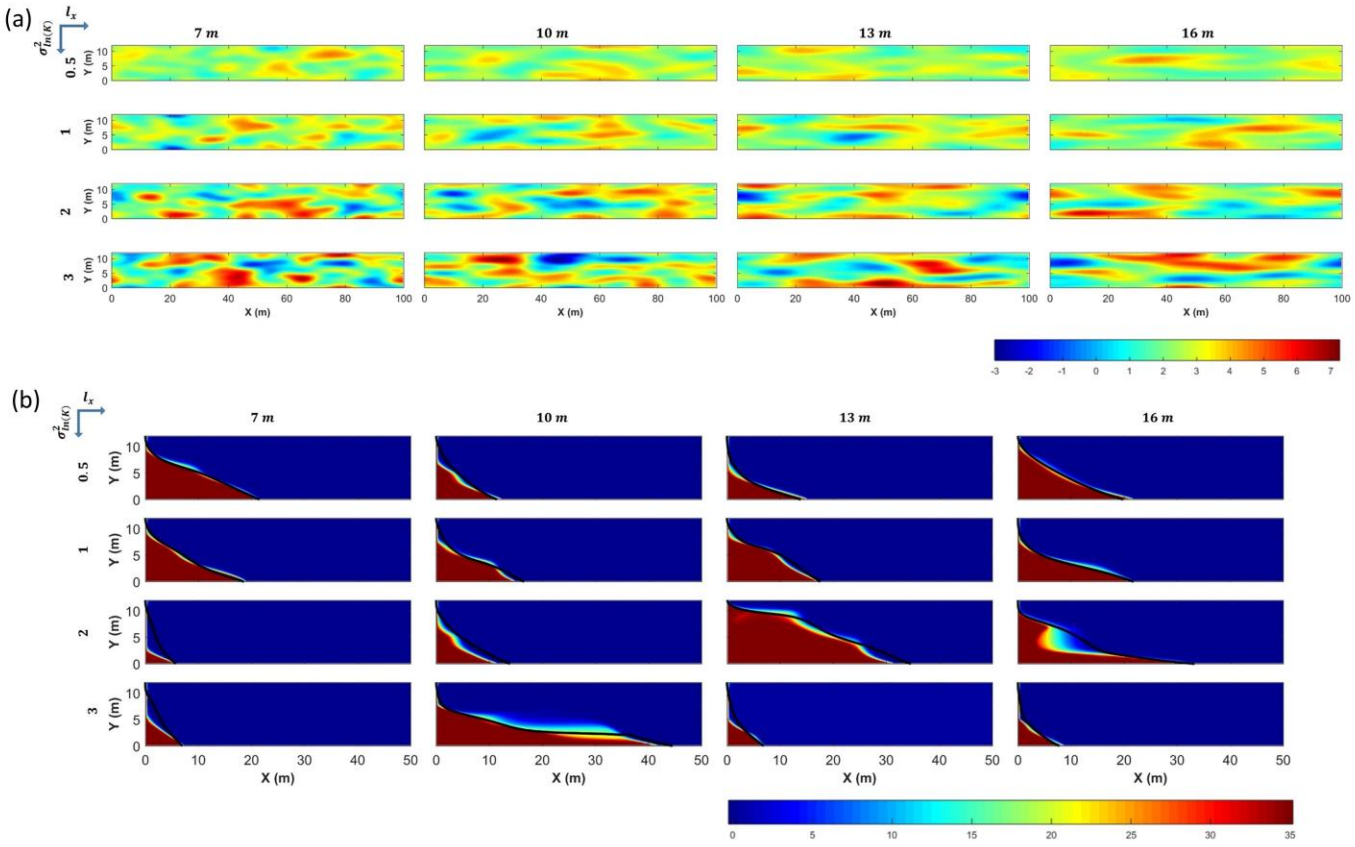

Figure 15 - (a) Heat maps of logarithmic conductivity fields generated using combinations of four different values of each l_x and σ^2_{lnK} as mentioned in Table 1; (b) Comparison of variable density flow simulation (map) and semi-analytical interface profile (black line) for four different values of each l_x and σ^2_{lnK} as mentioned in Table 7

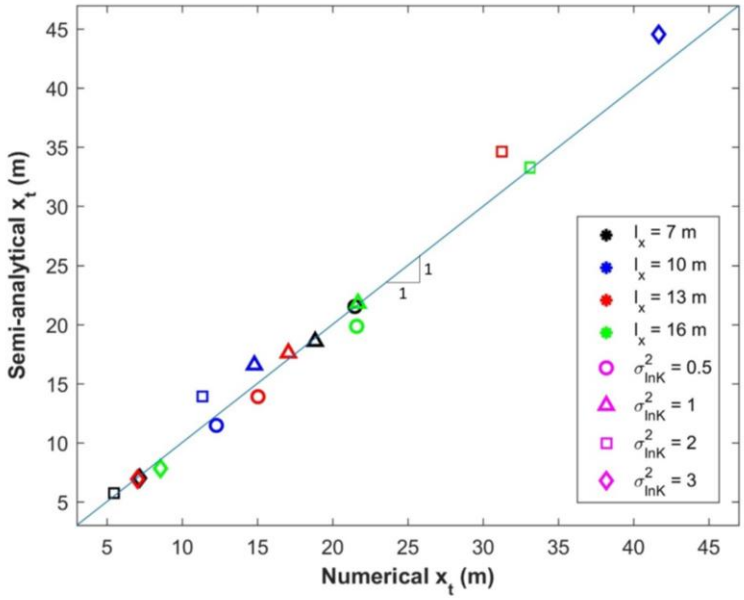

Figure 16 - Comparison of toe positions from the proposed semi-analytical method and numerical simulations (toe of the 50% isochlor)

5.5 Effect of 2D Heterogeneity on Seawater Intrusion

In this section, we analyze the effect of the spatial distribution of the hydraulic conductivity in a 2D domain on the interface profile. Theoretical analysis indicates that the SWI extent is only dependent on the transmissivity field above the seawater wedge (Rathore et al., 2019), which entails that the region of single density flow (landward of the toe position) and the region under the transition zone are insignificant in determining the extent of SWI. To verify this surprising insight, we conduct numerical experiments using realization 1 from Figure 14. We modify the hydraulic conductivities to 300 m/d in the "insignificant" regions (modified 1 case for seawater wedge and modified 2 cases for single density flow region) and found that SWI remained unchanged in the modified cases (Figure 17).

By observing spatial distributions of the conductivity values above the seawater wedge and the extent of SWI in different realization in Figure 14, it appears that the region close to the top of the aquifer and coastal is the most influential region. High hydraulic conductivities in the upper part of the aquifer near the coast results in greater SWI as in realization 1. This is because of the higher K results in a smaller head-gradient and milder slope of the interface for a given discharge. Mild interface slope in the upper part of the interface leads to longer toe-length than the mild slope of the interface near the aquifer bottom. More generally, toe position is more sensitive to the near-coast-near-top region of the aquifer.

This identification of the significant region has strong implications on optimizing the characterization of the hydraulic conductivity fields in the coastal aquifers.

Characterizing the significant near-coast-near-top region at finer resolution can reduce the uncertainty in the analysis. The relatively insignificant region away from the coast and near the aquifer bottom can be characterized sparsely. A detailed quantitative study is warranted to develop comprehensive guidelines for the characterization of coastal aquifers for SWI analysis.

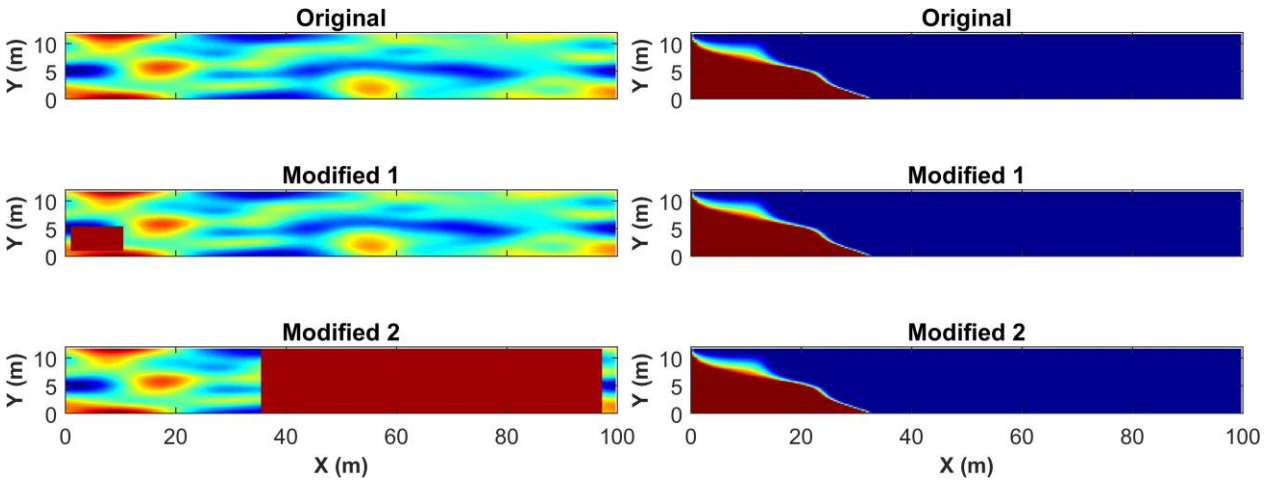

Figure 17 - Comparison of SWI in the modified and original hydraulic conductivity fields demonstrating the insignificance of the region under the transition zone and landward of the toe position

5.6 Summary and Conclusion

We propose a semi-analytical technique for the rapid computation of the interface profile in 2D heterogeneous aquifers. Our technique is based on the insight that the interface profile is a function of transmissivity centroid elevation of the flow domain above the interface (local transmissivity parameters proposed by Rathore et al. (2019) for stratified aquifers). We conceptualize the 2D heterogeneous aquifer as a series of columns stratified aquifers and assume that freshwater discharge redistributes abruptly in each column. Interface profiles computed in few seconds using the proposed technique agree very well with the numerical results which typically take a few hours. Although there was a deviation of the semi-analytical profile from numerical results in cases with steep interface near the coast because of the breakdown of horizontal flow assumption, the toe position still matched perfectly. We demonstrated the effectiveness of our technique for a wide range of heterogeneity parameters.

We numerically verified the implication from our analytical solution that the extent, not SWI is not influenced by the single-density flow zone and aquifer below the seawater-freshwater interface. Hence, the aquifer characterization can be made more efficient and uncertainty in the SWI model results can be lowered by characterizing the near-coast-near-top region at finer resolution and sparsely characterizing the region away from the coast and near the aquifer bottom. The proposed semi-analytical method allowed stochastic analysis in a 2D heterogeneous aquifer, the results of which are presented in the next chapter.

CHAPTER 6. STOCHASTIC ANALYSIS OF SEAWATER INTRUSION

6.1 Introduction

Heterogeneity due to spatial variations of hydraulic properties significantly influences groundwater flow and solute transport in geological formations. In coastal aquifers, heterogeneity often occurs in the form of stratification (Dagan and Zeitoun, 1998; Sacks and Tihansky, 1996) (Collins and Gelhar, 1971; Dafny et al., 2010; McClymonds and Franke, 1972), which results in a distinct seawater-freshwater interface and freshwater discharge pattern from those in homogeneous aquifers (Lu et al., 2013a; Rathore et al., 2018b; Strack and Ausk, 2015). Effects of deterministic stratification on seawater intrusion in coastal aquifers have been studied numerically, experimentally and analytically (Lu et al., 2013a; Mualem and Bear, 1974; Rathore et al., 2018b; Rumer and Shiau, 1968; Shi et al., 2018; Strack, 2017; Strack and Ausk, 2015). Our recent study (Rathore et al., 2018b) discovered that stratification effects in a given aquifer can be accounted for by a new parameter, the centroid elevation of the transmissivity field. Specifically, a higher transmissivity centroid elevation (TCE) corresponds to a more landward interface toe position and a larger groundwater discharge rate. This unique result indicates that in addition to mean hydraulic conductivity or total transmissivity, seawater intrusion is highly influenced by aquifer layer placement, which is not a factor for single density flow in stratified aquifers. In addition, Lu et al. (2013a) found that aquifer layer placement also affects the interface thickness due to flow refraction.

In aquifers with uncertain hydraulic conductivities, Dagan and Zeitoun (1998) modeled stratification as a one-dimensional random field in a coastal aquifer with a constant-flux inland boundary and derived the mean interface profile along with the associated variance based on the interface approximation. Held et al. (2005) used the homogenization theory for coupled variable-density flow and transport models and found that in isotropic media the effective permeability is the geometric mean of a randomly heterogeneous field, as under conditions without fluid density contrast. Numerical simulations based on randomly generated heterogeneous fields were conducted to investigate the effects of heterogeneity on mixing enhancement between freshwater and seawater (Abarca, 2006; Pool et al., 2015). None of these studies have recognized the effects of TCE or analyzed the results in terms of this newly-identified parameter. Moreover, the analytical solution in terms of TCE provides a much more convenient tool than the stochastic partial differential flow equation (Dagan and Zeitoun, 1998) to evaluate the uncertainty of the interface position and groundwater discharge rate for randomly stratified aquifers.

In this chapter, we extend the recently derived TCE-based approximate analytical solutions for deterministic stratification to randomly stratified coastal aquifers. We conduct stochastic analyses and provide explicit analytical solutions for the statistical moments of the interface toe position and discharge rate for both flux- and head-controlled coastal aquifers. Results are verified by Monte-Carlo simulations on randomly generated realizations with predefined spatial correlations. The solutions are then used to investigate how spatial correlation parameters affect the statistical behavior of seawater intrusion and discharge rate. For a 2D heterogeneous case, there is no detailed stochastic analysis

available because of the high computation cost to perform Monte Carlo ensemble computations using variable-density flow. However, we developed a new method for the rapid computation of the interface profile in a 2D heterogeneous field in the previous chapter. In this chapter, we perform stochastic analysis to quantify uncertainties in the SWI extent and groundwater discharge due to random 2D heterogeneity using MC simulations and perform sensitivity analysis for the uncertainties. We provide a method for stochastic upscaling for both randomly stratified and 2D heterogeneous aquifers.

6.2 Randomly Stratified Aquifers

6.2.1 Model Conceptualization

Figure 18 shows the formation configuration and conceptual model considered in this note. For simplicity, also similar to the previous setup in Dagan and Zeitoun (1998), we consider a two-dimensional confined aquifer with horizontal stratification in the hydraulic conductivity. The aquifer is underlain by an impermeable layer and bounded by vertical boundaries at the inland and coastal ends. The seaward freshwater discharge Q_x $[L^2/T]$ is assumed to be horizontal following Dupuit's assumption (Dupuit, 1863), which implies that the equipotential lines are vertical. The flow domain can be divided into two zones: an interface zone consisting of both freshwater and seawater (Zone 1) and zone consisting of only freshwater and no interface (Zone 2). Let the origin be at the point where the aquifer base meets coastline, the x axis along the top of the underlying impervious layer pointing towards inland, and the y axis along the vertical coastline pointing upwards. L $[L]$, H_s $[L]$ and x_t $[L]$ represent the distance of the inland boundary from the coastal boundary, seawater head at the coastal boundary, and interface toe position, respectively. The inland

boundary can be a constant total flux Q_x $[L^2/T]$ (in a flux-controlled system) or a constant head h_f $[L]$ (in a head-controlled system). In the confined aquifer, the layers are indexed from 1 to N from bottom to top (see Figure 18), where N is the total number of layers. For a particular ith layer, the thickness, center elevation, base elevation, and hydraulic conductivity are represented by b_i $[L]$, y_i $[L]$, d_i $[L]$ and K_i $[L/T]$, respectively. Note that the elevation is with respect to the base of the aquifer, unless mentioned otherwise. h $[L]$ is the freshwater head above sea level. B $[L]$ and T $[L^2/T]$ represent the total aquifer thickness and transmissivity, respectively.

$$B = \sum_{i=1}^{N} b_i \, , T = \sum_{i=1}^{N} T_i = \sum_{i=1}^{N} K_i b_i \tag{70}$$

A randomly stratified aquifer is conceptualized using thin layers with each layer arrangement having a unique y_c representing the elevation of the transmissivity field centroid (referred henceforth as Transmissivity-field Centroid Elevation or TCE) calculated as:

$$y_c = \frac{\sum_1^N T_j y_j}{T} \tag{71}$$

In chapter 3, we derived explicit analytical solutions for the toe-position Eq. (13) and discharge Eq. (12) for head-controlled and toe-position Eq. (9) for the flux-controlled system. These solutions accounted for stratification effects through TCE.

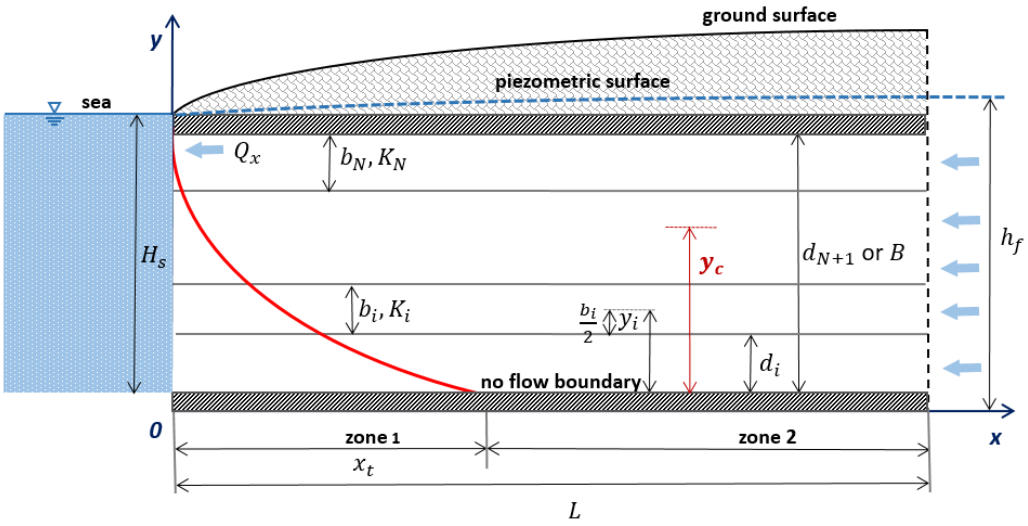

Figure 18 - Conceptual model for stratified coastal aquifer with y_c as one of the random parameters

6.2.2 Solutions in Random Stratification

In a randomly stratified aquifer, we assume the logarithmic K field as a stationary random function of y (elevation with respect to the aquifer base). A constant mean, variance and a two-point correlation function for the logarithmic K field are represented by μ_z, σ_z^2, and $\rho_z(y)$, respectively, where $z = lnK$ (Dagan and Zeitoun, 1998). Our solutions for x_t and Q_x, provided in the previous section, delineates the complex effects of stratification in terms of T and y_c (which are also random because of random K), making it convenient to perform a stochastic analysis of x_t and Q_x. We first evaluate the statistical moments of T and y_c (derivation provided in Appendix D):

$$\mu_T = \mu_K B \tag{72}$$

$$\sigma_T^2 = \sigma_K^2 I_1 \tag{73}$$

$$\mu_{y_c} = \frac{B}{2} + \frac{\sigma_K^2 (BI_1 - 2I_2)}{2\mu_K{}^2 B^2} \tag{74}$$

$$\sigma_{y_c}^2 = \frac{\sigma_K^2 (B^2 I_1 - 4BI_2 + 4I_3)}{4\mu_K{}^2 B^2} \tag{75}$$

where,

$$I_1 = \int_0^B \int_0^B \rho_K(h)\,dz\,dy;$$

$$I_2 = \int_0^B \int_0^B y\,\rho_K(h)\,dz\,dy; \tag{76}$$

$$I_3 = \int_0^B \int_0^B yz\,\rho_K(h)\,dz\,dy;$$

where $h = |y - z|$. The above derived moments for T and y_c are then used to evaluate the approximate moments of toe-positions and discharge described in Eqs. (9) - (13) and using the Taylor series expansion.

Statistical moments for the x_t in a flux-controlled system are given as (see Appendix E):

$$\mu_{x_t} = \frac{\mu_K H^2}{2\alpha Q_x} \tag{77}$$

$$\sigma_{x_t}^2 = \frac{\sigma_K^2}{\alpha^2 Q_x^2} I_3 \tag{78}$$

Statistical moments for Q_x in a head-controlled system are given as (see Appendix F):

$$\mu_{Q_x} = \frac{\mu_K B}{L}\left(\Delta h + \frac{B}{2\alpha}\right) \tag{79}$$

$$\sigma_{Q_x}^2 = \frac{\sigma_K^2}{L^2\alpha^2}(\alpha^2 \Delta h^2 I_1 + I_3 + 2\alpha \Delta h I_2) \tag{80}$$

The moments of x_t in a head-controlled system are presented in terms of μ_{y_c} and $\sigma_{y_c}^2$ for brevity (see Appendix F):

$$\mu_{x_t} = \frac{L\mu_{y_c}}{\alpha\Delta h + \mu_{y_c}} - \sigma_{y_c}^2 L \frac{\alpha\Delta h}{(\alpha\Delta h + \mu_{y_c})^3} \tag{81}$$

$$\sigma_{x_t}^2 = \sigma_{y_c}^2 \left(\frac{L\alpha\Delta h}{(\alpha\Delta h + \mu_{y_c})^2}\right)^2 \tag{82}$$

6.2.3 Validation

We conduct Monte-Carlo simulations to test the derived explicit solutions of the moments of x_t and Q_x in a randomly stratified aquifer with a constant-head inland boundary and x_t for a constant-flux inland boundary. A field-scale confined aquifer is considered with the geometrical, hydrogeological and random-K field parameters listed in Table 8. The logarithm of K field (m/d) is generated by assuming an exponential model for the spatial correlation:

$$\rho_z(h) = e^{-\frac{h}{l}} \tag{83}$$

The moments and the spatial correlation model for the corresponding K field can be obtained:

$$\mu_K = e^{\mu_Z + \sigma_Z^2/2} \tag{84}$$

$$\sigma_K^2 = e^{(2\mu_Z + \sigma_Z^2)}(e^{\sigma_Z^2} - 1) \tag{85}$$

$$\rho_K(h) = \frac{e^{\rho_Z(h)} - 1}{e - 1} \tag{86}$$

Using Eq. (76) and above equations for mean, variance and correlation function, I_1, I_2 and I_3 are evaluated, which are then used in the derived solutions to estimate statistical moments of Q_x and x_t.

Alternatively, the total aquifer thickness of 12 m is divided into 48 layers of 0.25 m thickness each, and then 50 realizations of the K field are generated using the considered lognormal distribution and exponential spatial correlation, Q_x and x_t values are estimated for each realization. Figure 19 shows their distributions along with the comparison of

ensemble moments and analytical moments, demonstrating that the moments of Q_x and x_t are well approximated by the proposed closed-form analytical solutions. The constant head at the inland boundary in the head-controlled case is h_f is 12.75 m. The constant flux at the inland boundary in the flux controlled case is 1 m^3/d, a rounded off value of the mean Q_x for the head controlled case. Main insights from the characterization and estimation of the moments are discussed in the next section.

Table 8 - Aquifer parameters for validation using Monte-Carlo simulation

Parameters	**Unit**	**Value**
Domain length ($\boldsymbol{L}$)	m	100
Domain thickness ($\boldsymbol{B}$)	m	12
Longitudinal dispersivity ($\boldsymbol{\alpha_L}$)	m	0.1
Transverse dispersivity ($\boldsymbol{\alpha_T}$)	m	0.01
Effective porosity ($\boldsymbol{n}$)	-	0.3
Constant seawater level ($\boldsymbol{H_s}$)	m	12
Seawater density ($\boldsymbol{\rho_s}$)	kg/m^3	1025
Freshwater density ($\boldsymbol{\rho_f}$)	kg/m^3	1000
Salt concentration in seawater ($\boldsymbol{C_s}$)	kg/m^3	35
Mean of lognormal $\boldsymbol{K}$ field ($\boldsymbol{\mu_Z}$)	-	2.5
Variance of lognormal $\boldsymbol{K}$ field ($\boldsymbol{\sigma_Z^2}$)	-	0.25
Spatial correlation length ($\boldsymbol{l}$)	m	4
Constant inland head **($\boldsymbol{h_f}$)**	m	12.75
Constant inland flux **($\boldsymbol{Q_x}$)**	m^3/d	1

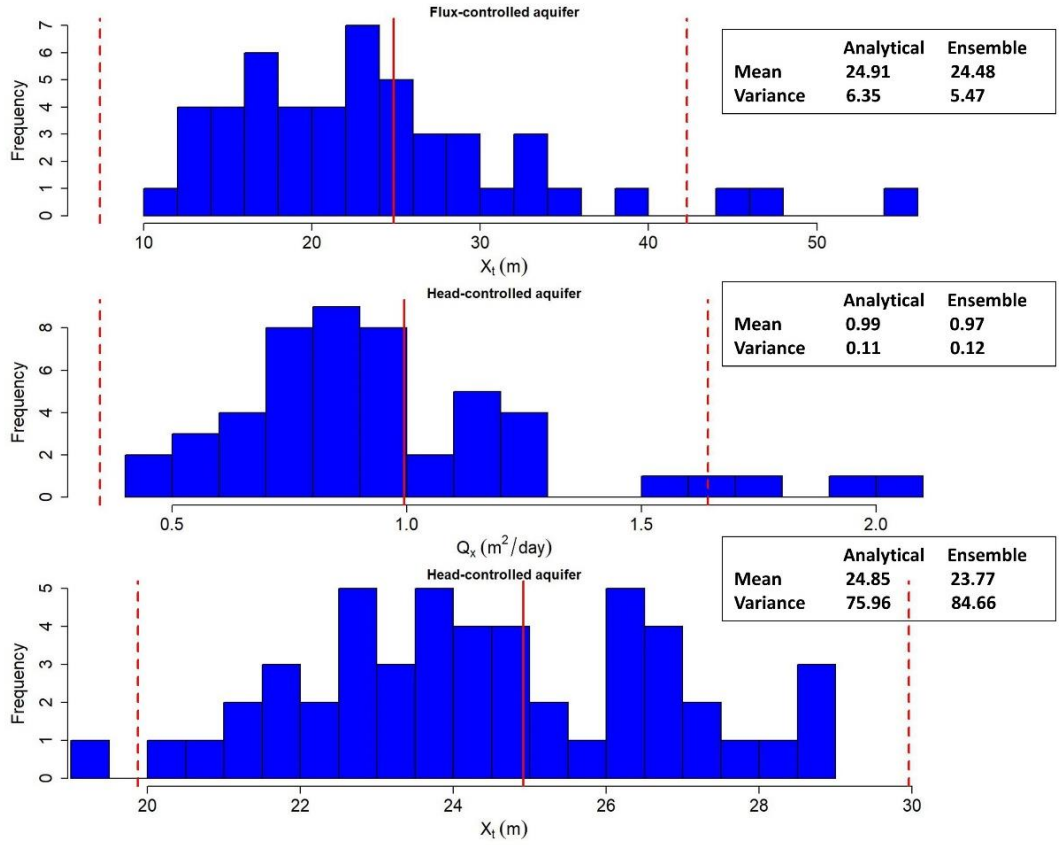

Figure 19 - Histogram represents the distribution of toe-positions in the flux-controlled system, and discharges and toe-positions in the head-controlled system for 50 K field realizations; Red lines represent analytical mean (solid) and 95% confidence intervals (dashed)

6.2.4 Discussion

Eqs. (77) to (82) present analytical solutions for the statistical moments of the toe-position and discharge in a randomly stratified aquifer and provide insight into how different parameters of the random K field influence uncertainties in SWI and GWD estimates. Randomly stratified K field results in a stochastic y_c (parameter encompassing stratification effects on SWI and GWD), with the mean (μ_{y_c}) and variance ($\sigma_{y_c}^2$) presented in Eqs. (74) and (75), respectively. Interestingly, both μ_{y_c} and $\sigma_{y_c}^2$ are linearly related to the ratio of the variance to mean squared, also known as statistical efficiency ($e_K = \sigma_K^2/\mu_K^2$), of the K field. The normalized μ_{y_c} and $\sigma_{y_c}^2$ are written as:

$$\frac{\mu_{y_c}}{B} = \frac{1}{2} + \frac{e_K}{2}\left(\frac{I_1}{B^2} - \frac{2I_2}{B^3}\right) \tag{87}$$

$$\frac{\sigma_{y_c}^2}{B^2} = \frac{e_K}{4}\left(\frac{I_1}{B^2} - \frac{4I_2}{B^2} + \frac{4I_3}{B^4}\right) \tag{88}$$

Hence, the uncertainty in y_c, plotted as confidence intervals, increases with the increasing e_K as shown in Figure 20(a). Note that μ_{y_c} does not change with e_K because for a stationary K field, the term $(BI_1 - 2I_2)$ is equal to zero. Figure 20(b) shows the influence of the correlation length l on the uncertainty. For l values changing from ten percent to ninety percent of the aquifer depth, the uncertainty increases rapidly for lower l values to reach a maximum at around forty percent of the depth, followed by a continuous-gradual decrease.

For a head-controlled system, Eqs. (79) and (80) indicate that the mean freshwater discharge and its variance, μ_{Q_x} and $\sigma_{Q_x}^2$, are linearly proportional to μ_K and σ_K^2, respectively. μ_{Q_x} is the same as that in a homogeneous interface flow with a constant

hydraulic conductivity equal to μ_K. The relation between $\sigma_{Q_x}^2$ and normalized l is shown in Figure 21.

Eqs. (81) and (82) relate the statistical moments of the toe-position in a head-controlled case in terms of the moments of y_c. Figure 21 shows that in a head-controlled case, the sensitivity of x_t to e_K and l is similar to that of y_c. However, in a flux-controlled case, statistical moments of x_t are not uniquely related to e_K, described by Eqs. (77) and (78), where μ_{x_t} is the same as that in a homogeneous case with a constant hydraulic conductivity equal to the arithmetic mean of the randomly stratified conductivity field. $\sigma_{x_t}^2$ is directly proportional to the variance of K and independent of the mean K. $\sigma_{x_t}^2$ monotonically increases with the increasing l, however, the rate of increase decreases for higher l (see Figure 21).

We also found an interesting fact that the variance of the toe-position in a flux-controlled case is significantly higher than that in the corresponding head-controlled case. This finding has serious implications on the conceptualization and interpretation of modeling results for the groundwater systems in which one or more boundaries do not represent clearly identifiable hydrological features, hence defined by the modeler. In our paper under preparation, we discuss in detail the effects of boundary types on uncertainties in seawater intrusion simulations for different cases of heterogeneities. These insights will have implications on modeling decisions and results interpretations.

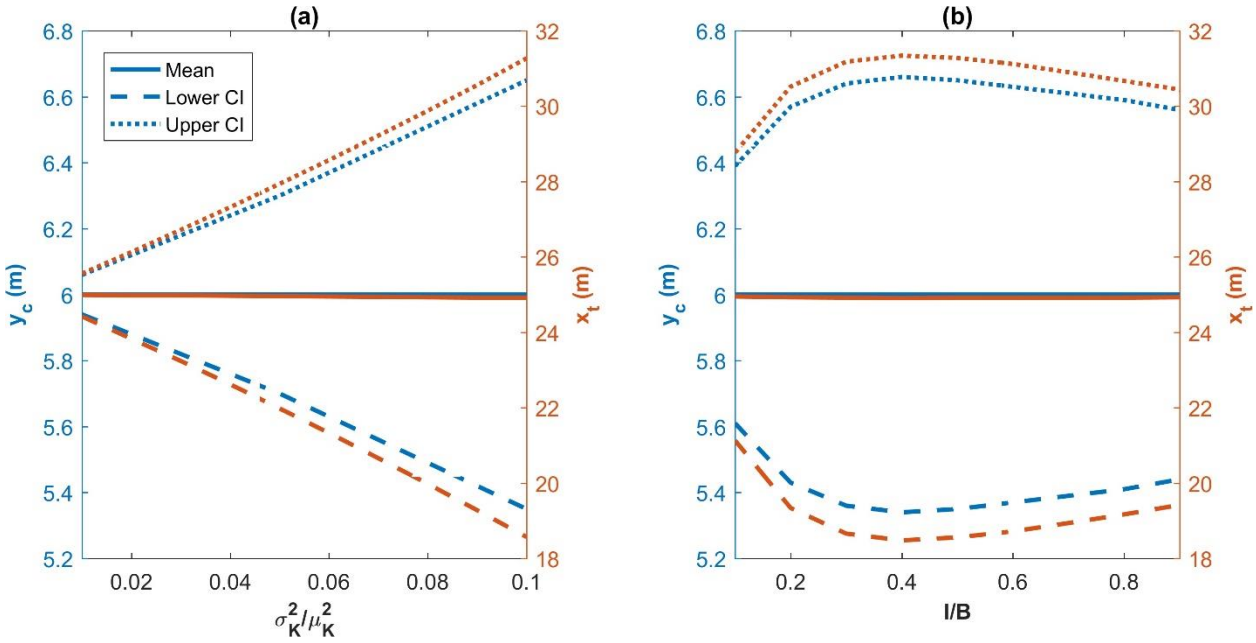

Figure 20 - Sensitivity of mean and confidence intervals (CI) of TCE (blue), and toe position in a head-controlled system (orange) to a) the ratio of variance to mean squared b) normalized correlation length

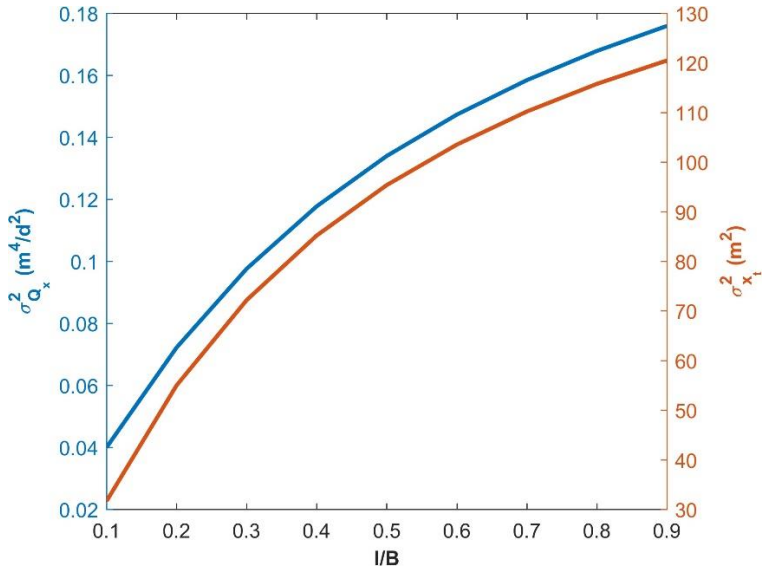

Figure 21 - Sensitivity to the normalized correlation length of K of the variance of the discharge rate in a head-controlled case (blue), the variance of the toe position in a flux-controlled case (orange)

6.3 2D Heterogeneous Aquifer

6.3.1 Quantification and Sensitivity Analysis of Uncertainty

With the ability to solve the interface rapidly using the proposed semi-analytical approach, we performed a stochastic analysis to understand the effect of the random heterogeneity parameters ($\sigma^2_{\ln K}$ and l_x) using the Monte-Carlo approach. We generated 500 realizations for each of 16 heterogeneity cases (sets of heterogeneity parameters) and computed interface profiles for each realization. We then evaluated ensemble mean, variance, 5th and 95th percentile for interface coordinates using evaluated 500 interfaces for each heterogeneity case. Figure 22 shows interface profiles for 50 randomly selected realizations (gray lines) along with ensemble mean (solid red line), 5th and 95th percentile (dashed red lines) interface profiles.

We found an interesting trend in the distribution of the x-coordinates of the interface with interface elevations. At higher interface elevation, x-coordinate distribution is strongly skewed to the right, and the skewness decreases with the decreasing elevation and nearly diminishes at the aquifer base, i.e., the toe-position was found to be normally distributed. Figure 23 shows this trend through histograms of the x coordinate of the interface at different interface elevations for 500 realizations of the base case ($\sigma^2_{\ln K} = 1$, $l_x = 10$ m). Due to this reason, we used percentiles instead of confidence intervals to depict the spread of the ensemble interface profiles in Figure 22.

We can see in Figure 22, both mean interface profile and spread of interface profiles are strongly influenced by the degree of heterogeneity and negligibly to be weakly influenced by the scale of the heterogeneity. To have a closer look, we plotted in Figure 24

ensemble means and variances of the toe position in all 16 heterogeneity cases with respect to variance and correlation length of the lognormal K field. Interestingly, the mean toe-position was found to be increasing monotonically with the degree of heterogeneity for all correlation lengths. The variance of the toe position showed similar trends of variation with respect to the degree of heterogeneity. Both the mean and variance of the toe position show slightly increasing trends with respect to the scale of heterogeneity.

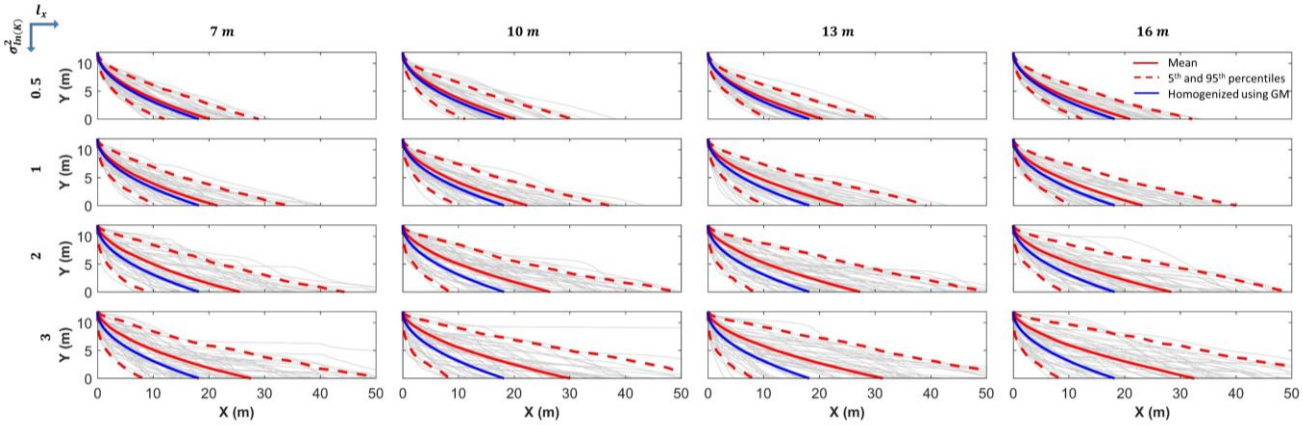

Figure 22 - Semi-analytical interface profiles for 50 realizations out of total 500 realizations for each combination of four different values of each l_x and σ^2_{lnK} as mentioned in Table 7; Ensemble mean and 5th and 95th percentile in red lines; Interface profile in the aquifer homogenized using the geometric mean

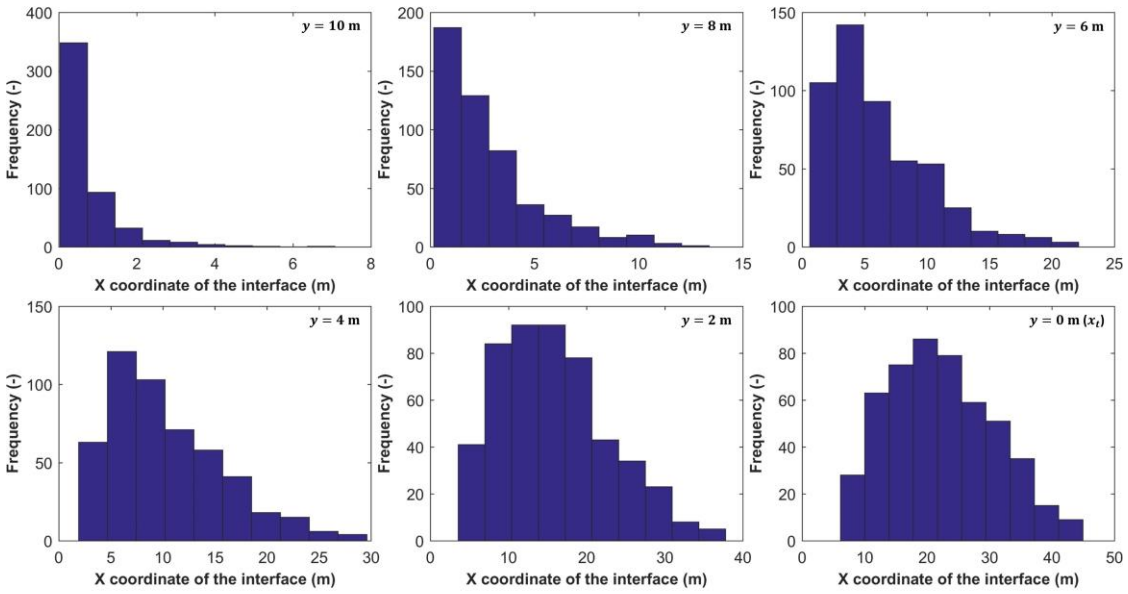

Figure 23 - Histograms of the x coordinate of the interface (semi-analytical) at different interface elevations for 500 realizations of the base case (σ^2_{lnK}= 1, l_x= 10 m)

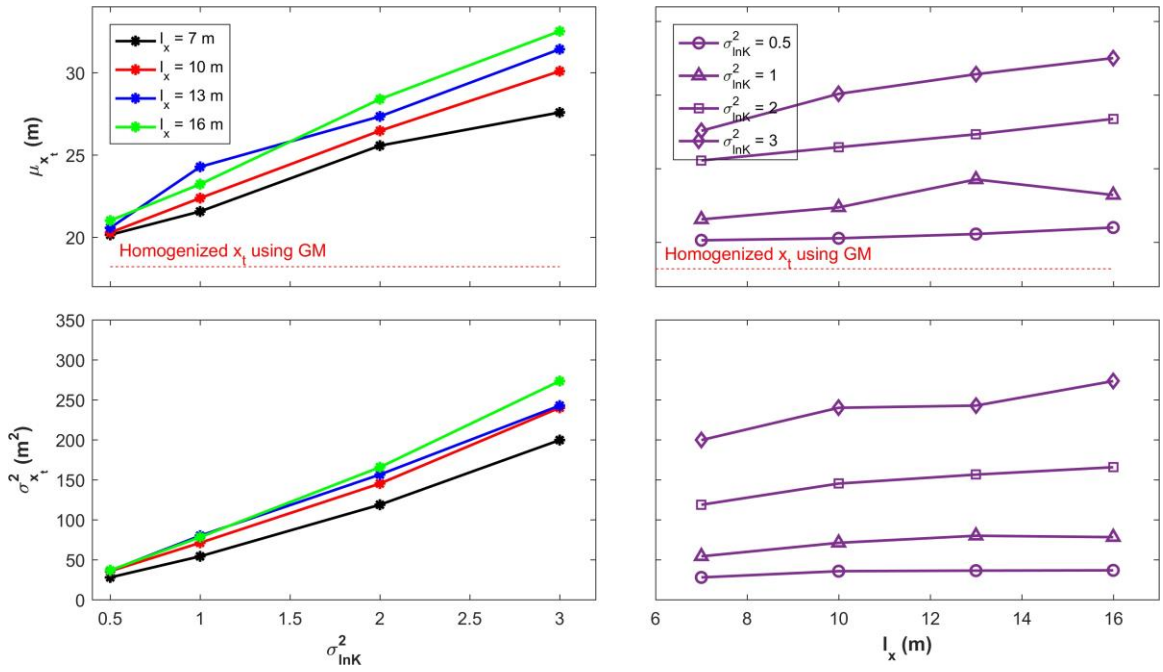

Figure 24 - Variation of ensemble mean and variance (500 realizations) of the toe-position (semi-analytical) with respect to σ^2_{lnK} and l_x

6.3.2 Stochastic Upscaling

To solve large-scale problems involving density-driven flows, upscaled parameterization is sought to make numerical simulations practical. Held et al. (2005) using homogenization theory proposed geometric mean (K_{GM}) as the effective hydraulic conductivity (K_{eff}) in the equivalent homogeneous field to reproduce the position of the saltwater wedge. However, it has been shown in recent studies (Lu et al., 2013a; Rathore et al., 2018b; Strack and Ausk, 2015) that unlike single-density flow, average hydraulic conductivity (be it arithmetic or geometric mean) cannot be used as effective conductivity because the spatial distribution of conductivities significantly influences the SWI. For stratified aquifers, Rathore et al. (2018b) provided effective-hydraulic conductivity solutions based on TCE which is a function of layer arrangement to reproduce the toe position and freshwater discharge in a homogenized aquifer. In a 2D heterogeneous case, as we can see in Figure 14, the interface profile varies significantly in the hydraulic-conductivity fields with the same geometric mean and variance but different spatial distribution.

If the field data for hydraulic conductivity is sparse and the flow domain cannot be characterized in a deterministic manner, the upscaling is performed in a stochastic framework wherein the effective parameter has associated uncertainty because of the uncertainty in the field characterization (Cushman et al., 2002). In the case of SWI with the toe-position and discharge as the dependent variables of interest, we obtain mean and variance of the hydraulic conductivity ($K_{eff}\,[L/T]$) for two types of heterogeneity conceptualizations: 1) Random stratification modeled as one dimensional random field, 2)

2D heterogeneous aquifer modeled as two-dimensional random fields. For randomly stratified aquifer, analytical statistical moments of the K_{eff} are derived using the TCE-based K_{eff} presented in chapter 3. For 2D heterogeneous case, we used MC simulations to semi analytically obtain an ensemble of K_{eff} for 500 realizations, and present the distribution and moments of K_{eff}.

It is interesting to note that using geometric mean to homogenize the aquifer cannot even reproduce the mean behavior of the interface for a 2D heterogeneous case (see Figure 22). The geometric mean as effective conductivity on average results in the underestimation of the SWI extent as seen in Figure 24 for each case of heterogeneity-field parameters. Figure 24 also shows the toe position estimated using K_{GM} is always underestimated compared with the ensemble mean toe position. The difference between the ensemble mean interface profile and homogenized interface profile increases significantly with the increasing conductivity variance and influenced weakly by the correlation length.

In order to study the effective hydraulic conductivity corresponding to the mean interface profile, we invert the equation of the toe-position from the Dupuit parabola and obtain K_{eff} corresponding to the mean profile for each of the 16 cases of heterogeneity parameters:

$$K_{eff} = \frac{2x_t Q_x \alpha}{B^2} \tag{89}$$

In Figure 25, we plot the variation of the K_{eff} corresponding to the mean toe position with respect to the heterogeneity parameters.

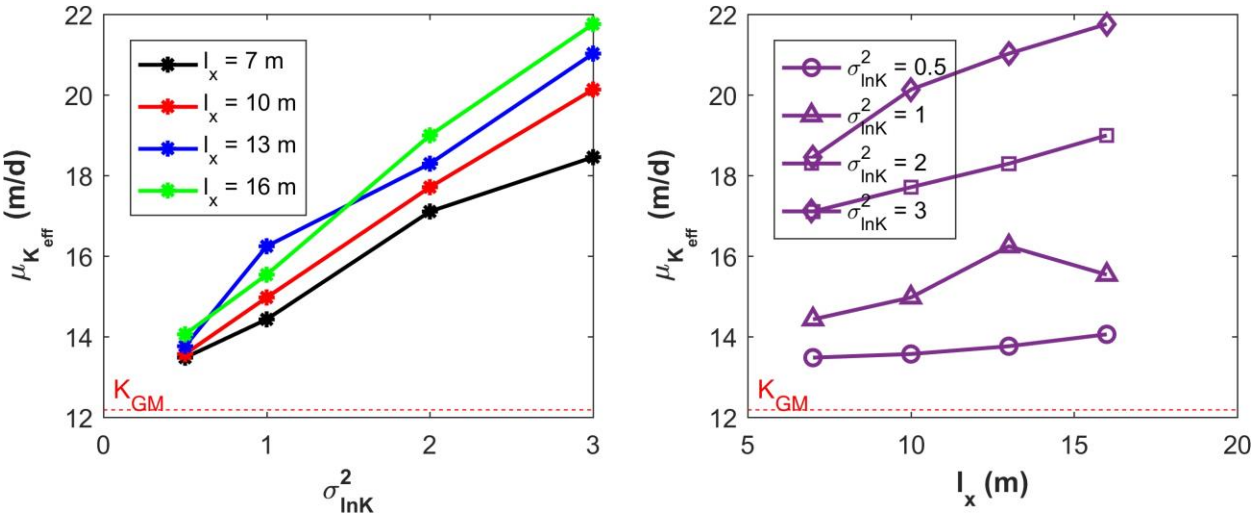

Figure 25 - Variation of K_{eff} corresponding to the mean toe position with respect to σ^2_{lnK} and l_x

K_{eff} sharply increases with the increasing variance of the log-conductivity field, and is weakly influenced by the correlation length. However, in all the cases, K_{eff} is found to be greater than K_{GM}, making K_{GM} a poor representative of the effect of hydraulic conductivity on the SWI in a homogenized aquifer.

For each case in Figure 22, we invert each of the 500 toe positions to obtain the distribution of K_{eff} (see Figure 26). For lower values of σ^2_{lnK}, the K_{eff} appears to be normally distributed, and with increasing σ^2_{lnK}, K_{eff} distribution skews to the left. The difference between K_{eff} and K_{GM} also appears to be increasing with the increasing σ^2_{lnK}.

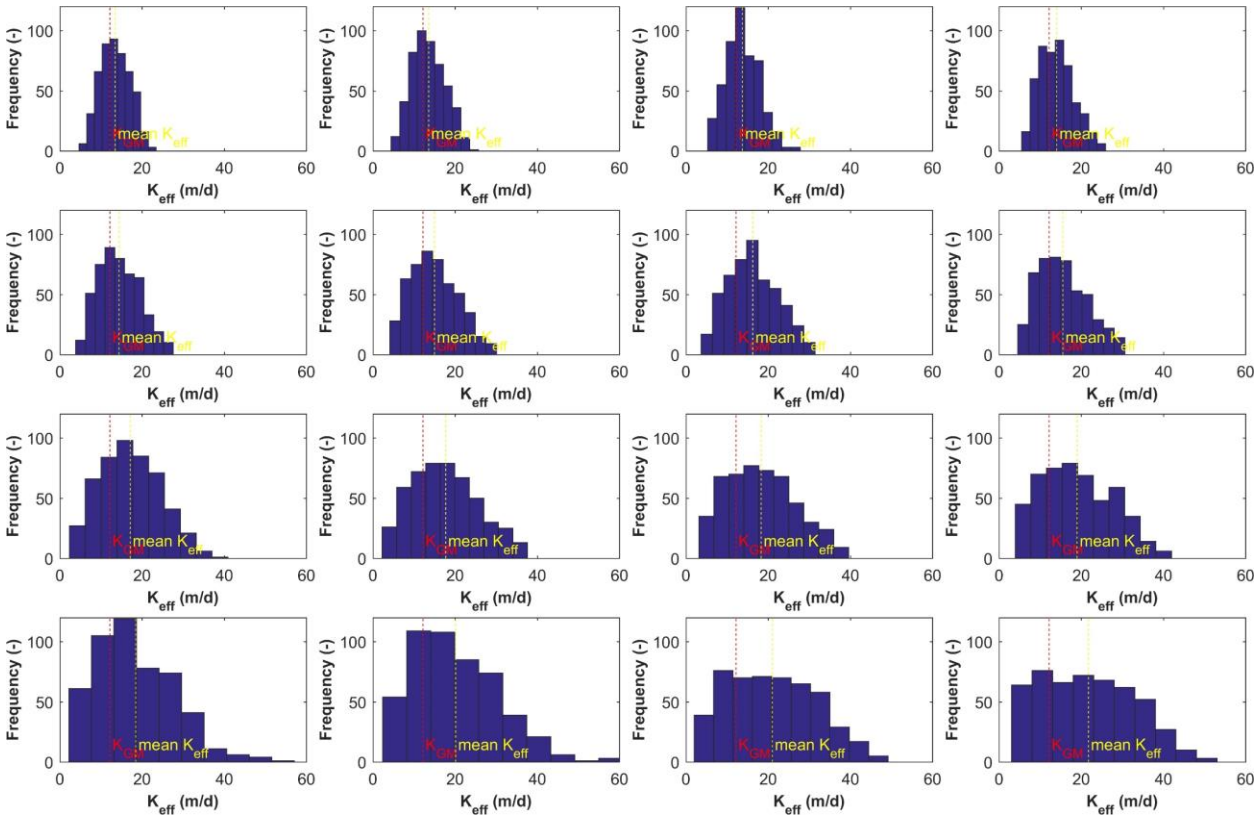

Figure 26 - Distribution of K_{eff} for each case of the heterogeneity parameter

6.4 Conclusion

Based on the solutions in terms of the transmissivity-centroid elevation (TCE) (Rathore et al., 2018b) in chapter 3, we derived explicit analytical solutions for the moments of toe-position and freshwater discharge rate in a head-controlled system and toe-position in a flux-controlled system in randomly stratified coastal aquifers. The solutions were validated using Monte-Carlo simulations based on numerical solutions on randomly generated lognormal K field and the ensemble moments. We found that in a flux-controlled system, the mean toe-position is the same as that in a homogeneous case with constant hydraulic conductivity equal to the arithmetic mean of the randomly stratified conductivity field, and is independent of the uncertainty parameters (variance and spatial correlation) in the hydraulic conductivity. However, in a head-controlled system, the mean toe-position, in addition, to mean hydraulic conductivity, is also dependent on the uncertainty parameters of the conductivity field. Mean discharge is found to be the same as that in a homogeneous interface flow with mean hydraulic conductivity. Variances of toe-position in flux- and head-controlled aquifers and discharges are linear functions of the variance of the hydraulic conductivity field but have different relationships with the spatial correlation function. The variance of the toe position in the flux-controlled system is found to be significantly higher than the corresponding head-controlled system. Proposed solutions provide convenient tools for uncertainty estimation and useful insights for modeling decisions for randomly stratified aquifers.

For a 2D heterogeneous case, capitalizing on the rapid computation ability of the interfaces presented in chapter 5, we performed the stochastic analysis by using 500 realizations for Monte Carlo simulation. The stochastic analysis revealed that the geometric

mean cannot be used to homogenize the aquifer as it cannot reproduce the mean behavior of the interface. The effective hydraulic conductivity obtained by plugging in the mean toe position in an inverted equation for the homogeneous toe-position was greater than the geometric mean of the K field for all degrees and scales of heterogeneity. We also found that the mean and variance of the toe-position increases with the increasing variance of the K field and mildly influenced by the correlation length. We also found that in a random K field, the interface profile near the aquifer top is heavily skewed to the right while the toe position is nearly Gaussian.

CHAPTER 7. TRANSIENT SEAWATER INTRUSION

7.1 Introduction

Seawater intrusion (SWI) is a commonly encountered phenomenon in coastal regions around the globe. The continuously increasing demand for water resulting from population growth and heavy industrialization in coastal areas has further aggravated the problem of SWI as a result of more extensive groundwater withdrawals from coastal aquifers (Chang et al., 2011). The extent of SWI is typically characterized in terms of the toe position, namely, the distance from the coastal boundary to the tip of the seawater wedge at the base of the aquifer. Most previous studies (Fahs et al., 2016; Lu et al., 2013b; Strack, 1976; Werner and Simmons, 2009) estimating the extent of SWI were based on the steady-state condition, and they have not taken into account the dynamic movement of the freshwater-seawater interface and its associated timescales. However, the transient nature of SWI is crucial for developing effective management strategies for controlling SWI (Watson et al., 2010). Furthermore, the dynamic movement of the interface causes significant changes in submarine groundwater discharge rates and chemical outputs into the sea (e.g., Li et al., 1999; Michael et al., 2005; Robinson et al., 2007).

An interesting finding in recent studies regarding transient SWI is the temporal asymmetry between SWI and seawater retreat (SWR), which represents the reversibility and remediation timescales of seawater-intruded coastal aquifers. Watson et al. (2010) explored the transience of SWI caused by sea-level rise (SLR) in an unconfined aquifer via numerical modeling (Diersch, 1998). Watson et al. (2010) chose the timescale associated with the toe position as a quantitative indicator and revealed the timescale disparity in SWI

and SWR. Chang and Clement (2012) conducted laboratory experiments to study the timescales of SWI and SWR in aquifer systems with specified flux as the inland boundary condition (referred to henceforth as "specified-flux boundary case"). They found that for the same magnitude of change in the boundary condition, the wedge took less time to recede from the aquifer than the time to advance into the aquifer. They showed that the SWI case exhibits two opposing flow fields with a distinct stagnation point at the aquifer bottom and a diffused stagnation zone along with the saltwater wedge, where the flow velocities reverse direction, while the SWR case supports a unidirectional flow field with all velocity vectors pointing toward the coastal boundary. They concluded that the difference in the flow fields during SWI and SWR resulted in the difference in their timescales. Lu and Werner (2013) conducted a numerical investigation of timescales associated with SWI and SWR and identified simple log-linear relationships between the timescale and specified-head values at the inland boundary (referred henceforth as "specified-head boundary case") in homogeneous aquifers. They presented the sensitivities of these relationships to aquifer parameters, reflected by the changes in regression coefficients. However, their analyses relied heavily on empirical relationships, and failed to reveal specific effects of various aquifer parameters on the timescale. In addition, a detailed numerical analysis of the effect of aquifer parameters and boundary conditions on the toe-response timescales is susceptible to excessive computational efforts. Other studies on the transience of SWI (Bratton, 2007; Cartwright et al., 2004; Essaid, 1990; Harrar et al., 2001; Meisler et al., 1984) are mostly restricted to site-specific complexities, such that the generalization of such research is challenging.

Because of the lack of field-scale transient SWI studies (Werner et al., 2013) and the limitations of numerical methods in simulating density-dependent problems, analytical methods offer an attractive alternative to more complex approaches to gain insights into the processes controlling SWI and SWR. Analytical solutions provide the ability of quick computation and may assist in identifying the relative influence of each parameter at a glance. Bear (1972) developed approximate analytical solutions for describing toe positions and discharge flow rates into the sea during the movement of the freshwater-seawater interface in a confined, homogeneous aquifer with an inland boundary as specified flux. Vappicha and Nagaraja (1976) obtained approximate solutions for toe positions in unconfined aquifers for a changing specified-flux boundary. Kiro et al. (2008) developed a simple analytical model to predict the timescale of the responses of the water table and the transition zone to a sea-level drop for an aquifer system with a specified-flux inland boundary. However, none of the previous studies provide a single explicit solution for the quick estimation of the timescales of SWI and SWR, or mathematically prove and analytically solve for the temporal asymmetry observed in numerical (Lu and Werner, 2013; Watson et al., 2010) and laboratory (Chang and Clement, 2012) studies. These studies highlight a need for an explicit analytical solution for estimating the timescale, an improvement in the theoretical reasoning, a quantification of the temporal asymmetry between SWI and SWR, and an examination of the effects of the hydrogeological parameters and boundary conditions on the temporal asymmetry. In addition, previous analytical studies were limited to specified-flux boundary cases, whereas there is a need to also evaluate specified-head boundary cases.

Previous studies provide us with the understanding of the flow dynamics and prediction capabilities related to steady-homogeneous (for e.g., Bakker, 2000; Bear, 1972; Kacimov and Obnosov, 2001; Strack, 1989; Strack, 1976; Verruijt, 1970), steady-stratified (e.g., Dagan and Zeitoun, 1998; Lu et al., 2013a; Mualem and Bear, 1974; Rumer and Shiau, 1968; Strack, 2017; Strack and Ausk, 2015) and transient-homogenous SWI (e.g., Lu and Werner, 2013; Vappicha and Nagaraja, 1976; Watson et al., 2010). However, to the best of our knowledge, to date, there is no study exploring transient-stratified SWI, which is of significant practical importance given that most of the field problems are heterogeneous. Horizontal layering or stratification is a common form of heterogeneity found in coastal aquifers because of their sedimentary nature (Dagan and Zeitoun, 1998), for example, Floridan Aquifer System (Sacks and Tihansky, 1996), coastal aquifers in Long Island, New York (McClymonds and Franke, 1972), Savannah, Georgia (Collins and Gelhar, 1971), and Israel (Dafny et al., 2010).

In this chapter, we aim to systematically analyze and quantify timescales associated with SWI and SWR for both homogeneous and stratified aquifers. For homogeneous aquifers, to the best of our knowledge, the explicit analytical solutions of the toe-response timescale are developed for the first time. We verify analytical solutions by numerical simulations, apply them to explain and quantify the temporal asymmetry between SWI and SWR and analyze the effects of hydrogeological conditions on timescales and asymmetry. Despite the assumptions made for the development of the analytical solutions, the insights offered by the solutions about the interface dynamics in coastal aquifers may be extended to real-field scenarios. For stratified aquifers, we explore the effects of stratification on the transient response of the aquifer. We propose an indicator representing the response time

of the interface that can be used to compare different layer arrangements or different aquifers in terms of their response timescale. We also analyze the transient response of the coastal aquifer with a preferential flow layer and explained the sensitivities of the response time to the elevation of the preferential flow layer and hydraulic conductivity contrast.

7.2 Transient Seawater Intrusion in Homogeneous Aquifers

7.2.1 Theoretical Derivation of the Explicit Timescale Solution

For the specified-flux boundary case, we analyze a 2-D vertical section of a confined, homogeneous, isotropic aquifer as our conceptual model, which is shown in Figure 27(a). The left side of the domain represents the inland boundary with a constant seaward freshwater flux, and the right side, a coastal boundary with a constant seawater head. For the fluxes, the first subscript, i.e., f or s, indicates water salinity, representing freshwater or seawater, respectively. The second subscript, i.e., 0 or L, gives a spatial distinction, representing the seaward boundary or inland boundary, respectively. The superscript 0 or $'$ give a temporal distinction, representing the initial or final value, respectively. The sign convention adopted for the fluxes is such that the direction towards the sea is positive. The toe position is measured from the coastal boundary. At the steady-state, the freshwater flux at the inland boundary Q_{fL}^{0} [L^2/T] is equal to the freshwater outflow into the sea at the coastal boundary Q_{f0}^{0} [L^2/T]. To simulate the moving interface, we assume an abrupt change in the freshwater flux at the inland boundary from Q_{fL}^{0} to Q_{fL}', resulting in unsteady flow conditions that cause the interface to move until the new equilibrium is reached. During this transition, the freshwater outflow into the sea $Q_{f0}(t)$ gradually changes from Q_{fL}^{0} to Q_{fL}'. We are interested in the time taken for this

change to occur. $Q_{s0}(t)$ [L^2/T] is the net seawater flux to the sea at any time t. $Q_f(x,t)$ [L^2/T] and η *(x,t)* [L] are the seaward freshwater flux and the depth of the interface measured from the top of the aquifer, respectively, at a distance x from the coastal boundary and at time t. $X(t)$ represents the toe position (the point where the interface meets the base of the aquifer).

The distribution of the flux over the seawater wedge affects the hydraulic head distribution which controls the interface shape and location. With the assumption of the linear variation of $Q_f(x,t)$ between the toe location and coastal boundary, the interface profile can be explicitly described in terms of the seaward freshwater outflow $Q_{f0}(t)$ only. Because the rate of the movement of the interface is controlled by $Q_{f0}(t)$ through the continuity of the flux, we can then derive the explicit solution for the timescale of the interface movement based on the solution for transient $Q_{f0}(t)$.

Bear (1972) derived an implicit solution (Eq. 90) for the transient freshwater outflow at the coastal boundary, $Q_{f0}(t)$, under the influence of an abrupt change in the freshwater flux at the inland boundary (from Q_{fL}^0 to Q'_{fL}). The derivation is briefly summarized in Appendix G. Their solution is based on the Dupuit approximation and the method of successive steady states (Kochina, 1962):

$$\frac{6t}{nK\varepsilon/B^3} = \frac{1}{{Q'_{fL}}^2} ln\frac{Q_{f0}(t)}{Q_{f0}^0} - \frac{1}{Q'_{fL}}\left(\frac{1}{Q_{f0}\,(t)} - \frac{1}{Q_{fo}^0}\right) - \frac{1}{{Q'_{fL}}^2} ln\frac{Q'_{fL}-Q_{f0}(t)}{Q'_{fL}-Q_{f0}^0} \qquad (90)$$

where n [-] is the porosity, K [L/T] is the hydraulic conductivity, ε [-] is the density ratio given by $\frac{\rho_s-\rho_f}{\rho_f}$, ρ_s [M/L^3] is the density of seawater, ρ_f [M/L^3] is the density of freshwater,

and B [L] is the depth of the aquifer. The hydraulic conductivity is assumed to be the same for both freshwater and seawater. The hydrostatic equilibrium at the interface defines the shape of the interface for a given $Q_{f0}(t)$:

$$\eta^2(x,t) = \left[\frac{2Q_{f0}(t)}{K\varepsilon}\right] x \tag{91}$$

The toe position $X(t)$ is obtained by substituting η with B in the above equation:

$$X(t) = \frac{K\varepsilon B^2}{2Q_{f0}(t)} \tag{92}$$

We use the timescale definition suggested by Watson et al. (2010) and adopted by Lu and Werner (2013), which describes a representative toe-response timescale as the time to reach 95% of the new steady state. As the transition from one steady-state to another is often characterized by the toe movement, the timescale can be defined as the time for the toe to travel a distance equal to 95% of the total toe-response distance. Thus, the toe position (X^T) corresponding to the toe-response timescale is given by:

$$X^T = X^0 + 0.95(X' - X^0) \tag{93}$$

where X^0 [L] is the initial toe position, and X' [L] is the final toe position at the steady-state after the change in the boundary condition.

Substituting the toe position expression from Eq. (92) into Eq. (93) yields:

$$\frac{K\varepsilon B^2}{2Q_{f0}(T)} = \frac{K\varepsilon B^2}{2Q_{fL}^0} + 0.95\left(\frac{K\varepsilon B^2}{2Q_{fL}'} - \frac{K\varepsilon B^2}{2Q_{fL}^0}\right) \tag{94}$$

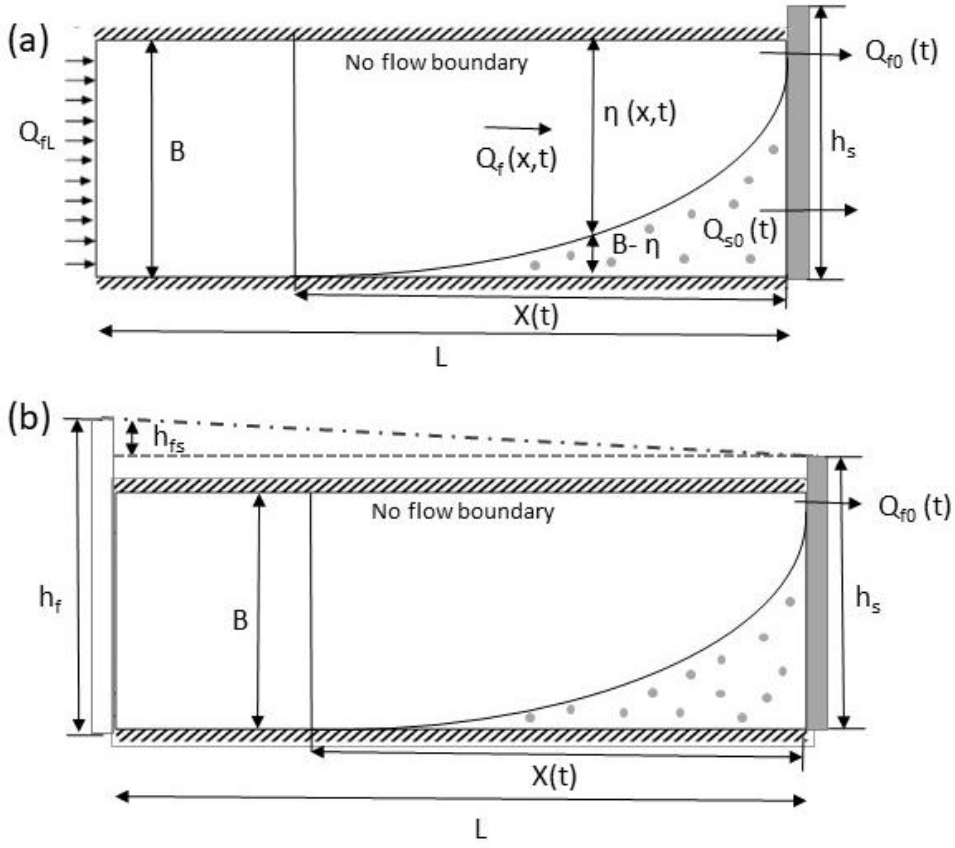

Figure 27 - Conceptual model for the (a) specified-flux boundary case, modified from Bear (1972); (b) specified-head boundary case

where T is the toe-response timescale.

Simplifyingthe above equation gives:

$$Q_{f0}(T) = \frac{1}{\frac{1}{Q_{fL}^0}+0.95\left(\frac{1}{Q'_{fL}}-\frac{1}{Q_{fL}^0}\right)} \tag{95}$$

By substituting $Q_{f0}(T)$ from the above equation into Eq. (90), we get an expression for T as:

$$T = \frac{nKB^3\varepsilon}{6(Q'_{fL})^2}\left(ln\frac{\beta}{\beta+0.95(1-\beta)} - \frac{0.95(1-\beta)}{1} - ln\frac{\beta-\frac{\beta}{\beta+0.95(1-\beta)}}{\beta-1}\right) \tag{96}$$

where β [-] is the ratio of the final freshwater flux to the initial freshwater flux at the inland boundary ($\beta = Q'_{fL}/Q^0_{fL}$), which is greater than 1 for SWR and less than 1 for SWI. Note that the above equation is not applicable to the condition of $\beta = 1$ (i.e., the boundary condition does not change).

Interestingly, we found that the complicated part of Eq. (96), namely, $E = ln\frac{\beta}{\beta+0.95(1-\beta)} - \frac{0.95(1-\beta)}{1} - ln\frac{\beta-\frac{\beta}{\beta+0.95(1-\beta)}}{\beta-1}$, can be converted into a simple linear expression $E = 0.95\,\beta + 2.046$ (see Appendix H). Hence, we can rewrite Eq. (96) in a simplified form:

$$T = \frac{nKB^3\varepsilon}{6\,{Q'_{fL}}^2}\left(0.95\,\frac{Q'_{fL}}{Q^0_{fL}} + 2.046\right) \tag{97}$$

Eq. (97) is a simple analytical solution in an explicit form for the timescale associated with the interface movement in response to an abrupt change in the specified-flux boundary.

Based on Eq. (97), we can conveniently extend the timescale solution for the specified-flux boundary case to the specified-head boundary case by expressing freshwater flux at the inland boundary in terms of the hydraulic heads using the relationship derived by Lu et al. (2015). For a 2-D vertical section of a homogeneous, isotropic, confined aquifer, as shown in Figure 27(b), the left side of the domain represents a specified-head inland boundary and the right side represents a specified-head coastal boundary. The head at the coastal boundary is h_s [L]. The initial head at the inland boundary and the initial head difference across the aquifer are represented as h_f^0 [L] and h_{fs}^0 [L], respectively. To simulate the moving interface, we assume an abrupt change in the inland-boundary head from h_f^0 to h_f'. L [L] and B [L] represents the length and depth of the aquifer, respectively. Lu et al. (2015) introduced a simple correction to the coastal heads as given in Eq. (98).

$$h_s^* = (1+\varepsilon)h_s - \frac{\varepsilon}{2}B \tag{98}$$

where h_s^* is the corrected coastal boundary head. We obtain the freshwater flux using corrected coastal boundary heads as:

$$Q_{fL} = KB\left(\frac{h_f - h_s^*}{L}\right) \tag{99}$$

By substituting Eqs. (98) and (99) into Eq. (97), we get an explicit analytical solution for the timescale for a specified-head boundary case:

$$T = \frac{nBL^2\varepsilon}{6K\left(h_f' - (1+\varepsilon)h_s + \frac{\varepsilon}{2}B\right)^2}\left(0.95\,\frac{h_f' - (1+\varepsilon)h_s + \frac{\varepsilon}{2}B}{h_f^0 - (1+\varepsilon)h_s + \frac{\varepsilon}{2}B} + 2.046\right) \tag{100}$$

To shorten the form of the equation, we rewrite the above equation as:

$$T = \frac{nBL^2\varepsilon}{6K\left(h_{fs^*}'\right)^2}\left(0.95\,\frac{h_{fs^*}'}{h_{fs^*}^0} + 2.046\right) \tag{101}$$

where $h_{fs^*} = h_f - h_s^* = h_f - (1+\varepsilon)h_s + \frac{\varepsilon}{2}B$

7.2.1.1 Quantification of Temporal Asymmetry

Analytical solutions, Eqs. (97) and (101), suggest that the toe responses during SWI and SWR are temporally asymmetrical. To quantify this asymmetry, we express the timescale equations for SWI and SWR, for the specified-flux boundary case. Q_H and Q_L represent two specific values of Q_{f0} such that $Q_H > Q_L$. The SWI and SWR cases involve Q_{f0} changing from Q_H to Q_L and Q_L to Q_H, respectively. The timescale equations are given as:

$$T_{SWI} = \frac{nKB^3\varepsilon}{6Q_L^2}\left(0.95\frac{Q_L}{Q_H} + 2.046\right) \tag{102}$$

$$T_{SWR} = \frac{nKB^3\varepsilon}{6Q_H^2}\left(0.95\frac{Q_H}{Q_L} + 2.046\right) \quad (103)$$

By dividing Eq. (102) by Eq. (103), we get the ratio of the SWI timescale to the SWR timescale, R_T, as:

$$R_T = \frac{T_{SWI}}{T_{SWR}} = \frac{0.95 + 2.046\,\sigma}{0.95 + 2.046/\sigma} \quad (104)$$

where $\sigma = \frac{Q_H}{Q_L} > 1$

This ratio is termed as the temporal asymmetry index, representing the resilience of a coastal aquifer in response to the SWI. Similarly, the temporal asymmetry index can be defined for the specified-head boundary case. h_H and h_L represent two specific values of head h_f [L] at the inland boundary such that $h_H > h_L$. The SWI and SWR processes are driven by changes to h_f, namely, h_H to h_L for SWI and h_L to h_H for SWR. The resulting equation for R_T is given by Eq. (104), except with $\sigma = \frac{h_H - h_S^*}{h_L - h_S^*}$.

The numerator in Eq. (104) is clearly greater than the denominator ($R_T > 1$), implying that T_{SWI} is greater than T_{SWR}, or in other words, the toe retreat is faster than the toe advance in both the specified-flux and specified-head boundary cases. This adds to the previous finding of temporal disparity observed in numerical (Lu and Werner, 2013; Watson et al., 2010) and laboratory (Chang and Clement, 2012) studies.

7.2.1.2 Dimensionless timescale

We can also express the timescale solution in the dimensionless form. By rearranging Eq. (97) for the specified-flux boundary case or Eq. (101) for the specified-head boundary case, we get:

$$\tau = \frac{T}{T^*} = \frac{1}{\beta^2}(0.95\beta + 2.046) \tag{105}$$

where the dimensionless timescale, τ, is normalized by $T^* = nKB^3\varepsilon/6{Q^0}_{fL}{}^2$ in the specified-flux boundary case or $T^* = nL^2B\varepsilon/6K{h^0_{fs^*}}^2$ in the specified-head boundary case. The dimensionless timescale shows the important relationships between the interface movement timescales and hydrogeological conditions.

7.2.2 Comparison with Numerical Results

To verify analytical solutions, Eqs. (97) and (101), we numerically solved the problems represented by the conceptual models shown in Figure 27, using SEAWAT, a MODFLOW/MT3DMS-based computer program designed to simulate three-dimensional variable-density flow (Langevin et al., 2003). The spatial discretization was determined according to the criteria based on Grid Peclet number [-] (Voss and Souza, 1987).

$$Pe = \frac{v\,\Delta x}{D_m + \alpha_L v} \approx \frac{\Delta x}{\alpha_L} \leq 4 \tag{106}$$

where v [L/T] is the average pore velocity, Δx [L] is the grid spacing, D_m [L^2/T] is the molecular diffusion coefficient, and α_L [L] is the longitudinal dispersion coefficient.

Lu and Werner (2013) suggested that the relationships between the timescales and the final head differences (between inland and coastal boundaries) for SWI can be described using simple log-linear equations. We used a similar log-log plot between the timescale and the final specified-flux or head at the inland boundary to compare the analytical and numerical timescales in Figure 28 and Figure 29 for the specified-head and specified-flux boundary cases, respectively. For the specified-head boundary case, we solved the scenarios presented by Lu and Werner (2013) with a wide range of hydrogeological parameters and boundary conditions. Figure 28 shows the comparison for a specific set of aquifer parameters (summarized in Table 9) and a range of boundary conditions (summarized in Table 10). For SWI, the logarithmic timescales ($\ln T_{SWI}$) are plotted against the final boundary-head differences ($\ln h'_{fs}$) for different changes in the head at the inland boundary (Δh_f). For SWR, the logarithmic timescales ($\ln T_{SWR}$) are plotted against the final boundary-head differences ($\ln h'_{fs}$) for different initial head values at the inland boundary (h_f^0).

Similarly, Figure 29 compares the numerical and analytical results for SWI and SWR in the specified-flux boundary case. For a specific set of aquifer parameters listed in Table 11, we numerically simulated 12 scenarios with different boundary conditions (summarized in Table 12).

Table 9 - Aquifer parameters for the specified-head boundary case

Input parameters	Values
Porosity, n	0.3
Aquifer length, L	1000 m
Aquifer depth, B	30 m
Fluid density of seawater, ρ_s	1025 kg/m^3
Fluid density of freshwater, ρ_f	1000 kg/m^3
Hydraulic conductivity, K	10 m/d
Longitudinal dispersivity, α_L	1 m
Transverse dispersivity, α_T	1/10 of α_L

Table 10 - Inland boundary head values (m) for the specified-head boundary case

Interface Advance						Interface Retreat			
h'_{fs}	Δh_f=0.1	Δh_f=0.25	Δh_f=0.5	Δh_f=0.75	Δh_f	h^0_{fs}=0.75	h^0_{fs}=1	h^0_{fs}=1.25	h^0_{fs}=1.5
	h^0_{fs}	h^0_{fs}	h^0_{fs}	h^0_{fs}		h'_{fs}	h'_{fs}	h'_{fs}	h'_{fs}
0.75	0.85	1	1.25	1.5	0.1	0.85	1.1	1.35	1.6
1	1.1	1.25	1.50	1.75	0.25	1	1.25	1.5	1.75
1.25	1.35	1.5	1.75	2	0.5	1.25	1.5	1.75	2
1.5	1.6	1.75	2	2.25	0.75	1.5	1.75	2	2.25
1.75	1.85	2	2.25	2.5	1	1.75	2	2.25	2.5
2	2.1	2.25	2.5	2.75	1.25	2	2.25	2.5	2.75
2.25	2.35	2.5	2.75	3	1.5	2.25	2.5	2.75	3
					2	2.75	3	3.25	3.5

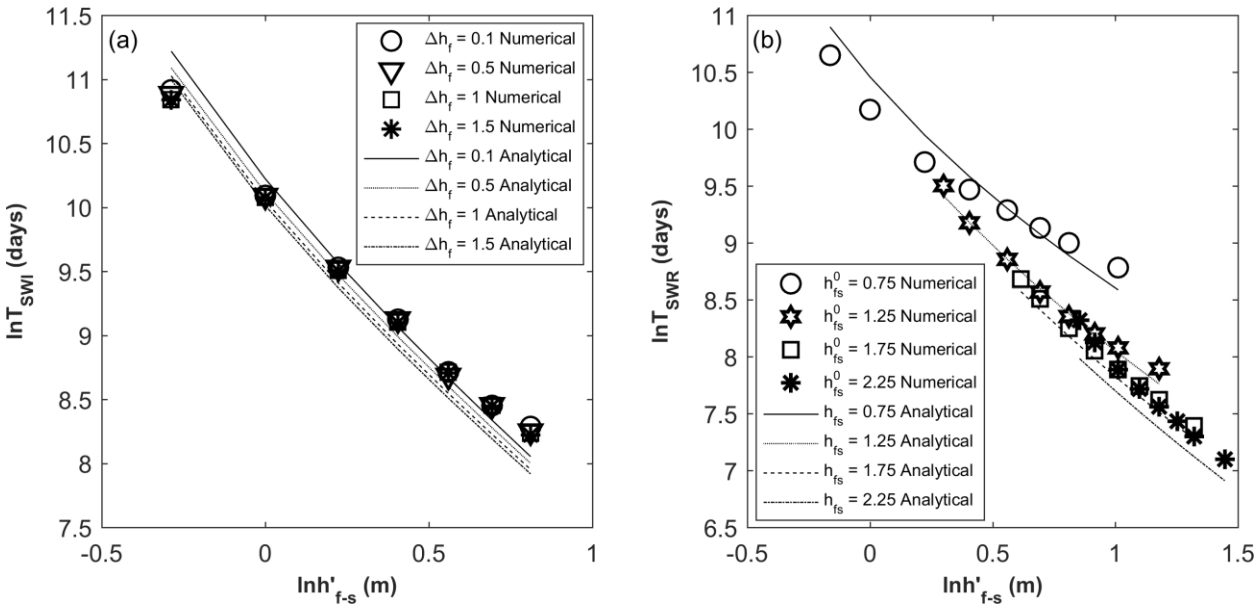

Figure 28 - Comparison of analytical and numerical results for (a) SWI and (b) SWR timescales for the specified-head boundary case

Table 11 - Aquifer parameters for the specified-flux boundary case

Input parameters	Values
Porosity, n	0.2
Aquifer length, L	1000 m
Aquifer depth, B	30 m
Fluid density of seawater, ρ_s	1025 kg/m^3
Fluid density of freshwater, ρ_f	1000 kg/m^3
Hydraulic conductivity, K	10 m/d
Longitudinal dispersivity, α_L	1 m
Transverse dispersivity, α_T	1/10 of α_L

Table 12 - Inland boundary flux values (m2/d) in the specified-flux boundary case

Interface Advance				Interface Retreat			
Q'_{fL}	$Q^0{}_{fL}$= 0.7	$Q^0{}_{fL}$=0.8	$Q^0{}_{fL}$= 0.9	Q'_{fL}	$Q^0{}_{fL}$= 0.3	$Q^0{}_{fL}$= 0.4	$Q^0{}_{fL}$= 0.5
	ΔQ_f	ΔQ_f	ΔQ_f		ΔQ_f	ΔQ_f	ΔQ_f
0.3	0.4	0.5	0.6	0.6	0.3	0.2	0.1
0.4	0.3	0.4	0.5	0.7	0.4	0.3	0.2
0.5	0.2	0.3	0.4	0.8	0.5	0.4	0.3
0.6	0.1	0.2	0.3	0.9	0.6	0.5	0.4

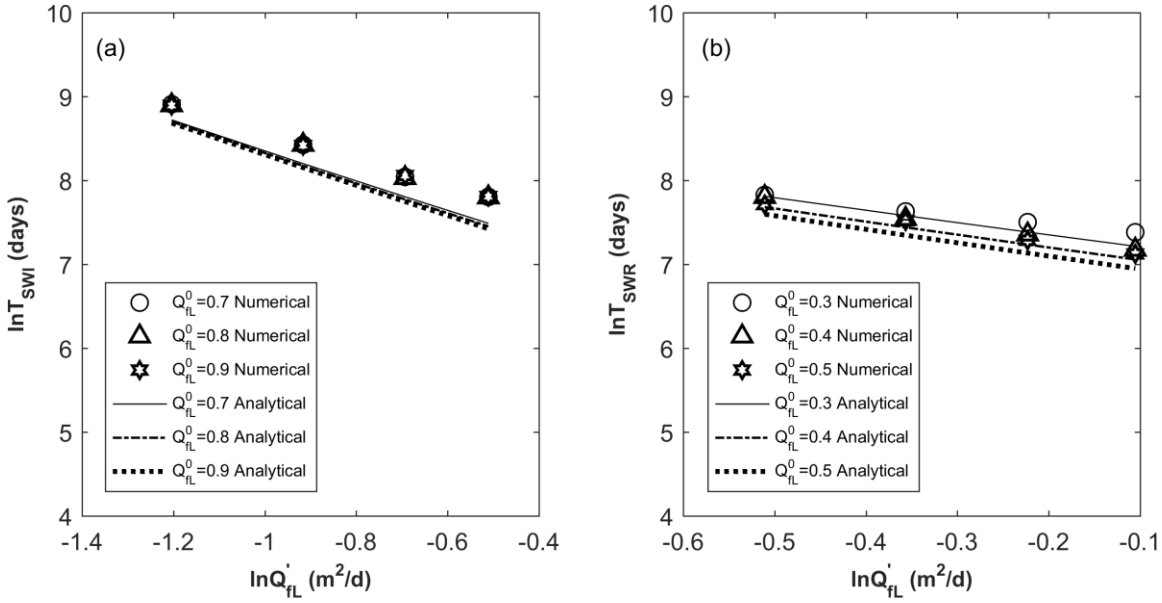

Figure 29 - Comparison of analytical and numerical results for (a) SWI and (b) SWR timescales for the specified-flux boundary case; lnT vs lnQ'_{fL} for different Q^0_{fL}

Overall, analytical solutions agree well with numerical results. Small deviations maybe because of the assumption that the seawater-freshwater interface instantaneously responses to the changes in the freshwater outflow into the sea. In reality, however, a time lag exists between a change in the freshwater outflow and in the interface profile. Another possible reason may be the sharp-interface approximation, which does not consider dispersive effects (Pool and Carrera, 2011). Kiro et al. (2008), however, argued that the sharp-interface approximation is reasonable for studying the transience of the interface movement at a large spatial scale. We also conducted numerical simulations for doubled dispersivity values and found that the change in the timescale value was less than 5% for both SWI and SWR, indicating the relative insensitivity of toe-response timescales to the dispersivity values for the considered range of aquifer parameters. In addition, the derived analytical solutions show that the relationship between the timescale and final boundary condition value is not perfectly log-linear as suggested by Lu and Werner (2013).

7.2.3 Analysis and Discussion

7.2.3.1 Dynamics Controlling the Timescale

The timescale of the toe movement in response to an abrupt change in the boundary conditions is controlled by the distance and rate of the toe movement. For the successive steady-state, the toe-response distance can be determined by the hydrostatic equilibrium across the interface in agreement with the hydraulic gradient, and the movement rate is controlled by the resultant seawater flux at the coastal boundary, which can be determined by the flow continuity in the aquifer.

Since the freshwater outflow at the coastal boundary Q_{f0} is equal to the inflow flux at the inland boundary Q_{fL} at the large-time steady state, the difference between them during the interface movement can be a good measure of the degree of disequilibrium. Prior to an abrupt change in the inland boundary condition, the system is in equilibrium (i.e., $Q_{fL} = Q_{f0}$), and $Q_{s0} = 0$ (i.e., the seawater volume in the aquifer remains constant). An instantaneous change in Q_{fL} results in the disequilibrium with the degree of $\Delta Q = Q'_{fL} - Q^0_{fL}$, which leads to an instantaneous increase in Q_{s0} from zero to ΔQ to satisfy the flow continuity. Driven by the disequilibrium ΔQ, Q_{f0} gradually changes along with the corresponding interface movement to maintain hydrostatic equilibrium. The interface moves at the rate for which the resulting seawater flux (described by the rate of the seawater volume change as a consequence wedge movement, $\frac{ndU_s(t)}{dt} = Q_{s0}$) satisfies the condition of flow continuity at the coastal boundary ($Q_{s0} = Q'_{fL} - Q_{f0}$), as also depicted in Figure 30.

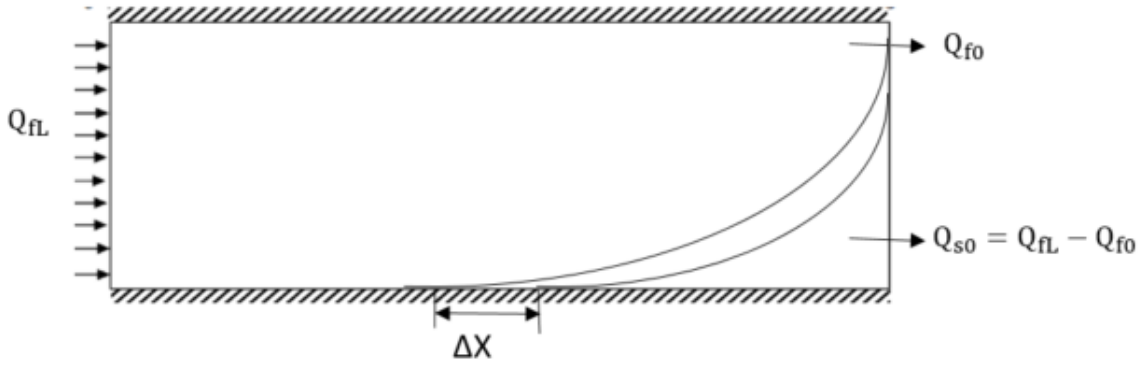

Figure 30 - Schematic representation of the freshwater flux at the inland boundary, freshwater and seawater fluxes at the coastal boundary in the specified-flux boundary case

7.2.3.2 Temporal Asymmetry Between SWI and SWR

We can conveniently explain the temporal asymmetry between SWI and SWR through the framework discussed above. During SWI, the degree of the disequilibrium is maximum ($\Delta Q = Q'_{fL} - Q^0_{fL}$) right after the abrupt change at the inland boundary, resulting in the maximum magnitude of both Q_{s0} and the rate of the interface movement. However, interface profiles corresponding to higher initial Q_{f0} values are more vertical and have shorter toe displacements (ΔX) per unit change in Q_{f0}. When the system is about to reach the new equilibrium, the degree of the disequilibrium and Q_{s0} are small but the toe displacements are longer corresponding to the smaller final Q_{f0} values. This essentially means that during SWI, longer toe displacements are traveled at lower rates and shorter toe displacements are traveled at higher rates. While in the SWR case this trend is reversed, i.e., longer toe displacements are traveled at higher rates and shorter toe displacements are traveled at lower rates (see Figure 31). Since the total toe displacement distance is the same in both cases for two given bounding steady states, the time taken by the toe to advance into the aquifer is longer than the time to recede into the sea, resulting in the temporal asymmetry between SWI and SWR. The non-dimensional forms of the variables of interest can help to generalize the analysis (Chang and Clement, 2013; Smith, 2004a). We present Q_{s0} and ΔX in non-dimensional forms, Q^*_{s0} and ΔX^*, respectively, where, Q_{s0} is normalized by its maximum value ΔQ, and ΔX is normalized by the total toe displacement. For a specific case with inland-boundary flux values of 0.3 and 0.6 m^2/d, and aquifer parameters listed in Table 11, we present Q^*_{s0} vs ΔX^* in Figure 31, showing the temporal disparity between SWI and SWR.

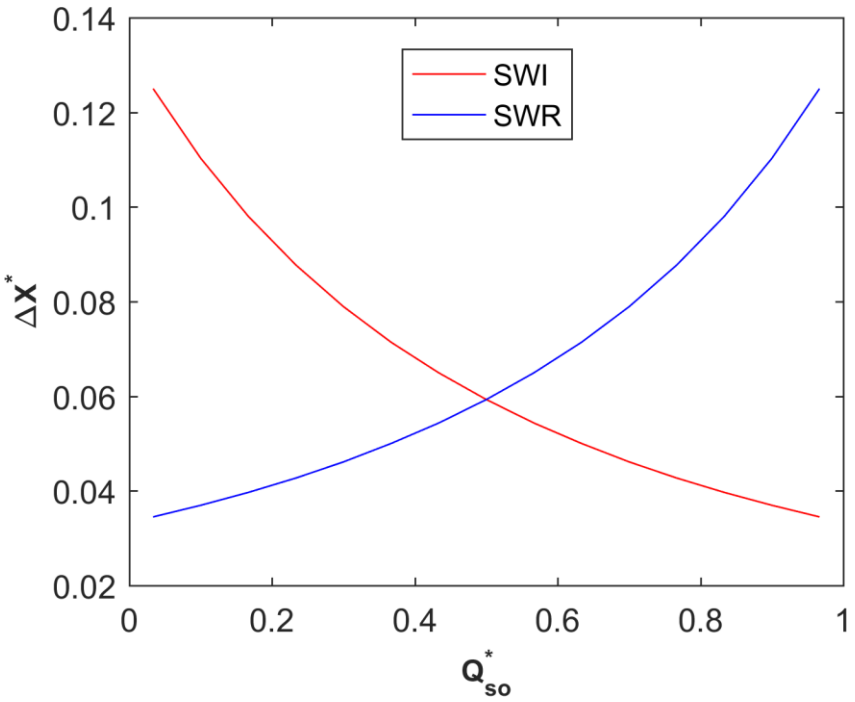

Figure 31 - Non-dimensional toe displacements vs corresponding non-dimensional net seawater flux (also representing the rate of the seawater wedge movement) in response to an abrupt change in the freshwater flux at the inland boundary (0.6 m^2/d to 0.3 m^2/d for SWI and 0.3 m^2/d to 0.6 m^2/d for SWR)

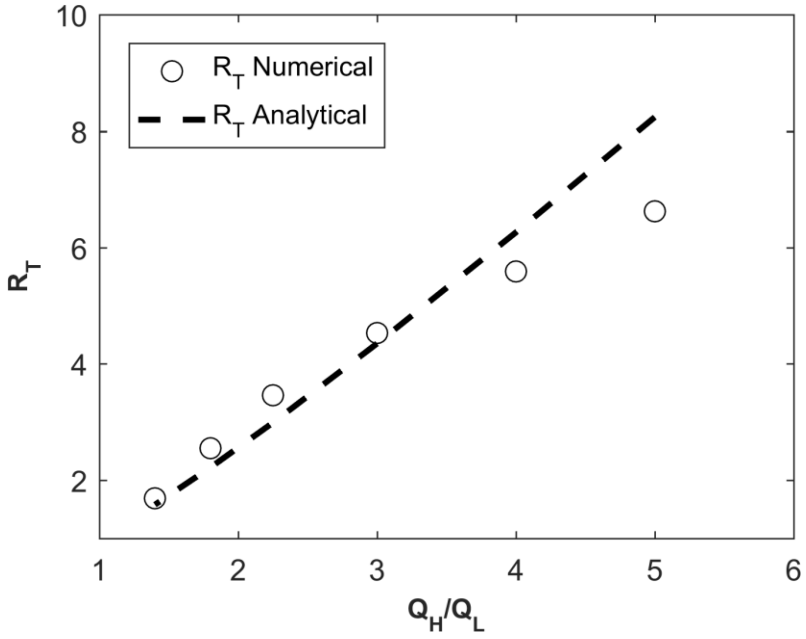

Figure 32 - Comparison of the temporal asymmetry index, R_T obtained analytically and numerically for different ratios of higher to lower inland boundary fluxes (Q_H/Q_L)

Eq. (104) quantifies the temporal asymmetry index R_T for the specified-flux boundary case and describes its relationship with the changing flux at the inland boundary. Figure 32 shows a good agreement between the numerical and analytical results of R_T for Q_H/Q_L values less than 4. Discrepancy at high ratios of Q_H/Q_L could be due to the potentially significant impact of dispersive mixing on the interface movement, which is ignored in our analytical solution.

Eq. (104) also suggests that aquifer parameters do not influence R_T. Table 13 shows the R_T values estimated from numerical simulations for aquifer systems with four different sets of parameters. Q_H and Q_L values are constant (0.7 m^2/d and 0.5 m^2/d, respectively) in all cases. The numerical results confirm that R_T is predominantly governed by boundary conditions and insignificantly influenced by other hydrogeological parameters in the specified-flux boundary case. R_T for the specified-head boundary case has a similar form as that for the specified-flux boundary case (Eq. 104). However, σ in the specified-head boundary case is also dependent on B, which makes the temporal asymmetry dependent of the aquifer depth, unlike the specified-flux boundary case.

Table 13 - Aquifer systems with different parameters and respective R_T values estimated using numerical simulations

	Case-1	Case-2	Case-3	Case-4
Hydraulic conductivity, K (m/d)	10	5	30	1
Porosity, n (-)	0.2	0.3	0.2	0.5
Aquifer Length, L (m)	1000	1000	500	500
Aquifer Depth, B (m)	30	30	25	100
Transverse Dispersivity, α_T (m)	0.1	0.2	0.1	0.1
R_T	1.70	1.73	1.73	1.80

7.2.4 Effects of Inland-Boundary Condition and Aquifer Parameters on the Timescale

We further explore the log-linearity of the timescale with respect to the freshwater flux at the inland boundary using the dimensionless timescale equation for the specified-flux boundary case. By taking the logarithm of both sides of Eq. (105), we get:

$$log\,\tau = -2\,log\,\beta + log(0.95\beta + 2.046) \tag{107}$$

Figure 33 shows the variation of $\log\tau$ with $\log\beta$ obtained analytically and numerically for a typical range of β from 0.01 to 100, whereby the freshwater flux decreases to only 1% of or increases to 100 times the original value. As evidenced by Eq. (107) and seen in Figure 33, the relationship is not perfectly linear over the entire range, but maybe approximated by two linear functions with different slopes for SWI and SWR, respectively. In fact, for the cases of large changes in the boundary flux, i.e., $\beta \ll 1$ for SWI and $\beta \gg 1$ for SWR, Eq. (107) implies that the relation tends to be linear with the slope equal to -2 and -1, respectively.

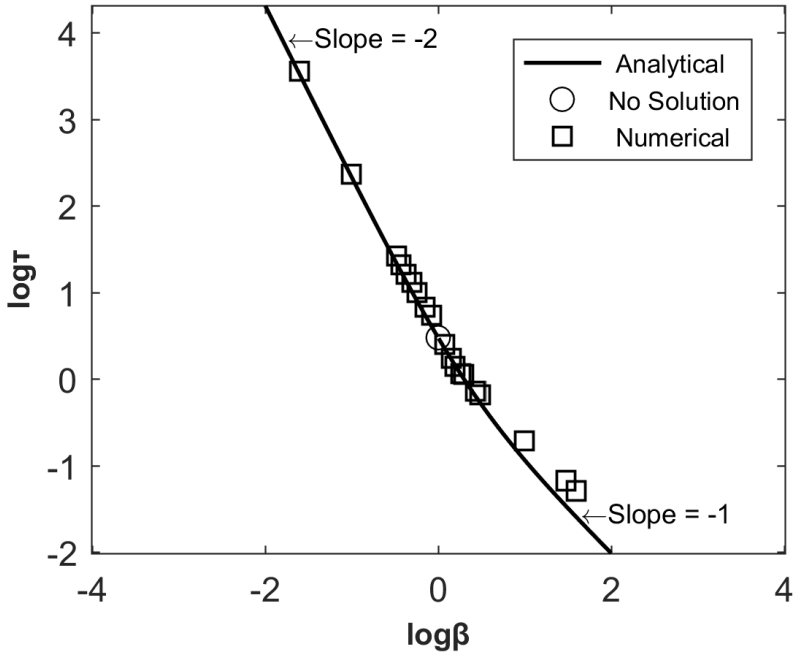

Figure 33 - Logarithmic τ vs logarithmic β obtained analytically and numerically for the specified-flux boundary case

7.2.5 Sensitivity of Timescales

Eqs. (97) and (101) explicitly provide the relationship between different hydrogeological parameters and the toe response timescale. For the specified-flux boundary case, the analytical solution reveals that the timescale increases linearly with the porosity, hydraulic conductivity, density ratio, and cubic aquifer thickness, and is not affected by the sea level and aquifer length. Figure 34 shows sensitivity results from numerical simulations for hydraulic conductivity, aquifer depth and porosity. In addition, numerical simulations were also conducted for different sea levels (30 m, 40 m, and 50 m) and different aquifer length values (1000 m, 2000 m, and 500 m), and the resulting timescales were almost the same in all cases.

For a specified-head boundary case, the analytical solution reveals that the timescale is directly proportional to the porosity, aquifer thickness, density ratio, coastal-boundary head, and squared aquifer length, and is inversely proportional to the hydraulic conductivity. Figure 35 compares the sensitivity results of SWI and SWR timescales obtained from the derived explicit analytical solution Eq. (101) and numerical simulations results obtained by Lu and Werner (2013) for a specified-head boundary case. The analytical solution matches the numerical results of sensitivities with good accuracy.

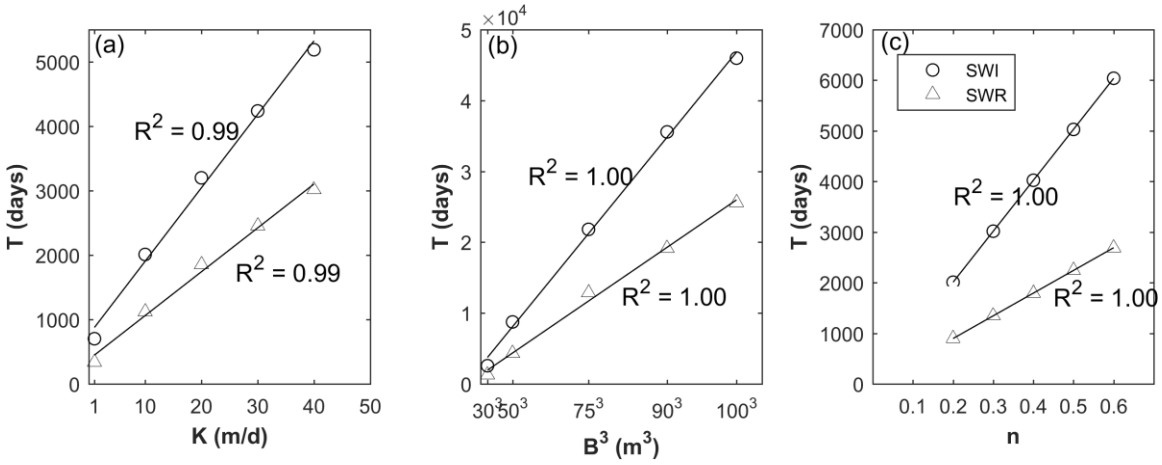

Figure 34 - Variation of the toe-response timescale with (a) hydraulic conductivity; (b) cubic depth; and (c) porosity, for SWI and SWR in the specified-flux boundary case

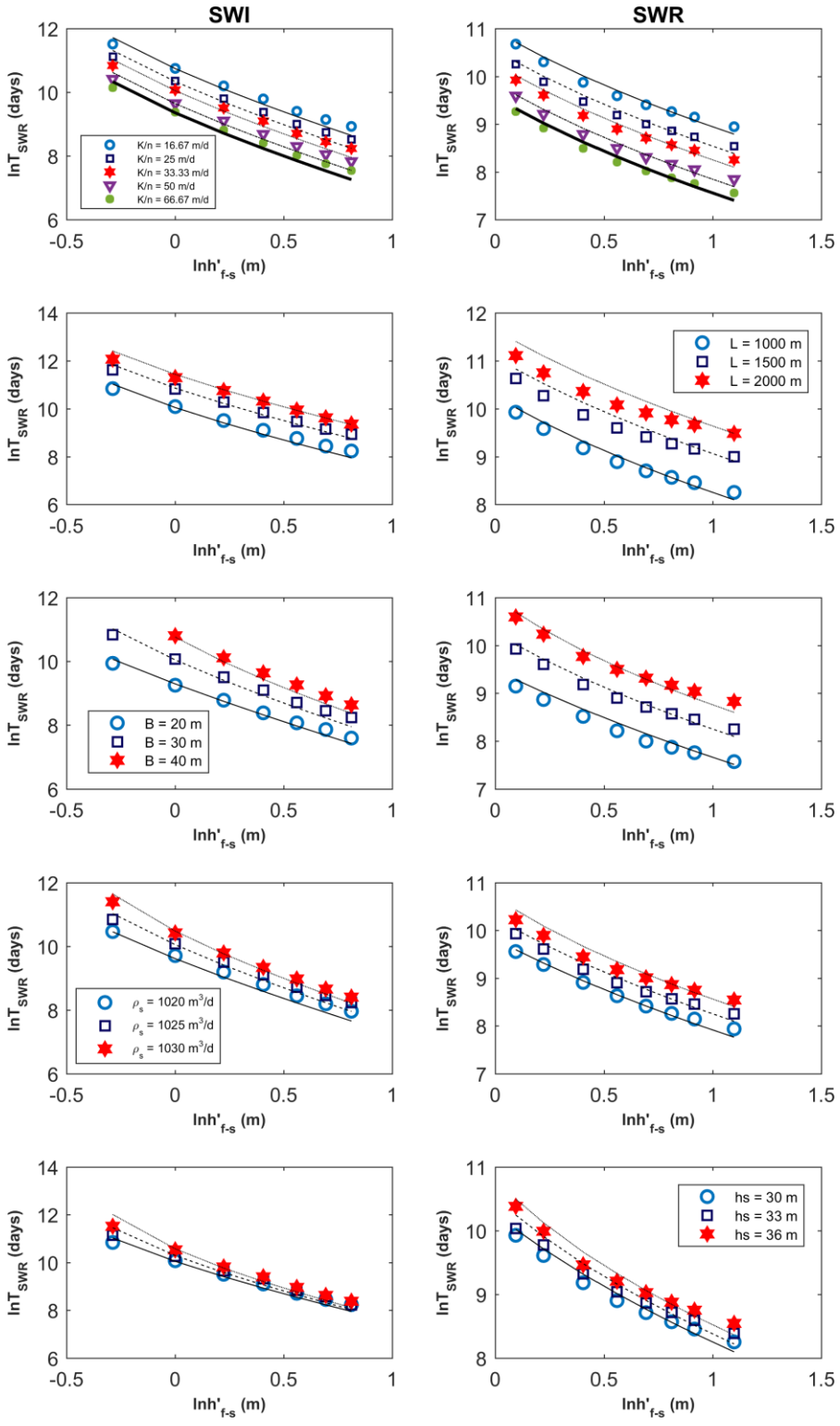

Figure 35 - Sensitivity of the SWI and SWR timescales to different aquifer parameters and boundary conditions; Lines- Analytical Eq. (12), Points - Numerical (Lu and Werner, 2013)

As discussed we explained based on the dynamics of SWI, the effects of different aquifer parameters on the timescales can be understood by analyzing their effects on: i) the head-gradient controlling the toe location in accordance with the hydrostatic equilibrium across the interface; and ii) flow continuity controlling the rate of the interface movement. Porosity n and aquifer thickness B have similar effects on the timescale for both specified-flux and specified-head boundary cases. An increase in n or B will not only increase the total volume of seawater to be displaced to reach the new steady-state but also the volume of seawater displaced per unit displacement of the seawater wedge. This results in the slower movement of the wedge to maintain flow continuity, thus a longer timescale. In the specified-flux boundary case, the timescale is directly proportional to K whereas in the specified-head boundary case, the timescale is inversely proportional. In the specified-flux boundary case, an increase in K decreases the hydraulic gradient. The lower hydraulic gradient results in a shallower interface angle and a longer toe response distance, thus a longer timescale. In the specified-head boundary case, a higher K results in a higher degree of disequilibrium in terms of the magnitudes of the freshwater flux, leading to faster wedge movement to yield a higher Q_{s0}, thus a shorter timescale. The aquifer length L and sea level h_s do not affect toe response distance or the toe-travel rate in the specified-flux boundary case, thus do not influence the timescale. In the specified-head boundary case, an increase in h_s or L results in a lower head gradient and thus a longer toe-response distance to satisfy the hydrostatic equilibrium. In addition, a higher h_s or L leads to a lower freshwater flux and a lower degree of disequilibrium, causing the lower travel rate of the interface to satisfy flow continuity. Therefore, the longer toe-distance and a lower rate of the movement of the

interface result in a longer timescale for a higher h_s or L in the specified-head boundary case.

7.3 Numerical and Analytical Analysis of Transient SWI in Stratified Aquifers

7.3.1 Conceptual Model:

We consider a sharp interface in a two-dimensional confined aquifer with uniform thickness and horizontal stratification in the hydraulic conductivity, as shown in Figure 36. The aquifer is bounded by impermeable layers at the top and bottom, and vertical boundaries at the inland and coastal ends. All the discharges are assumed to be horizontal following Dupuit's assumption (Dupuit, 1863) implying that equipotential lines are vertical. Let the origin be at the point where the aquifer base meets the coastline and the x axis along the top of the underlying impervious layer pointing towards the inland and y axis along the vertical coastline pointing upwards. For the discharges, the first subscript (f or s) indicates water salinity (freshwater or seawater, respectively), and the second subscript (0 or L) is a spatial indicator (seaward or inland boundary, respectively). The superscript (0 or ') is a temporal indicator (initial or final, respectively). The abrupt change in the inland boundary discharge (Q_{fL}^{0} $[L^2/T]$ to Q'_{fL} $[L^2/T]$) is assumed to simulate the transient conditions and the moving interface. The key transient variables for our analysis are - freshwater outflow $Q_{f0}(t)$ $[L^2/T]$, the corresponding interface profile $\zeta(x,t)$ $[L]$ and net seawater discharge in any ith layer $Q_{si}(t)$.

L $[L]$ and H_s $[L]$ represent the distance between the inland boundary and the coastal boundary, and the seawater head at the coastal boundary. For a particular ith layer, the

thickness, center elevation, base elevation and the hydraulic conductivity are represented by b_i $[L]$, y_i $[L]$, d_i $[L]$ and K_i $[L/T]$, respectively. B $[L]$ and T $[L^2/T]$ represent the total aquifer thickness and transmissivity, respectively. Note that in this manuscript, by "elevation" we mean elevation with respect to the aquifer base unless specified otherwise.

7.3.2 Numerical Analysis:

We choose toe position as the indicator of the state of the aquifer, hence define timescale as the time taken by the toe to move from the initial to the final steady position. Timescale is essentially governed by two factors (Rathore et al., 2018a): 1) the interface shape and position (controlled by the hydrostatic equilibrium) which defines the volume of intruded seawater, and 2) the rate of the interface movement (controlled by flow-continuity) which defines the net seawater discharge at the coastal boundary. In this section, we study using numerical simulations how stratification affects two governing factors of timescale and the roles of individual layers in the transient response of the aquifer.

We consider a four-layer confined head-controlled aquifer with parameter values as follows: $B = 12$ m, $L = 100$ m, $H_s = 12$ m. longitudinal dispersivity $\alpha_L = 0.1$ m, and transverse dispersivity $\alpha_T = \alpha_L/10$. Each layer is 3 m thick with the hydraulic conductivity values as 60, 30, 15 and 5 m/d, respectively, with total transmissivity $T = 330$ m^2/d. Numerical simulations are conducted using SEAWAT, a MODFLOW/MT3D-based computer program to simulate 3D variable-density flow. From the 24 possible layer arrangements, we consider 4 special layer arrangements. S1 (bottom to top [5 60 30 15]) and S2 ([15 30 60 5]) are cases with TCE is equal to 6 m ($B/2$) same as in the homogeneous

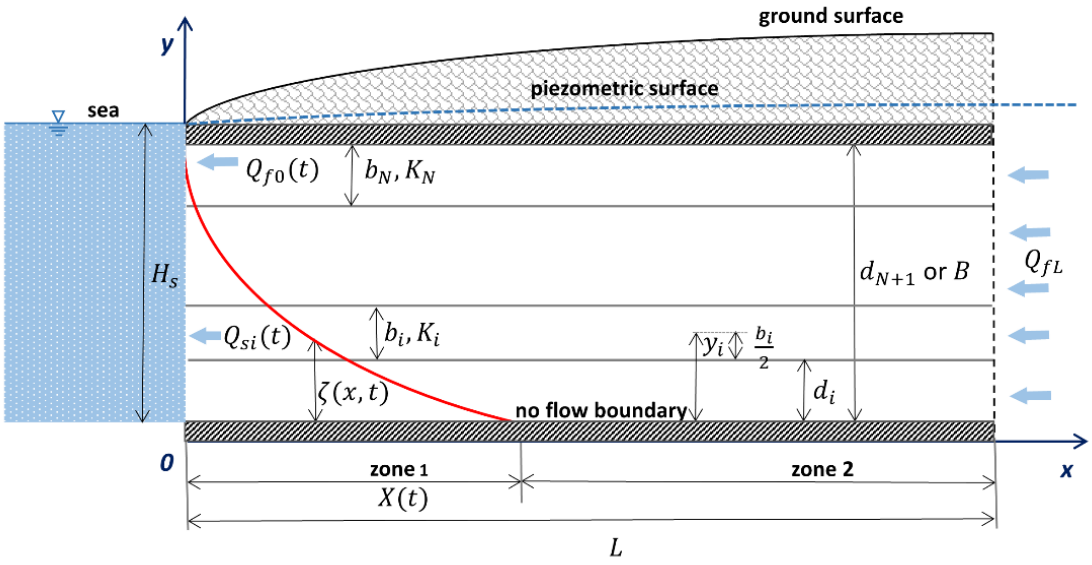

Figure 36 - Conceptual model for the confined stratified aquifer for transient analysis

case with $K = 27.5$ m/day. E1 ([5 15 30 60]) and E2 ([60 30 15 5]) are extreme cases with the highest and lowest TCE values resulting from an ascending and descending layer-transmissivity values, respectively. To simulate the SWI, the inland freshwater head is abruptly dropped from 13 m to 12.75 m, and vice versa for SWR. The resulting timescale values are presented in Table 14 in the increasing order.

Table 14 - Timescales in 5 Special Stratified Cases in the Increasing Order

Case	SWI Timescale (d)	SWR Timescale (d)
E1	31.5	16
Homogeneous	84.5	50
S2	130	79.5
S1	339	190
E2	416	238.5

Aquifer response is fastest in the E1 stratification scenario, which has the lowest volume of the intruded seawater (lowest TCE), and slowest in E2, which has the highest volume of the intruded seawater. Interesting cases are S1, S2, and Homogeneous in which the discharge and toe-position in both the bounding steady states are the same because of the same TCE (Rathore et al., 2018b), but timescales are different - homogenous being the fastest and S1 being the slowest case. To explain this difference and identify the key factor controlling the timescale in stratified aquifers, we take a closer look at the individual layer responses.

To visualize the volume of seawater displaced, we plot in Figure 37, the initial and final interface profiles for each of the five cases described above, where solid and dashed lines represent initial and final interfaces, respectively, in the case of SWI. Corresponding to the overall aquifer response, each layer undergoes a change in the intruded seawater volume, which is dependent on TCE and layer position. Lower layers naturally have higher intruded seawater volume per unit thickness than upper layers because of the wedge shape of the intruded seawater volume. To visualize the discharge in each layer during the transition, we plot in Figure 38, the velocity vectors right after the abrupt lowering in the inland boundary head. The plots are in order of increasing timescale, from the fastest case E1 to the slowest case E2. As seen in Figure 38, during the transition, the seawater discharge in each layer is a function of the layer hydraulic conductivity. Therefore, for a particular layer, given the change in the seawater volume and discharge corresponding to the aquifer response, we can conceptualize a characteristic timescale of the layer response. Higher seawater volume in the layer contributes to longer characteristic layer timescale and higher layer-discharge contributes to the shorter. Overall aquifer response is essentially the

expression of the simultaneous individual layer responses linked together through complex processes and criteria like the continuity of the interface. The layer with the slowest response acts as a bottleneck and eventually decide the total response time of the aquifer. We refer to this layer as the critical layer.

The critical layer will be the layer with high seawater volume and low discharge, or in other words, located close to the bottom of the aquifer and have low hydraulic conductivity, respectively. To visualize the responses of the individual layers, we plot (see Figure 39) the movement of the point on the interface at the center of each layer and toe-position which is our indicator for the overall aquifer response. As we can see, the L1 layer is the slowest layer in all five cases, which governs the toe-response timescale. E1 case has the shortest response timescale because its critical layer has the smallest volume of intruded seawater and highest hydraulic conductivity. As expected, E2 has the longest timescale because of the highest seawater volume and lowest hydraulic conductivity in the critical layer. The interesting comparison is between S1, S2 and Homogeneous cases where despite the same initial and final toe positions, and discharges, the transient-toe movement is very different. Aquifer response (characterized by the toe response) is slowest in S1 and fastest in the homogeneous case which conforms to the response of the critical layer which is also slowest in S1 and fastest in the homogeneous case. It is interesting to see that the response of the L2 layer is fastest in S1 and slowest in the homogeneous case, contrary to the overall aquifer response governed by critical layer response. This is because K in L2 is highest in S1 (60 m/d) and lowest in homogeneous case (27.5 m/d).

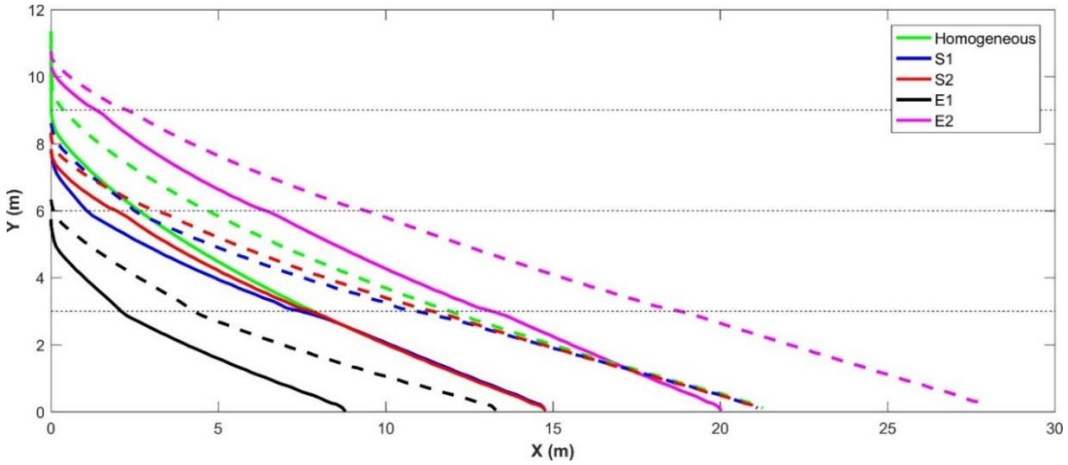

Figure 37 - Initial (solid) and final (dashed) interfaces for five special cases – Homogeneous, S1 S2, E1, E2

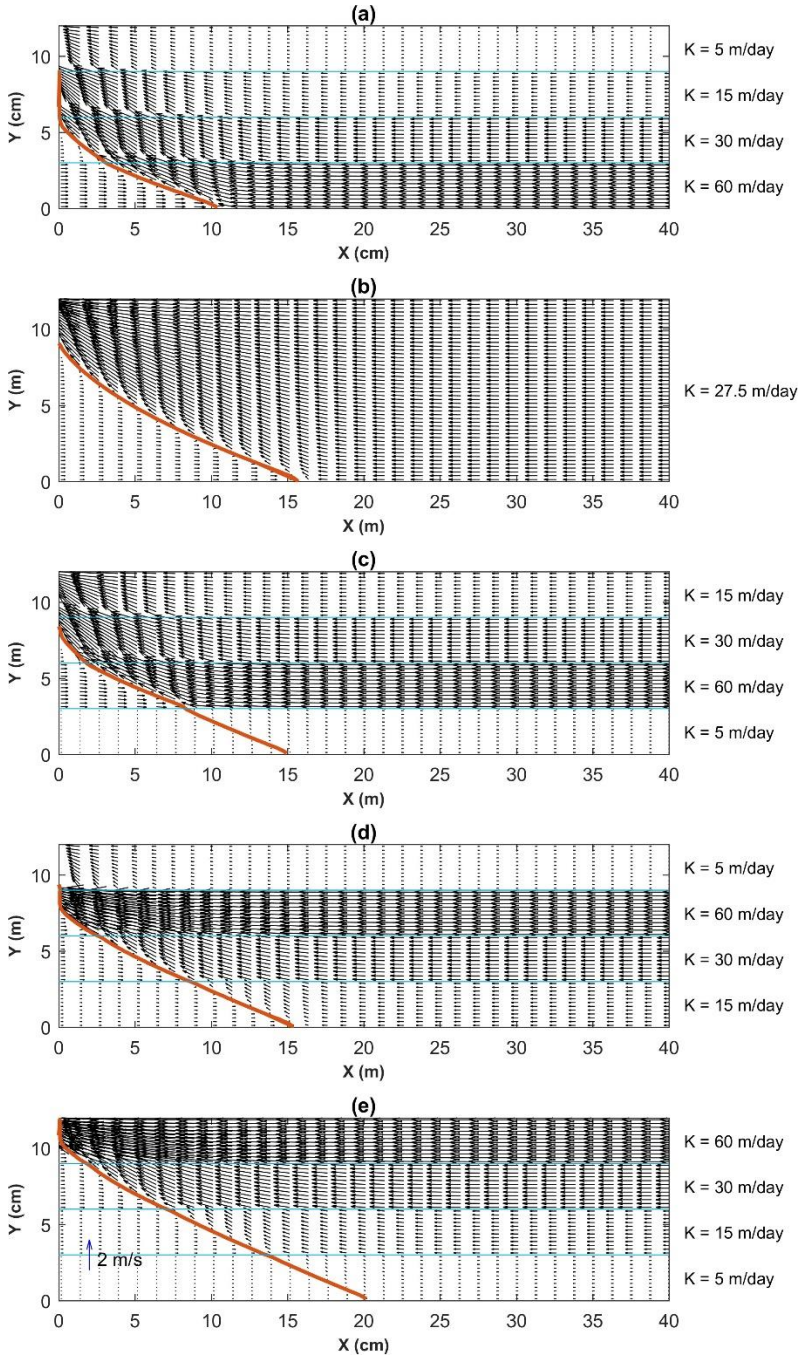

Figure 38 - Interfaces and velocity vectors right after the abrupt boundary change during SWI in (a) E1, (b) Homogeneous, (c) S1, (d) S2, and (e) E2

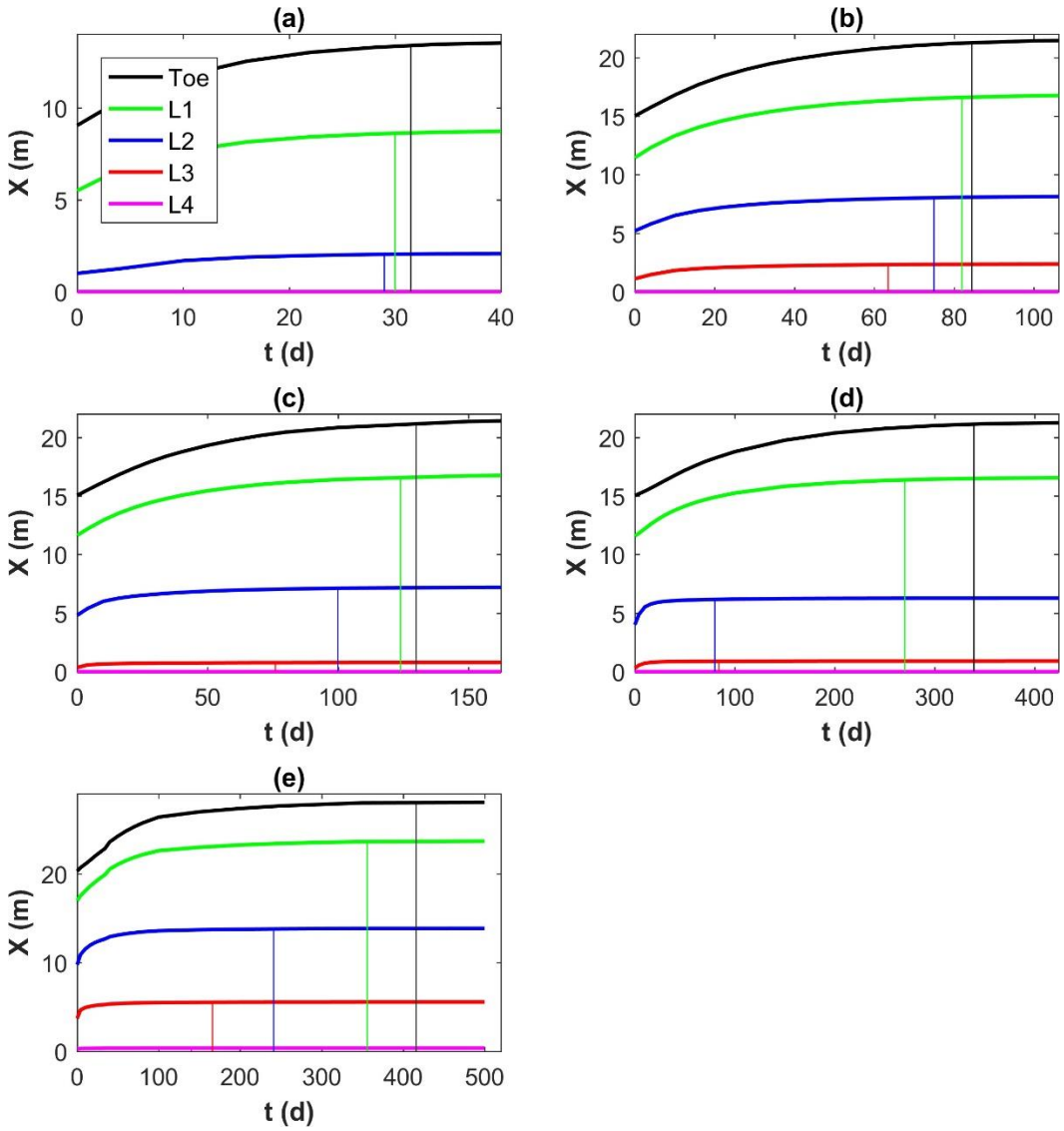

Figure 39 - Individual layer responses characterized by the movement of the center of the interface section in the layer for (a) E1, (b) Homogeneous, (c) S1, (d) S2, and (e) E2

7.3.3 Response Timescale Indicator

We can compute the intruded-seawater volume by integrating the explicit interface profile given by Rathore et al. (2018) (c) to perform a timescale analysis for stratified aquifers, similar to homogeneous aquifers done by Rathore et al. (2018a). However, we need to include the discharge distribution resulting from the stratification instead of uniform discharge across the depth of the seawater wedge as assumed in the homogeneous case (Rathore et al., 2018a). Uniform discharge assumption will lead to a conclusion that layer arrangements with the same TCE will result in the same timescale, which is false as we numerically demonstrated in the previous section that S1, S2 and homogeneous cases have different timescales despite same discharge and toe position.

In this study, our aim is to develop a Response-Timescale Indicator (RTI) which can help us compare the transient responses of different stratification scenarios. We first quantify the characteristic timescale of the individual layers in the form of layer RTIs. Then we propose an RTI for the aquifer representative of all layers which can be used to compare response timescales in different stratification cases.

For a particular layer, the response to an abrupt boundary change is essentially governed by two factors, namely, change in the volume of seawater intruded in the aquifer and net-seawater discharge in the layer corresponding to the boundary change. Net-seawater discharge is equal to the rate of change of seawater volume in the layer. We can write the above volumetric balance for an i^{th} layer as:

$$\frac{dV_{si}}{dt} = Q_{si} \tag{108}$$

where V_{si} is the volume of seawater intruded and Q_{si} is the net seawater discharge in the i[th] layer. V_{si} can be evaluated by integrating the interface profile over the layer thickness. Q_{si} is the component of net seawater discharge (Q_s) at the coastal boundary proportional to its transmissivity. Q_s is the difference between freshwater discharge at the inland boundary (Q_{fL}) and freshwater outflow at the coastal boundary (Q_{f_o}), satisfying the flow continuity. Therefore, Eq. (108) can be rewritten as:

$$\theta \frac{d}{dt}\left(\int_{d_i}^{d_{i+1}} x(\zeta, t) d\zeta\right) = \frac{T_i}{T}(Q_{f_o}(t) - Q'_{fL}) \tag{109}$$

where $x(\zeta, t)$ is the transient interface profile, Q'_{fL} is the final discharge at the inland boundary after the abrupt change and $Q_{f_o}(t)$ is the freshwater outflow at time t. Rathore et al. (2018) (c) provided an explicit analytical solution of the interface profile in a stratified aquifer for a given outflow value:

$$x(\zeta, t) = \frac{1}{\alpha Q_{f0}}\left[T_{Ui}(y_{ci} - \zeta) - \frac{K_i}{2}(d_{i+1} - \zeta)^2\right] \tag{110}$$

where T_{Ui} and y_{ci} are the total transmissivity and TCE for the region above the i[th] layer.

$$\frac{\theta}{\alpha}\frac{d}{dt}\left[\frac{1}{Q_{f0}(t)}\int_{d_i}^{d_{i+1}}\left(T_{Ui}(y_{ci} - \zeta) - \frac{K_i}{2}(d_{i+1} - \zeta)^2\right)d\zeta\right] = \frac{T_i}{T}(Q_{f_o}(t) - Q'_{fL}) \tag{111}$$

After integrating the above equation and rearranging terms, we get:

$$\frac{\theta}{\alpha}\frac{d}{dt}\left[\frac{b_i}{Q_{f0}(t)}\left(T_{Ui}(y_{ci}-y_i)+\frac{T_i b_i}{6}\right)\right]=\frac{T_i}{T}\left(Q_{f_o}(t)-Q'_{fL}\right) \tag{112}$$

Time-independent terms containing layer thicknesses and hydraulic conductivities are collectively replaced by D_i^2 $[L^2]$ in the above equation resulting in:

$$\frac{\theta T D_i^2}{\alpha}\frac{d}{dt}\left(\frac{1}{Q_{f0}(t)}\right)=\left(Q_{f_o}(t)-Q'_{fL}\right) \tag{113}$$

where

$$D_i^2=\frac{T_{Ui}}{T_i}b_i(y_{ci}-y_i)+\frac{b_i^2}{6} \tag{114}$$

After rearranging the terms, we get the integral equation:

$$\frac{dQ_{f0}}{Q_{f_o}(Q_{f_o}-Q'_{fL})}=\frac{dt}{\theta T D_i^2/\alpha} \tag{115}$$

After solving the above equations, we get:

$$\frac{6t}{\theta T D_i^2/\alpha}=\frac{1}{{Q'_{fL}}^2}ln\frac{Q_{f0}(t)}{Q^0_{fL}}-\frac{1}{Q'_{fL}}\left(\frac{1}{Q_{f0}\,(t)}-\frac{1}{Q^0_{fL}}\right)-\frac{1}{{Q'_{fL}}^2}ln\frac{Q'_{fL}-Q_{f0}(t)}{Q'_{fL}-Q^0_{fL}} \tag{116}$$

The above equation gives us insight into how an i[th] layer in a particular stratification scenario influences the timescale of the aquifer response to an abrupt change in the boundary discharge from Q^0_{fL} to Q'_{fL}. D_i^2 encapsulates the effect of both – properties of the i[th] layer and overall layer arrangement on the contribution of the i[th] layer to the overall

aquifer response. We can now quantify the layer-characteristic timescale (corresponding to 95% of the transition) as the Response-Timescale Indicator for the i[th] layer (τ_i $[T]$) in a given stratification, following the derivation process adopted in Rathore et al. (2018a):

$$\tau_i = \frac{\theta T D_i^2}{\alpha {Q'_{fL}}^2}\left(0.95\frac{Q'_{fL}}{Q^0_{fL}} + 2.046\right) \tag{117}$$

τ_i equation looks very similar to timescale solution by Rathore et al. (2018a), here representing the contribution of the i[th] layer to the timescale of a stratified aquifer. We can express the inland boundary discharges in terms of boundary heads using the TCE-based solution for the freshwater discharge (Rathore et al., 2018b) to yield τ_i ethe quation for the head-controlled system.

$$\tau_i = \frac{\theta L^2 D_i^2}{\alpha T\left(h'_{fL} - H_s\left(1+\frac{1}{\alpha}\right)+\frac{y_c}{\alpha}\right)^2}\left(0.95\frac{\left(h'_{fL} - H_s\left(1+\frac{1}{\alpha}\right)+\frac{y_c}{\alpha}\right)}{\left(h^0_{fL} - H_s\left(1+\frac{1}{\alpha}\right)+\frac{y_c}{\alpha}\right)} + 2.046\right) \tag{118}$$

where h^0_{fL} $[L]$ and h'_{fL} $[L]$ represents initial and final inland boundary heads, respectively, and y_c $[L]$ represents the TCE.

In the equations for τ_i, D_i^2 encompasses the effect of the i[th] layer in a particular layer arrangement on the overall transient response of the aquifer. Other terms in Eqs. (117) and (118) are independent of layer arrangement representing the effects of boundary conditions (boundary discharge and head values), density differences (α) and other aquifer parameters like porosity and aquifer dimensions.

The greater D_i^2 means the i[th] layer contributes towards the longer timescale of the aquifer. In the D_i^2 the expression we can see the two opposing factors as discussed in the previous section that controls a particular layer's temporal response. The numerator of the first term $T_{Ui}b_i(y_{ci} - y_i)$ and the second term $b_i^2/6$ are the measure of the volume of the intruded seawater. High $T_{Ui}b_i(y_{ci} - y_i)$ resulting from high transmissivity values of the layer above the i[th] layer leads to a mild slope of the interface and a more landward interface, which results in high intruded seawater volume in the i[th] layer. High $b_i^2/6$ will naturally result in high intruded seawater volume in the i[th] layer. Denominator T_i is the measure of discharge rate. Therefore, D_i^2 contains both the factors related to stratification parameters governing timescale and is a reasonable indicator to response timescale of a layer. The layer with the highest D_i^2 is the critical layer that is slowest to respond to the boundary change, hence act as a bottleneck and control the response of the aquifer. Maximum of the characteristic timescales of layers which corresponds to layer with maximum D_i^2 representing the critical later is chosen as the indicator for the overall aquifer response.

$$RTI = maximum(\tau_1, \tau_2, \dots, \tau_N) \tag{119}$$

Using RTI we can rank 5 special cases analyzed using numerical simulations in the order of fastest to slowest response in Table 15, which is in agreement with the numerical results.

Table 15 - Characteristic timescale for each layer and RTI for the aquifer for five special

Case	τ_i's [L1 L2 L3 L4]	RTI (d)
E1	[**23.8** 15.9 6.5 3.2]	23.8
Homogeneous	[**92.7** 46.4 15.5 2.6]	92.7
S2	[**170.0** 36.1 1.3 2.6]	170.0
S1	[**509.9** 15.5 7.8 2.6]	509.9
E2	[**23.8** 15.9 6.5 3.2]	23.8

7.4 Summary and Conclusion

This chapter analyzes the transient SWI in homogeneous and stratified aquifers. For the homogeneous case, there are three main contributions of this study. First, we derived, for the first time, a simple explicit analytical solution for the timescale of the interface movement in response to an abrupt change in the freshwater flux at the inland boundary, allowing quick assessment of the SWI and SWR timescales. The solution was extended to the case of the specified hydraulic head at the inland boundary condition. These solutions can be potentially used as a first-order prediction tool for estimating the timescale of SWI and SWR. Second, we theoretically verified the temporal disparity between SWI and SWR and quantified it using a temporal asymmetry index. Third, we proposed a two-mechanism based theoretical framework to explain the temporal asymmetry and analyzed the effects of aquifer parameters and boundary conditions on the timescales.

The analytical solutions provide many useful insights into SWI and SWR timescales, albeit within the constraints of the approximation of a sharp interface in a confined, homogenous, isotropic aquifer. For specified-flux boundary cases, the timescale is linearly proportional to porosity, hydraulic conductivity, and cubic aquifer thickness, and is insensitive to the aquifer length and the coastal boundary head. For specified-head boundary cases, the timescale is directly proportional to the porosity, aquifer thickness, density ratio, coastal boundary head and squared aquifer length, and inversely proportional to the hydraulic conductivity. The close agreement in the sensitivity results of analytical and numerical solutions demonstrates the robustness of the analytical solutions. More importantly, we conveniently explained and quantified the temporal asymmetry between SWI and SWR. Given two bounding steady states defined by specified-fluxes or heads at

the inland boundary, longer toe-displacements are traveled at lower rates and shorter toe-displacements are traveled at higher rates in SWI, but this trend reverses in SWR, such that the timescales of SWR are shorter than those of SWI. The temporal asymmetry index, defined as the ratio between SWI and SWR timescales, was found to be heavily dependent on changing boundary conditions and weakly influenced by aquifer parameters. Furthermore, we theoretically examined the log-linearity relationship between the timescale and the freshwater flux at the inland boundary, recently identified by numerical simulations (Lu and Werner, 2013). We found that the relationship is not perfectly linear over the entire flux change range, but maybe approximated by two linear functions with different slopes for SWI and SWR, respectively. For the cases of large changes in the boundary flux for SWI and SWR, the log-linearity slope tends to be -2 and -1, respectively

For the stratified case, for the first time, we studied the effects of stratification on the transient response of the seawater-freshwater interface. We hypothesized that each layer has a characteristic response timescale and the layer with the longest characteristic timescale acts as a bottleneck and controls the aquifer response timescale. We propose an indicator for the response timescale of the interface to compare timescales for different layer arrangements. We demonstrated the effectiveness of the indicator using numerical simulations.

The present study is limited by the sharp-interface approximation. Hence, the proposed analytical approach does not explain the effect of the dispersivity on the timescale. However, it is possible to include a correction factor similar to that introduced by Pool and Carrera (2011) to account for dispersive mixing. This study also neglects the time lag between the change in the boundary head and the corresponding change in the flux

for the specified-head boundary case. Other hydrogeological conditions, such as tidal effects, and aquifer slopes, may also affect timescales. Nonetheless, the analytical nature of the solution enables us to develop a new understanding of the conditions controlling SWI and SWR timescales for both specified-flux and specified-head boundary cases in a homogeneous case. For the stratified case, there is a need for further investigations for better prediction capabilities.

CHAPTER 8. CONCLUSIONS AND FUTURE WORK RECOMMENDATIONS

8.1 Conclusions

This thesis investigated the effects of heterogeneity on seawater intrusion and submarine groundwater discharge using analytical and numerical methods. The main conclusions are provided below:

1) The effects of stratification in coastal aquifers can be represented by the Transmissivity Centroid Elevation (TCE). Higher TCE, which implies higher discharges in the upper part of the aquifer and lower discharges in the lower part, results in a greater extent of SWI. Effective parameters to homogenize the stratified aquifers and reproduce the toe-position and discharge are functions of TCE taking into account the effect of layer placements. For the preferential flow layer setting, the elevation of the layer is critical and the hydraulic conductivity contrast does not have significant effects on SWI.
2) The extent of SWI at any elevation is a function of local transmissivity parameters—transmissivity and TCE of the region above the interface. This local TCE concept enables the explicit analytical solution of the interface profile which can be integrated to evaluate the volume of intruded seawater, a critical parameter for transient SWI analysis. Based on the derived solutions, it is found that the boundary potential in Strack's discharge potential theory essentially represents the first moment of the transmissivity. The delineation of the interface profile is crucial

as it controls the pathways of solutes transported with groundwater discharge into the sea.

3) A 2D heterogeneous aquifer can be conceptualized as a series of columns of stratified aquifers assuming that freshwater discharge redistributes abruptly in each column. This allows us to apply the concept of local TCE to the 2D heterogeneous case to compute the interface profile rapidly without solving non-linear PDEs solving variable-density flow. The computed interface profile shows excellent agreement with numerical simulations for variable-density flow. The extent of SWI is not influenced by the conductivity values in the single-density flow region (i.e. region inland of the toe position) and the region below the seawater-freshwater interface.

4) In an aquifer with heterogeneity modeled as random stratification, the mean toe-position in a flux-controlled system is the same as that in a corresponding homogeneous aquifer with mean hydraulic conductivity. On the contrary, the mean toe position in a head-controlled case is dependent on the variance and correlation length as well in addition to mean hydraulic conductivity. Variances of toe-position in flux- and head-controlled aquifers and discharges are linear functions of the variance of the hydraulic conductivity field but have different relationships with the correlation length. The variance of the toe position in a flux-controlled system is found to be significantly higher than the corresponding head-controlled system. In a 2D heterogeneous case, the variance of the field has a much stronger influence on the variance of the interface profile compared with the correlation length of the field. Geometric mean cannot be used as an effective parameter as it underestimates

the mean interface profile. This underestimation increases with the variance of the random field.

5) The temporal disparity quantified as the ratio of intrusion to retreat timescale is heavily influenced by boundary conditions and weakly influenced by the aquifer parameters. For specified-flux boundary cases, the timescale is linearly proportional to porosity, hydraulic conductivity, and cubic aquifer thickness, and is insensitive to the aquifer length and the coastal boundary head. For specified-head boundary cases, the timescale is directly proportional to the porosity, aquifer thickness, density ratio, coastal boundary head and squared aquifer length, and inversely proportional to the hydraulic conductivity. The transient response in stratified aquifers is controlled by a critical layer, a layer with the longest characteristic timescale among all layers. This layer typically has a large volume of seawater to be displaced and small discharge due to low conductivity, hence it acts as a bottleneck for the whole aquifer response.

8.2 Implications

This dissertation presents a significant advance in the theoretical understanding of the effects of heterogeneity on seawater intrusion and submarine groundwater discharge. The derived elegant analytical solutions provide key parameters, understanding of underlying mechanisms and first-order prediction tools albeit within the constraints of simplifications of the interface assumption. Based on the novel insights obtained and tools developed, following research and engineering objectives are met for different settings of heterogeneity:

1) Fast delineation of freshwater-seawater interface and estimation of submarine groundwater discharge
2) Improved control of seawater intrusion
3) Impacts of the preferential flow path
4) Aquifer homogenization and upscaling
5) Quantification and management of uncertainty
6) Optimizing the extent of SWI in the region of influence
7) Analysis of transience of seawater intrusion

8.3 Limitations

The studies in this thesis adopted a sharp interface approximation to quantify the extent of seawater intrusion and submarine groundwater discharge analytically. Though for most studies concerning SWI, the interface is a good approximation of the mixing zone, karst aquifer like Biscayne aquifer in Florida displays a wide mixing zone (about 1 kilometer) in which case the mixing zone cannot be ignored.

The adoption of a two-dimensional vertical slice of the coastal aquifer makes it difficult to analyze the effects of pumping which exhibits radial flow. Although insights about the effects of heterogeneity on SWI and SGD are transferable to 3D cases, there is a need to extend this analysis to 3D in order to study mode complicated scenarios like pumping and land inundations.

8.4 Recommendations for Future Work

8.4.1 Developing a Semi-analytical Technique to Compute the Seawater-freshwater Interface in 3D

There is a possibility of extending the developed semi-analytical technique from 2D to 3D given that lateral flux distributions are properly accounted for. If successful, other factors like land inundations and pumping can be incorporated in the analyses offering a powerful tool for rapid delineation of the extent of SWI in 3D heterogeneous coastal aquifers.

8.4.2 Inverse Modeling of the Conductivity from Field Salinity Measurements

Characterization of the hydraulic conductivity field requires a combination of multiple methods and measurements. Traditionally, hydraulic head measurements in conjunction with the tracer test were used to invert flow and transport models to estimate the hydraulic conductivity. In coastal aquifers, the salinity distribution influenced by seawater intrusion can provide additional information about the hydraulic conductivity field using inverse modeling. However, inverse modeling requires solving thousands of scenarios which is impractical with variable-density flow simulations. Using our proposed methodology to compute interface profile semi-analytically, inverse modeling can be performed to estimate bulk parameters above the interface (Figure 40). Note that this approach needs to be used in conjunction with other methods to improve the estimate.

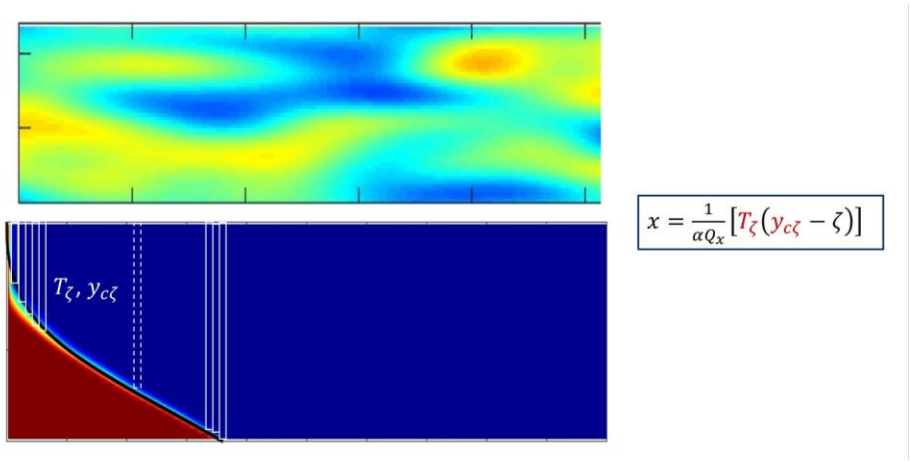

Figure 40 - Using salinity values for inverse modeling to estimate hydraulic conductivity field

8.4.3 Modeling the Effects of Heterogeneity on Solute Transport into Estuary Ecosystems

The solute path near the coast is only dependent on the hydraulic conductivity field but also strongly influenced by the seawater wedge (Figure 41). It is highly desirable to develop a near-coast transport model (conservative and reactive) and identify key-parameters similar to TCE for flow models that can account for the effects of heterogeneity.

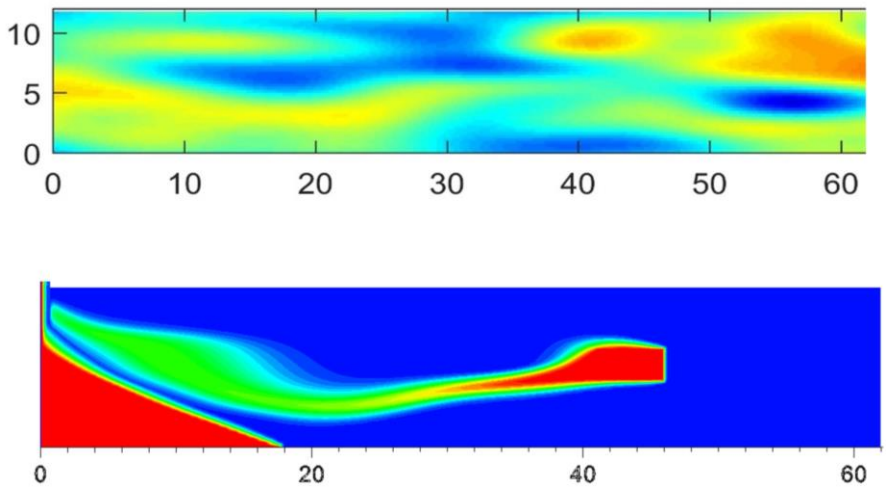

Figure 41 - Influence of seawater wedge on the solute pathways near the coastal boundary

8.4.4 Effects of Heterogeneity on Dense Contaminants

The transport and mixing of contaminants are governed by advection, convection, and dispersion. All three processes are influenced by aquifer heterogeneity (Figure 42). It is critical to understand these heterogeneity effects and develop models to predict the spreading of dense contaminants.

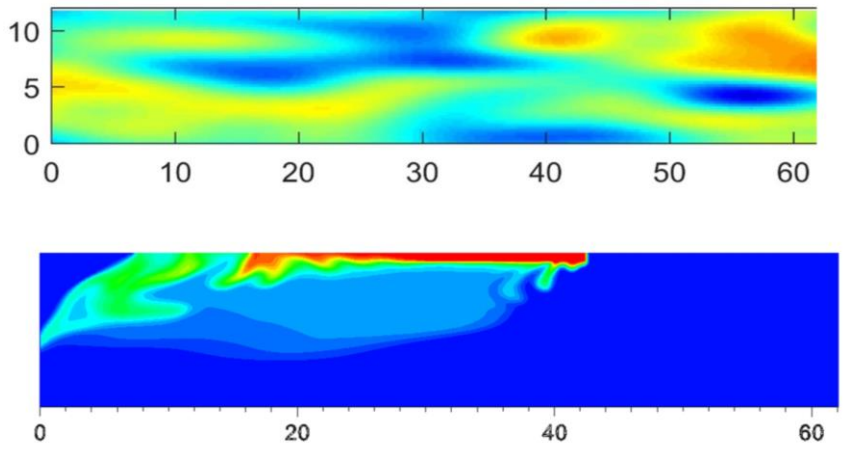

Figure 42 - Spreading of a dense contaminant in a heterogeneous aquifer

8.4.5 Estimation of the Salinity Fluxes at the Coastal Boundary

There is a continuous exchange of saline fluxes between the sea and coastal aquifer through the seawater wedge. The circulating seawater intakes seawater containing chemicals and microorganisms and processes them under biogeochemical conditions in the wedge before outputting them into the sea. The output into the sea is dependent on the residence time of pathlengths. Figure 43 depicts the velocity vectors of the recirculating saline fluxes. There are mainly two research questions to be answered:

1) At the steady-state, the net seawater flux at the coastal boundary is zero (mass balance). Hence, it is extremely difficult to estimate and model the volume of circulating seawater. There is a need for innovative field or laboratory measurements and mathematical models to quantify these saline fluxes.
2) It is of high interest to model the travel-time distribution of chemicals and microorganisms in the saline fluxes for the reactive transport model. An approach similar to the transient storage model can be adopted.

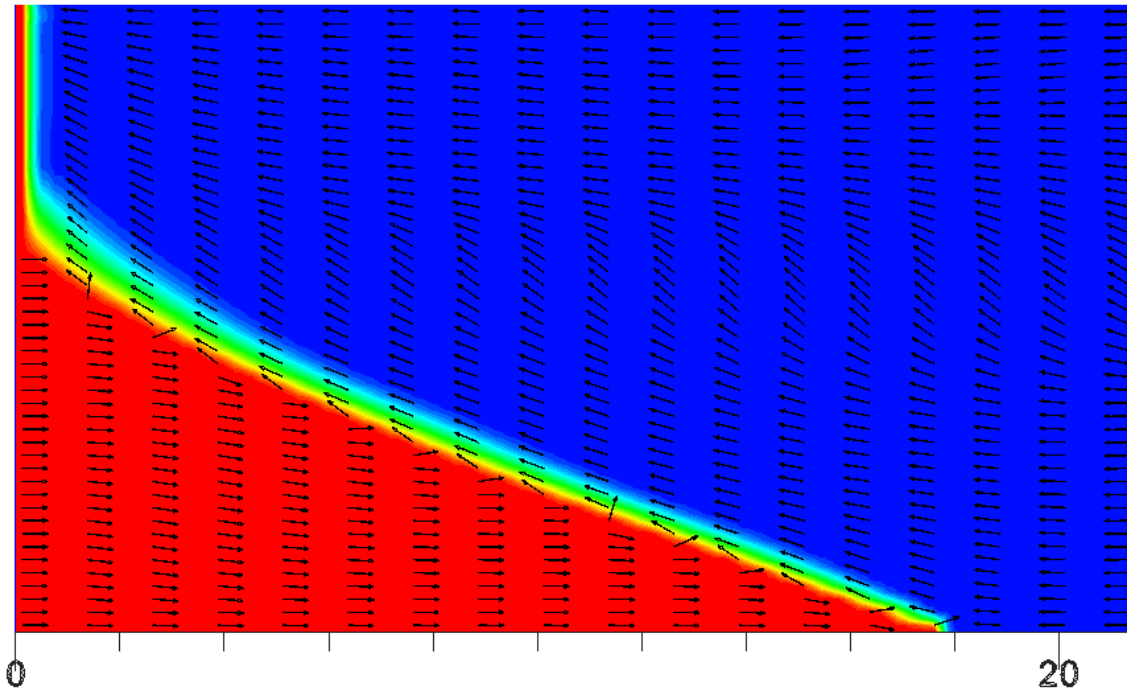

Figure 43 - Velocity vectors depicting recirculating seawater

8.4.6 Integrated Modeling of Water and Solute exchanges between Groundwater, River, Sea and Human Activities in Coastal Areas

There is a pressing need to understand the earth system as a whole in order to predict climate change impacts on various earth subsystems. Figure 44 depicts key processes in the coastal area. With the advancement in computing abilities outpacing the modeling of earth systems, it is essential to model various earth systems together with analyses at multiple scales. U.S. Department of Energy started an initiative called Energy Exascale Earth System Model (E3SM), which is a state-of-the-science high-resolution earth system modeling, simulation, and prediction using exascale computing. Integrated Coastal Modeling (ICoM) project under E3SM aims to model the interactions between human-land-river-ocean with a focus on modeling the water, heat, sediment and nutrient fluxes. Analytical solutions like developed in this study have a great utility for such applications and can be used as a subgrid level to represent coastal processes in a particular grid cell at the coast.

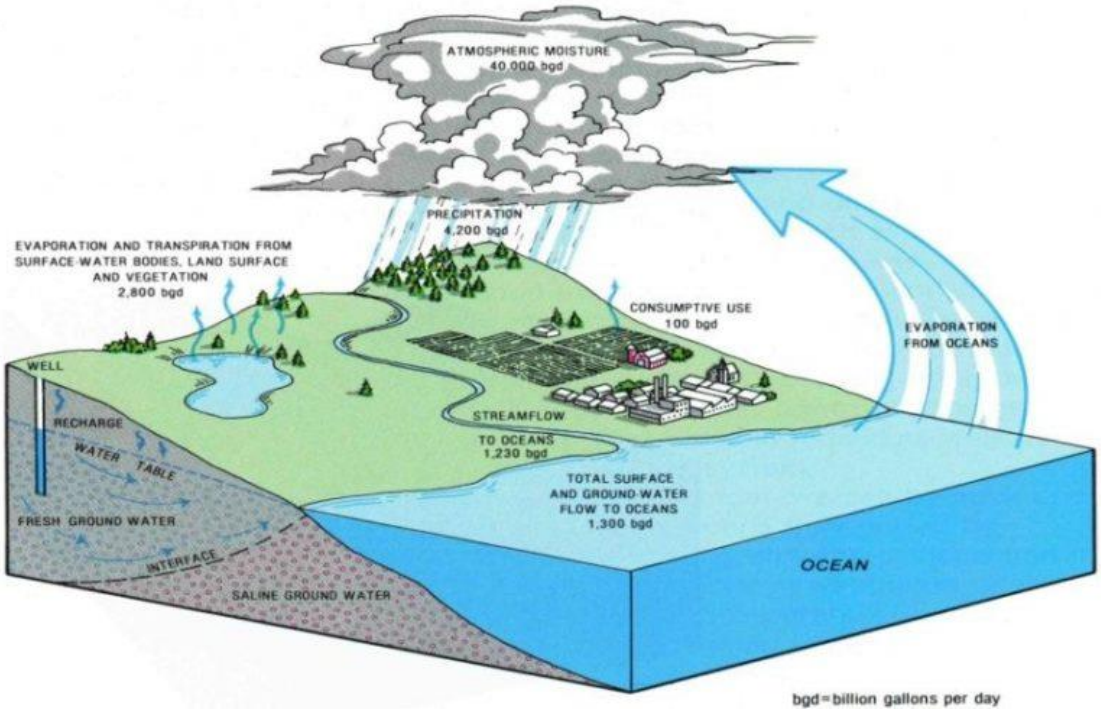

http://sonomavalleygroundwater.org/gw/

Figure 44 - Key processes in the coastal areas

APPENDIX A: COMPUTING THE INTEGRATION CONSTANT FOR A GENERAL i^{th} LAYER

We show the computation of C_i only for a confined aquifer. The reader can follow the same procedure to obtain C_i for an unconfined aquifer. We can rewrite Eq. (37) as:

$$C_{i-1} = C_i + \frac{d_i^2}{2\alpha Q_x}(K_i - K_{i-1}) \quad \text{A1}$$

Using the above relation and C_N from Eq. (35), C_{N-1} can be computed as:

$$C_{N-1} = -\frac{K_N B^2}{2\alpha Q_x} + \frac{d_N^2}{2\alpha Q_x}(K_N - K_{N-1}) \quad \text{A2}$$

Similarly, for any general i^{th} layer, C_i can be computed as:

$$C_i = -\frac{K_N B^2}{2\alpha Q_x} + \frac{1}{2\alpha Q_x}\sum_{j=i}^{N-1} d_{j+1}^2\left(K_{j+1} - K_j\right) \quad \text{A3}$$

The summation term is rearranged so as to get differences of consecutive d_j^2 terms for each K_j:

$$C_i = \frac{1}{2\alpha Q_x}[-K_N(B^2 - d_N^2) - K_{N-1}(d_N^2 - d_{N-1}^2) \ldots - K_{i+1}(d_{i+2}^2 - d_{i+1}^2) - K_i d_{i+1}^2] \quad \text{A4}$$

Expanding the difference-of-square terms:

$$C_i = \frac{1}{\alpha Q_x}\Big[-K_N(B - d_N)\frac{(B+d_N)}{2} - K_{N-1}(d_N - d_{N-1})\frac{(d_N+d_{N-1})}{2} \ldots - K_{i+1}(d_{i+2} - d_{i+1})\frac{(d_{i+2}+d_{i+1})}{2} - \frac{K_i d_{i+1}^2}{2}\Big] \quad \text{A5}$$

Substituting $(d_{i+2} - d_{i+1})$ as the thickness of the $(i+1)^{th}$ layer, b_{i+1}, and $(d_{i+2} + d_{i+1})/2$ as the elevation of the center of the $(i+1)^{th}$ layer, y_{i+1}:

$$C_i = \frac{1}{\alpha Q_x}\left[-K_N b_N y_N - K_{N-1} b_{N-1} y_{N-1} \ldots - K_{i+1} b_{i+1} y_{i+1} - \frac{K_i d_{i+1}^2}{2}\right] \quad \text{A6}$$

$$C_i = -\frac{1}{\alpha Q_x}\left(\sum_{i+1}^{N} T_j\, y_j + \frac{K_i d_{i+1}^2}{2}\right) \quad \text{A7}$$

APPENDIX B: SOLUTION OF THE FRESHWATER FLUX IN A STRATIFIED UNCONFINED AQUIFER

We follow the approach adopted by Rathore et al. (2018b) in confined aquifers of applying Darcy's law between the inland boundary and the seawater-freshwater interface toe, which essentially contains a single-density flow region. The freshwater flowrate in an unconfined aquifer (Q_x) can be divided into two components: 1) below the sea-level (Q_1); 2) above the sea-level (Q_2).

Q_1 can be given as:

$$Q_1 = -T\left(\frac{h_f - h_t}{L - x_t}\right) \quad \text{B1}$$

$$Q_2 = -\frac{K_{N+1}}{L - x_t}\left[\frac{h_f^2 - h_t^2}{2} - H_s(h_f - h_t)\right] \quad \text{B2}$$

where h_t is given by $H_s(1 + 1/\alpha)$. Adding two components of discharges ($Q_x = Q_1 + Q_2$) and rearranging, we get:

$$Q_x = -\frac{h_f - h_t}{L - x_t}\left[T + K_{N+1}\left(\frac{h_f + h_t}{2} - H_s\right)\right] \quad \text{B3}$$

Substituting x_t in terms of Q_x from Eq. (959) into equation (B3) and rearranging, we get:

$$Q = -\frac{h_f - h_t}{L}\left[T + K_{N+1}\left(\frac{h_f + h_t}{2} - H_s\right)\right] - \frac{T}{\alpha L}\left(y_c + \frac{K_{N+1}H_s^2}{2\alpha T}\right) \quad \text{B4}$$

Substituting h_t as $H_s(1 + 1/\alpha)$ and simplifying, we get:

$$Q_x = -\frac{T}{L}\left[h_f - H_s\left(1+\frac{1}{\alpha}\right)+\frac{y_c}{\alpha}\right] - \frac{K_{N+1}}{2L}\left(h_f - H_s\right)^2 \qquad \text{B5}$$

It is interesting to note that, the first term with the square bracket is essentially the discharge solution for the confined aquifer, in this case, bounded by sea-level at the top.

APPENDIX C: PROOF FOR THE MATHEMATICAL SAMENESS OF OUR SOLUTION FOR THE INTERFACE PROFILE AND STRACK AND AUSK (2015)

We here start with Eq. (56) of Strack and Ausk (2015) which relates comprehensive potential to the piezometric head for confined aquifers:

$$\phi^2 + \frac{A_m}{B_m}\phi - \left(\Phi - C_{m_s} + \frac{1}{2}k_N b_{N+1}^2\right)/B_m = 0 \qquad \text{C1}$$

For the special 2D case considered in their paper, potential as a function of position and boundary potential is given as:

$$\Phi = -Q_{x_0}x + \Phi_0 \qquad \text{C2}$$

The piezometric head ϕ is related to signed elevation of the interface h_s as:

$$\phi = -h_s/\alpha \qquad \text{C3}$$

A_m and B_m are constants in terms of aquifer properties, defined as:

$$A_m = \sum_{m+1}^{N} k_j H_j + k_m b_{m+1} \qquad B_m = \frac{1}{2}\alpha k_m \qquad \text{C4}$$

The potential at the coastal boundary Φ_0 is a function of aquifer parameters:

$$\Phi_0 = \frac{1}{2\alpha}\sum_{j=2}^{N}\left(k_j - k_{j-1}\right)b_j^2 + \frac{1}{2\alpha}k_1 H_s^2 - \frac{1}{2}\left(1 + \frac{1}{\alpha}\right)k_N b_{N+1}^2 \qquad \text{C5}$$

And the constant C_{m_s} to ensure the continuity of the potential at the intersections of the interface with layer boundaries is given as:

$$C_{m_s} = \frac{1}{2\alpha}\left[\sum_{j=2}^{m}\left(k_j - k_{j-1}\right)b_j^2 + k_1 H_s^2\right] \quad \text{C6}$$

Eqs. C1 – C6 are directly from Strack and Ausk (2015), where all the elevations are measured from the sea-level and are signed.

Substituting Φ from Eq. C2 into Eq. C1, and after rearranging, x can be explicitly expressed as:

$$x = -\frac{1}{Q_x}\left\{B_m\phi^2 + A_m\phi - \Phi_0 + C_{m_s} - \frac{1}{2}K_N b_{N+1}^2\right\} \quad \text{C7}$$

Substituting Eqs. C3 – C6 in Eq. C7;

$$x = -\frac{1}{Q_x}\left\{\frac{1}{2\alpha}k_m h_s^2 - \left(\sum_{m+1}^{N} k_j H_j + k_m b_{m+1}\right)\frac{h_s}{\alpha} - \left[\frac{1}{2\alpha}\sum_{j=2}^{N}\left(k_j - k_{j-1}\right)b_j^2 + \frac{1}{2\alpha}k_1 H_s^2 - \frac{1}{2}\left(1 + \frac{1}{\alpha}\right)k_N b_{N+1}^2\right] + \frac{1}{2\alpha}\left[\sum_{j=2}^{m}\left(k_j - k_{j-1}\right)b_j^2 + k_1 H_s^2\right] - \frac{1}{2}K_N b_{N+1}^2\right\} \quad \text{C8}$$

We simplify Eq. C8 to:

$$x = \frac{1}{\alpha Q_x}\left\{-\frac{1}{2}k_m b_{m+1}^2 - \sum_{j=m+1}^{N} T_j y_j' + \left(\sum_{j=m+1}^{N} T_j + k_m b_{m+1}\right)h_s - \frac{k_m}{2}h_s^2\right\} \quad \text{C9}$$

where y_j' is the signed elevation of the center of a layer. Our paper considered all elevations with respect to the aquifer based. Hence, we transform elevation variables are follows:

$$d_i = b_i + H_s \quad \text{C10}$$

$$y_i = y_i' + H_s \quad \text{C11}$$

$$\zeta = h_s + H_s \quad \text{C12}$$

where d_i and y_i are the layer-base and-center elevation, respectively, and ζ is the elevation of the interface, measured from the aquifer base. Substituting Eqs. C10-C12 into Eqs. C9 and simplifying, we get the solution proposed by us in the paper:

$$\boldsymbol{x = \frac{1}{\alpha(-Q_x)}\left\{\sum_{j=m+1}^{N} T_j\,(y_{cm} - \zeta) + \frac{K_m}{2}(d_{m+1} - \zeta)^2\right\}}$$

APPENDIX D: MOMENTS OF y_c AND T

y_c encompasses the effects of the layer arrangement in the solutions derived for the Q_x and x_t.

$$y_c = \frac{\sum_{i=1}^{N} T_i y_i}{T}, \text{ or} \tag{D1}$$

$$y_c = \frac{\int_0^H yK(y)dy}{\int_0^H K(y)dy} \tag{D2}$$

It is also important to note that when we do not have an exact characterization of the stratification of K, we can model K as a random field in 1D with known mean, variance, and spatial correlation structure, to perform the stochastic analysis. We first evaluate statistical moments for the continuous case, then we extend it for the discrete case.

D1. $K(y)$ as a continuous variable

We first evaluate the statistical moments of the numerator (N) and denominator (D).

$$y_c = \frac{\int_0^H yK(y)dy}{\int_0^H K(y)dy} = \frac{N}{D}$$

$$\mu_N = E[N] = E[\int_0^H yK(y)\,dy] = \int_0^H yE[K(y)]\,dy = \mu_K \int_0^H y\,dy = \boldsymbol{\frac{\mu_K H^2}{2}} \tag{D3}$$

$$\mu_D = E[N] = E[\int_0^H K(y)\,dy] = \int_0^H E[K(y)]\,dy = \mu_k \int_0^H dy = \boldsymbol{\mu_K H} \tag{D4}$$

$$\sigma_N^2 = E[N^2] - \mu_N^2; \qquad \{\because \sigma_X^2 = E[X^2] - \mu_X^2\} \tag{D5}$$

Evaluating $E[N^2]$:

$$E[N^2] = E\left[\left(\int_0^H yK(y)\,dy\right)^2\right] = E\left[\int_0^H \int_0^H zK(z)\,yK(y)\,dzdy\right] =$$

$$E\left[\int_0^H \int_0^H K(z)\,K(y)zy\,dzdy\right] \qquad \left\{\because \left(\int_0^H f(x)\,dx\right)^2 = \int_0^H \int_0^H f(x)\,f(y)\,dxdy\right\}$$

$$= \int_0^H \int_0^H E[K(z)\,K(y)]\,zy\,dzdy = \int_0^H \int_0^H \big(Cov\big(K(y),K(z)\big) + E[K(y)]\,E[K(z)]\big)\,zy\,dzdy$$

$$\{\because E[xy] = Cov(x,y) + E[x]\,E[y]\}$$

$$E[N^2] = \int_0^H \int_0^H (\sigma_K^2\,\rho(h) + \mu_K^2)\,zy\,dzdy = \sigma_K^2 \int_0^H \int_0^H \rho(h)zydzdy + \mu_K^2 \frac{H^4}{4} \qquad \text{(D6)}$$

where, $\rho_K(h)$ is a correlation function with $h = |z - y|$

Substituting μ_N and $E[N^2]$ from Eq. (D3) and Eq. (D6), respectively, into Eq. (D5) to get σ_N^2:

$$\sigma_N^2 = E[N^2] - \mu_N^2 = \sigma_K^2 \int_0^H \int_0^H \rho_K(h)zydzdy + \mu_K^2 \frac{H^4}{4} - \mu_K^2 \frac{H^4}{4}$$

$$\sigma_N^2 = \sigma_K^2 \int_0^H \int_0^H \rho_K(h)zydzdy \qquad \text{(D7)}$$

On similar lines, we get ${\sigma_D}^2$ as:

$$\sigma_D^2 = E[D^2] - \mu_D^2; \qquad \text{(D8)}$$

Evaluating $E[D^2]$:

$$E[D^2] = E\left[\left(\int_0^H K(y)\,dy\right)^2\right] = E\left[\int_0^H \int_0^H K(z)\,K(y)\,dzdy\right] =$$

$$E\left[\int_0^H \int_0^H K(z)\,K(y)\,dzdy\right]$$

$$= \int_0^H \int_0^H E[K(z)\,K(y)]\,dzdy = \int_0^H \int_0^H \big(Cov\big(K(y),K(z)\big) +$$

$$E[K(y)]\,E[K(z)]\big)\,dzdy$$

$$E[D^2] = \int_0^H \int_0^H (\sigma_K^2\,\rho_k(h) + \mu_K{}^2)\,dzdy = \sigma_K^2 \int_0^H \int_0^H \rho_K(h)dzdy + \mu_K^2\,H^2 \qquad \text{(D9)}$$

Substituting μ_D and $E[D^2]$ from Eq. (D3) and Eq. (D9), respectively, into Eq. (D8) to get σ_D^2:

$$\sigma_D^2 = E[D^2] - \mu_D{}^2 = \sigma_K^2 \int_0^H \int_0^H \rho_K(h)dzdy + \mu_K^2\,H^2 - \mu_K^2\,H^2$$

$$\sigma_D^2 = \sigma_K^2 \int_0^H \int_0^H \rho_K(h)dzdy \qquad \text{(D10)}$$

We also need to evaluate the covariance between N and D.

$$Cov(N,D) = E[ND] - E[N]E[D] = E\left[\left(\int_0^H yK(y)\,dy\right)\left(\int_0^H K(y)\,dy\right)\right] - \mu_N\mu_D$$

$$= E\left[\int_0^H \int_0^H yK(y)\,K(z)\,dydz\right] - \mu_N\mu_D$$

$$= \int_0^H \int_0^H E[K(z)\,K(y)]\,ydydz - \mu_N\mu_D$$

$$= \int_0^H \int_0^H (\sigma_K^2\,\rho_k(h) + \mu_K^2\,)\,y\,dzdy - \mu_N\mu_D = \sigma_K^2 \int_0^H \int_0^H \rho_K(h)y\,dzdy +$$

$$\mu_K^2\,\frac{H^3}{2} - \mu_K^2\,\frac{H^3}{2}$$

$$Cov(N,D) = \sigma_K^2 \int_0^H \int_0^H \rho_K(h) y \, dz dy \tag{D11}$$

We can now evaluate the mean and variance of y_c using method of approximate moments:

$$y_c(N,D) = \frac{N}{D} = \frac{\int_0^H yK(y)dy}{\int_0^H K(y)dy}$$

$$y_c(N,D) \approx y_c(\mu_N,\mu_D) + (N-\mu_N)\left[\frac{\partial y_c(N,D)}{\partial N}\right]_{\substack{N=\mu_N \\ D=\mu_D}} + (D-\mu_D)\left[\frac{\partial y_c(N,D)}{\partial D}\right]_{\substack{N=\mu_N \\ D=\mu_D}} + \frac{1}{2}(N-$$

$$\mu_N)^2\left[\frac{\partial^2 y_c(N,D)}{\partial N^2}\right]_{\substack{N=\mu_N \\ D=\mu_D}} + \frac{1}{2}(D-\mu_D)^2\left[\frac{\partial^2 y_c(N,D)}{\partial D^2}\right]_{\substack{N=\mu_N \\ D=\mu_D}} + (N-\mu_N)(D-$$

$$\mu_D)\left[\frac{\partial^2 y_c(N,D)}{\partial N \partial D}\right]_{\substack{N=\mu_N \\ D=\mu_D}} \tag{D12}$$

$$\mu_{y_c} = \frac{\mu_N}{\mu_D} + \frac{1}{2}\sigma_N^2\left[\frac{\partial^2 y_c(N,D)}{\partial N^2}\right]_{\substack{N=\mu_N \\ D=\mu_D}} + \frac{1}{2}\sigma_D^2\left[\frac{\partial^2 y_c(N,D)}{\partial D^2}\right]_{\substack{N=\mu_N \\ D=\mu_D}} + Cov(N,D)\left[\frac{\partial^2 y_c(N,D)}{\partial N \partial D}\right]_{\substack{N=\mu_N \\ D=\mu_D}} \tag{D13}$$

$$\sigma_{y_c}^2 = \sigma_N^2\left[\frac{\partial y_c(N,D)}{\partial N}\right]_{\substack{N=\mu_N \\ D=\mu_D}}^2 + \sigma_D^2\left[\frac{\partial y_c(N,D)}{\partial D}\right]_{\substack{N=\mu_N \\ D=\mu_D}}^2 + 2Cov(N,D)\left[\frac{\partial y_c(N,D)}{\partial N}\frac{\partial y_c(N,D)}{\partial D}\right]_{\substack{N=\mu_N \\ D=\mu_D}} \tag{D14}$$

After evaluating the derivatives and substituting the values of μ_N, μ_D, σ_N^2, σ_D^2 and $Cov(N,D)$ from Eqs. (D3), (D4), (D7), (D10) and (D11), respectively, we get:

$$\mu_{y_c} = \frac{H}{2} + \frac{{\sigma_K}^2}{2{\mu_K}^2 H^2}\int_0^H \int_0^H \rho_K(H-2y)dzdy \tag{D15}$$

$$\sigma_{y_c}^2 = \frac{{\sigma_K}^2}{4{\mu_K}^2 H^2}\int_0^H \int_0^H \rho_K(4yz + H^2 - 4Hy)dzdy \tag{D16}$$

Essentially, we need to evaluate the following three different integrals involving $\rho_K(h)$:

$I_1 = \int_0^H \int_0^H \rho_K(h)dzdy;$

$I_2 = \int_0^H \int_0^H y\,\rho_K(h)dzdy\,;$

$I_3 = \int_0^H \int_0^H yz\,\rho_K(h)dzdy;$ (D17)

where $h = |y - z|$

We can rewrite μ_{y_c} and $\sigma_{y_c}^2$ in terms of I_1, I_2, and I_3 as follows:

$\mu_{y_c} = \frac{H}{2} + \frac{\sigma_K^2[HI_1 - 2I_2]}{2\mu_K{}^2H^2}$ (D18)

$\sigma_{y_c}^2 = \frac{\sigma_K^2[H^2I_1 - 4HI_2 + 4I_3]}{4\mu_K{}^2H^2}$ (D19)

D2. $\boldsymbol{K(y)}$ set of discrete variables

Expressing in the form of K as a random vector (discrete stratification):

$\mu_{y_c} = \frac{H}{2} + \frac{1}{2\mu_K{}^2H^2}\sum_{i=1}^N \sum_{j=1}^N Cov(K_i, K_j)H_iH_j(H - 2y_i)$ (D20)

$\sigma_{y_c}^2 = \frac{1}{4\mu_K^2H^2}\sum_{i=1}^N \sum_{j=1}^N Cov(K_i, K_j)H_iH_j(4y_iy_j + H^2 - 4Hy_i)$ (D21)

APPENDIX E: MOMENTS OF x_t IN A FLUX-CONTROLLED SYSTEM

For the flux-controlled system, x_t is given in Eq. (9), which can be simplified to calculated moments as:

$$x_t = \frac{N}{\alpha Q_x} \tag{E1}$$

where $N = \int_0^H yK(y)dy$ and its moments are evaluated in Appendix A.

$$\mu_{x_t} = E[x_t] = E\left[\frac{N}{\alpha Q_x}\right] = \frac{E[N]}{\alpha Q_x} = \frac{\mu_K H^2}{2\alpha Q_x} \tag{E2}$$

$$\sigma_{x_t}^2 = Var[x_t] = Var\left[\frac{N}{\alpha Q_x}\right] = \frac{Var[N]}{\alpha^2 Q_x^2} = \frac{\sigma_K^2 I_3}{\alpha^2 Q_x^2} \tag{E3}$$

APPENDIX F: MOMENTS OF Q_x AND x_t IN A HEAD-CONTROLLED SYSTEM

We estimate the moments of Q_x and x_t using Taylor series approximation, the same approach as used in Appendix A for the moments of y_c.

Moments of Q_x

Q_x is a function of two random variables, i.e. T and y_c.

$$Q_x(T, y_c) = \frac{T}{L}\left(\Delta h + \frac{y_c}{\alpha}\right) \quad \text{(F1)}$$

where $\Delta h = h_f - H_s(1 + 1/\alpha)$

The moments of both T (mentioned as D in Appendix A) and y_c are already calculated in Appendix A. $Cov(y_c, T)$ can be given as:

$$Cov(y_c, T) = E[y_c T] - E[y_c]E[T]$$

$$= E[N] - E[y_c]E[D] \qquad \left\{\because y_c = \frac{N}{D}, T = D\right\}$$

$$= -\sigma_K^2 \frac{HI_1 - 2I_2}{2\mu_K H} \quad \text{(F2)}$$

The moments of Q_x can, therefore, be given as:

$$\mu_{Q_x} = Q_x(\mu_{y_c}, \mu_T) + \frac{1}{2}\sigma_{y_c}^2 \left[\frac{\partial^2 Q_x(y_c,T)}{\partial {y_c}^2}\right]_{\substack{\beta=\mu_{y_c} \\ T=\mu_T}} + \frac{1}{2}\sigma_T^2 \left[\frac{\partial^2 Q_x(y_c,T)}{\partial T^2}\right]_{\substack{y_c=\mu_{y_c} \\ T=\mu_T}} +$$

$$Cov(y_c, T)\left[\frac{\partial^2 Q_x(y_c,T)}{\partial y_c \partial T}\right]_{\substack{y_c=\mu_{y_c} \\ T=\mu_T}} \quad \text{(F3)}$$

$$\sigma_{Q_x}^2 = \sigma_{y_c}^2 \left[\frac{\partial Q_x(y_c,T)}{\partial y_c}\right]^2_{\substack{y_c=\mu_{y_c} \\ T=\mu_T}} + \sigma_T^2 \left[\frac{\partial Q_x(y_c,T)}{\partial T}\right]^2_{\substack{y_c=\mu_{y_c} \\ T=\mu_T}} +$$

$$2Cov(y_c, T)\left[\frac{\partial Q_x(y_c,T)}{\partial y_c}\frac{\partial Q_x(y_c,T)}{\partial T}\right]_{\substack{y_c=\mu_{y_c} \\ T=\mu_T}} \quad \text{(F4)}$$

Substituting moments of y_c and T from Appendix A, and $Cov(y_c, T)$ from Eq. (B2), into Eq. (F3) and Eq. (F4), we get:

$$\mu_{Q_x} = \frac{\mu_K H}{L}\left(\Delta h + \frac{H}{2\alpha}\right) \quad \text{(F5)}$$

$$\sigma_{Q_x}^2 = \frac{\sigma_K^2}{L\alpha}[\alpha^2 \Delta h^2 I_1 + I_3 + 2\alpha \Delta h I_2] \quad \text{(F6)}$$

Moments of x_t

x_t is only a function of y_c.

$$x_t(y_c) = \frac{L y_c}{\alpha \Delta h + y_c} \quad \text{(F7)}$$

Therefore, we evaluate the moments of x_t in terms of the moments of y_c using the Taylor series approximation. We have already derived the moments of y_c.

$$\mu_x = x_t(\mu_{y_c}) + \frac{1}{2}\sigma_{y_c}^2 \left[\frac{\partial^2 x_t(y_c)}{\partial {y_c}^2}\right]_{y_c=\mu_{y_c}} \quad \text{(F8)}$$

$$\sigma_x^2 = \sigma_{y_c}^2 \left[\frac{\partial x_t(y_c)}{\partial y_c}\right]^2_{y_c=\mu_{y_c}} \tag{F9}$$

Evaluating derivatives and simplifying, we get:

$$\mu_{x_t} = \frac{L\mu_{y_c}}{\alpha\Delta h+\mu_{y_c}} - \sigma_{y_c}^2 L \frac{\alpha\Delta h}{(\alpha\Delta h+\mu_{y_c})^3} \tag{F10}$$

$$\sigma_{x_t}^2 = \sigma_{y_c}^2 \left(\frac{L\alpha\Delta h}{(\alpha\Delta h+\mu_{y_c})^2}\right)^2$$

APPENDIX G: SOLUTION FOR TRANSIENT FRESHWATER DISCHARGE INTO THE SEA IN A FLUX BOUNDARY CASE BY BEAR (1972)

The method discussed below by Bear (1972) is suggested by Kochina (1962) and is also known as an approach of successive steady states or approximate quasi-steady approach. As per this approach, $Q_f(x,t)$ is assumed to be varying from Q'_{fL} at $x = L$, $\eta = B$, to Q_{f0} at $x = 0$, $\eta \approx 0$. The freshwater discharge $Q_{f0}(t)$ is an unknown variable for the analysis. $U_s(t)$ is the volume of aquifer intruded by seawater. For the conceptual model and variables, refer Figure 27(a).

By applying conditions of continuity in the aquifer:

$$\frac{ndU_s(t)}{dt} = Q_{f0}(t) - Q'_{fL} \tag{G1}$$

$$U_s(t) = \int_{\eta=0}^{B} x(\eta,t)d\eta \tag{G2}$$

Substituting the value of $U_s(t)$ from (A.2) into (A.1):

$$n\frac{d}{dt}\int_{\eta=0}^{B} x(\eta,t)d\eta = Q_{f0}(t) - Q'_{fL} \tag{G3}$$

From the Ghyben-Herzberg approximation:

$$\eta = \frac{\gamma_f}{\gamma_s-\gamma_f}\emptyset_f - \frac{\gamma_s}{\gamma_s-\gamma_f}\emptyset_s \tag{G4}$$

where $\emptyset_f$ and $\emptyset_s$ are freshwater and seawater potentials, respectively, and γ_f and γ_s are freshwater and seawater specific weights, respectively. Potential $\emptyset$ is given as $z + p/\gamma$, where z is the elevation head and p is the pressure head. By differentiating equation (A.4) w.r.t. x:

$$\frac{\partial \eta}{\partial x} = \frac{\gamma_f}{\gamma_s - \gamma_f}\frac{\partial \emptyset_f}{\partial x} - \frac{\gamma_s}{\gamma_s - \gamma_f}\frac{\partial \emptyset_s}{\partial x} \tag{G5}$$

Using Darcy's Law,

$$Q_f = K_f \frac{\partial \emptyset_f}{\partial x}\, \eta \tag{G6}$$

$$Q_s = K_s \frac{\partial \emptyset_s}{\partial x}(B - \eta) \tag{G7}$$

Substituting $\frac{\partial \emptyset_f}{\partial x}$ and $\frac{\partial \emptyset_s}{\partial x}$ from Eq. (G6) and Eq. (G7) into Eq. (G5):

$$\frac{\partial \eta}{\partial x} = \frac{Q_f}{K_f \varepsilon \eta} - \frac{Q_s}{K_s \varepsilon (B - \eta)} \tag{G8}$$

In a coastal aquifer, it is fair to assume $K_f \approx K_s$ as viscosities of the seawater and freshwater are not much different. By using $Q'_{fL} = Q_f + Q_s$ and rearranging:

$$\frac{\partial \eta}{\partial x} = \frac{Q_f\, B}{K \varepsilon \eta (B - \eta)} - \frac{Q'_{fL}}{K \varepsilon (B - \eta)} \tag{G9}$$

The suggested method can be implemented by the following 3 steps.

a) A function is assumed for the variation of $Q_f(\eta, t)$ in terms of Q_{fL}, Q_{f0}, η.

$Q_f(x, t) \equiv Q_f(Q_{fL}, Q_{f0}, \eta)$ should satisfy following:

At $x = 0$; $Q_f(x,t) = Q_{f0}$, $\eta = 0$

At $x = L$; $Q_f(x,t) = Q_{fL}$, $\eta = B$

Bear (1972) assumed a linear variation of $Q_f(x,t)$ with η such that $Q_f(x,t)$ varies linearly from Q'_{fL} at $x = L$ (where $\eta = B$) to $Q_{f0}(t)$ at $x = 0$ (where $\eta \approx 0$), which is as follows

$$Q_f(\eta,t) = Q'_{fL} + [Q_{f0}(t) - Q'_{fL}]\frac{(B-\eta)}{B}$$

$$= Q_{f0}(t) - [Q_{f0}(t) - Q'_{fL}]\frac{\eta}{B} \quad \text{(G10)}$$

b) Insert Q_f from Eqs. (G10) into Eq. (G9) and integrate to get η as a function of x and Q_{f0}:

$$\eta^2(x,t) = \left[\frac{2Q_{f0}(t)}{K'}\right]x \quad \text{(G11)}$$

c) Then substitute this η in Eq. (G3) and integrate to get:

$$\frac{6t}{nK\varepsilon B^3} = \frac{1}{(Q'_{fL})^2} ln\frac{Q_{f0}(t)}{Q^0_{f0}} - \frac{1}{Q'_{fL}}\left(\frac{1}{Q_{f0}(t)} - \frac{1}{Q^0_{fo}}\right) - \frac{1}{Q'_{fL}{}^2} ln\frac{Q'_{fL}-Q_{f0}(t)}{Q'_{fL}-Q^0_{f0}} \quad \text{(G12)}$$

Eq. (G12) gives the implicit solution for the transient freshwater discharge into the sea $Q_{f0}(t)$ controlled by the change in the freshwater flux $Q_{fL}(t)$ at the inland boundary.

APPENDIX H: SIMPLIFICATION OF THE TIMESCALE EXPRESSION

This section provides the conversion of $E = ln\frac{\beta}{\beta+0.95(1-\beta)} - \frac{0.95(1-\beta)}{1} - ln\frac{\beta-\frac{\beta}{\beta+0.95(1-\beta)}}{\beta-1}$ into $E = 0.95\beta + 2.046$ for the simplification of the timescale expression used in this paper.

$$E = ln\frac{\beta}{\beta+0.95(1-\beta)} - \frac{0.95(1-\beta)}{1} - ln\frac{\beta-\frac{\beta}{\beta+0.95(1-\beta)}}{\beta-1}$$

$$= ln\left(\frac{\beta}{\beta + 0.95(1-\beta)}\frac{\beta-1}{\beta-\frac{\beta}{\beta+0.95(1-\beta)}}\right) - \frac{0.95(1-\beta)}{1}$$

$$= 0.95\beta - 0.95 + ln\left(\frac{\beta}{\beta + 0.95(1-\beta)}\frac{\beta-1}{\beta-\frac{\beta}{\beta+0.95(1-\beta)}}\right)$$

$$= 0.95\beta - 0.95 + ln\left(\frac{1}{\beta + 0.95(1-\beta)}\frac{\beta-1}{\frac{\beta+0.95(1-\beta)-1}{\beta+0.95(1-\beta)}}\right)$$

$$= 0.95\beta - 0.95 + ln\left(\frac{\beta-1}{\beta+0.95(1-\beta)-1}\right)$$

$$= 0.95\beta - 0.95 + ln\left(\frac{\beta-1}{0.05\beta-0.05}\right)$$

Assuming $\beta \neq 1$

$$= 0.95\beta - 0.95 + ln(20) = 0.95\beta + 2.046$$

REFERENCES

. Abarca, E., 2006. Seawater intrusion in complex geological environments. Universitat Politècnica de Catalunya.

Abarca, E., Carrera, J., Sánchez-Vila, X., Dentz, M., 2007a. Anisotropic dispersive Henry problem. Advances in Water Resources, 30(4): 913-926. DOI:10.1016/j.advwatres.2006.08.005

Abarca, E., Carrera, J., Sánchez-Vila, X., Voss, C.I., 2007b. Quasi-horizontal circulation cells in 3D seawater intrusion. Journal of Hydrology, 339(3-4): 118-129.

Abdollahi-Nasab, A., Boufadel, M.C., Li, H., Weaver, J.W., 2010. Saltwater flushing by freshwater in a laboratory beach. Journal of Hydrology, 386(1-4): 1-12. DOI:10.1016/j.jhydrol.2009.12.005

Appelo, C., Willemsen, A., 1987. Geochemical calculations and observations on salt water intrusions, I. A combined geochemical/minxing cell model. Journal of Hydrology, 94(3-4): 313-330.

Back, W., Hanshaw, B.B., Pyle, T.E., Plummer, L.N., Weidie, A., 1979. Geochemical significance of groundwater discharge and carbonate solution to the formation of Caleta Xel Ha, Quintana Roo, Mexico. Water Resources Research, 15(6): 1521-1535.

Badon Ghyben, W., 1888. Nota in Verband met de Voorgenomen Putboring nabij Amsterdam. Tijdshrift van het koninklyk Instituut van Ingenieurs, 21.

Bakker, M., 1998. Transient Dupuit interface flow with partially penetrating features. Water resources research, 34(11): 2911-2918.

Bakker, M., 2000. The size of the freshwater zone below an elongated island with infiltration. Water Resources Research, 36(1): 109-117.

Bakker, M., 2006. Analytic solutions for interface flow in combined confined and semi-confined, coastal aquifers. Advances in Water Resources, 29(3): 417-425. DOI:https://doi.org/10.1016/j.advwatres.2005.05.009

Bakker, M., Essink, G.H.O., Langevin, C.D., 2004a. The rotating movement of three immiscible fluids—a benchmark problem. Journal of Hydrology, 287(1-4): 270-278.

Bakker, M., Oude Essink, G.H.P., Langevin, C.D., 2004b. The rotating movement of three immiscible fluids - A benchmark problem. Journal of Hydrology, 287(1-4): 270-278. DOI:10.1016/j.jhydrol.2003.10.007

Barlow, P.M., Reichard, E.G., 2010. Saltwater intrusion in coastal regions of North America. Hydrogeology Journal, 18(1): 247-260.

Barwell, V., Lee, D.R., 1981. Determination of horizontal-to-vertical hydraulic conductivity ratios from seepage measurements on lake beds. Water Resources Research, 17(3): 565-570.

Bear, J., 1972. Dynamics of fluids in porous media. American Else-vier, New York.

Bear, J., 1979. Hydraulics of Groundwater.

Bear, J., 2013. Dynamics of fluids in porous media. Courier Corporation.

Bear, J., Dagan, G., 1964. Moving interface in coastal aquifers. J. Hydraul. Div. Am. Soc. Civ. Eng, 99: 193-215.

Bear, J., Shamir, U., Gamliel, A., Shapiro, A.M., 1985. Motion of the seawater interface in a coastal aquifer by the method of successive steady states. Journal of Hydrology, 76(1): 119-132. DOI:http://dx.doi.org/10.1016/0022-1694(85)90093-9

Bear, J., Zhou, Q., Bensabat, J., 2001. Three dimensional simulation of seawater intrusion in heterogeneous aquifers, with application to the coastal aquifer of Israel, the proceedings of the First International Conference on Saltwater Intrusion and Coastal Aquifers-Monitoring, Modeling, and Management, Essaouira, Morocco, April. Citeseer, pp. 23-25.

Berner, R.A., 1980. Early diagenesis: a theoretical approach. Princeton University Press.

Boufadel, M.C., 2000. A mechanistic study of nonlinear solute transport in a groundwater-surface water system under steady state and transient hydraulic conditions. Water Resources Research, 36(9): 2549-2565. DOI:10.1029/2000WR900159

Boufadel, M.C., Xia, Y., Li, H., 2011. Modeling solute transport and transient seepage in a laboratory beach under tidal influence. Environmental Modelling and Software, 26(7): 899-912. DOI:10.1016/j.envsoft.2011.02.005

Bower, J., Motz, L., Durden, D., 1999. Analytical solution for determining the critical condition of saltwater upconing in a leaky artesian aquifer. Journal of Hydrology, 221(1-2): 43-54.

Boyle, J.M., Saleem, Z., 1979. Determination of recharge rates using temperature-depth profiles in wells. Water Resources Research, 15(6): 1616-1622.

Bratton, J.F., 2007. The importance of shallow confining units to submarine groundwater flow. IAHS Proceedings and Reports, 312. IAHS Press, Wallingford, U. K.

Bredehoeft, J.D., Papaopulos, I., 1965. Rates of vertical groundwater movement estimated from the Earth's thermal profile. Water Resources Research, 1(2): 325-328.

Burnett, W.C., 1996. Tracing groundwater flow into surface waters using natural super (222) RN. LOICZ Reports Studies(8): 22-36.

Burnett, W.C. et al., 2006. Quantifying submarine groundwater discharge in the coastal zone via multiple methods. Science of The Total Environment, 367(2): 498-543. DOI:https://doi.org/10.1016/j.scitotenv.2006.05.009

Burnett, W.C., Bokuniewicz, H., Huettel, M., Moore, W.S., Taniguchi, M., 2003. Groundwater and pore water inputs to the coastal zone. Biogeochemistry, 66(1): 3-33. DOI:10.1023/b:Biog.0000006066.21240.53

Cable, J.E., Bugna, G.C., Burnett, W.C., Chanton, J.P., 1996. Application of 222Rn and CH4 for assessment of groundwater discharge to the coastal ocean. Limnology and Oceanography, 41(6): 1347-1353.

Carneiro, J.F. et al., 2010. Evaluation of climate change effects in a coastal aquifer in Morocco using a density-dependent numerical model. Environmental Earth Sciences, 61(2): 241-252. DOI:10.1007/s12665-009-0339-3

Cartwright, N., Li, L., Nielsen, P., 2004. Response of the salt–freshwater interface in a coastal aquifer to a wave-induced groundwater pulse: field observations and modelling. Advances in Water Resources, 27(3): 297-303. DOI:http://doi.org/10.1016/j.advwatres.2003.12.005

Chang, S.W., Clement, T.P., 2012. Experimental and numerical investigation of saltwater intrusion dynamics in flux-controlled groundwater systems. Water Resources Research, 48(9): n/a-n/a. DOI:10.1029/2012WR012134

Chang, S.W., Clement, T.P., 2013. Laboratory and numerical investigation of transport processes occurring above and within a saltwater wedge. J Contam Hydrol, 147: 14-24. DOI:10.1016/j.jconhyd.2013.02.005

Chang, S.W., Clement, T.P., Simpson, M.J., Lee, K.-K., 2011. Does sea-level rise have an impact on saltwater intrusion? Advances in Water Resources, 34(10): 1283-1291. DOI:http://dx.doi.org/10.1016/j.advwatres.2011.06.006

Charette, M.A., Buesseler, K.O., Andrews, J.E., 2001. Utility of radium isotopes for evaluating the input and transport of groundwater-derived nitrogen to a Cape Cod estuary. Limnology and Oceanography, 46(2): 465-470.

Cheng, A.D., Halhal, D., Naji, A., Ouazar, D., 2000. Pumping optimization in saltwater-intruded coastal aquifers. Water Resources Research, 36(8): 2155-2165.

Cherubini, C., Pastore, N., 2011. Critical stress scenarios for a coastal aquifer in southeastern Italy. Natural Hazards and Earth System Science, 11(5): 1381-1393. DOI:10.5194/nhess-11-1381-2011

Church, T.M., 1996. An underground route for the water cycle. Nature, 380(6575): 579-580.

Cihan, A., Zhou, Q., Birkholzer, J.T., Kraemer, S.R., 2014. Flow in horizontally anisotropic multilayered aquifer systems with leaky wells and aquitards. Water Resources Research, 50(1): 741-747. DOI:10.1002/2013WR013867

Collins, M.A., Gelhar, L.W., 1971. Seawater intrusion in layered aquifers. Water Resources Research, 7(4): 971-979. DOI:10.1029/WR007i004p00971

Corbett, D.R., Dillon, K., Burnett, W., Chanton, J., 2000. Estimating the groundwater contribution into Florida Bay via natural tracers, 222Rn and CH4. Limnology and Oceanography, 45(7): 1546-1557.

Crotwell, A.M., Moore, W.S., 2003. Nutrient and radium fluxes from submarine groundwater discharge to Port Royal Sound, South Carolina. Aquatic Geochemistry, 9(3): 191-208.

Cushman, J.H., Bennethum, L.S., Hu, B.X., 2002. A primer on upscaling tools for porous media. Advances in Water Resources, 25(8): 1043-1067. DOI:https://doi.org/10.1016/S0309-1708(02)00047-7

Custodio, E., 2010. Coastal aquifers of Europe: an overview. Hydrogeology Journal, 18(1): 269-280.

Dafny, E., Burg, A., Gvirtzman, H., 2010. Effects of Karst and geological structure on groundwater flow: The case of Yarqon-Taninim Aquifer, Israel. Journal of Hydrology, 389(3): 260-275. DOI:10.1016/j.jhydrol.2010.05.038

Dagan, G., Zeitoun, D.G., 1998. Seawater-freshwater interface in a stratified aquifer of random permeability distribution. Journal of Contaminant Hydrology, 29(3): 185-203. DOI:10.1016/S0169-7722(97)00013-2

Darling, W.G., Edmunds, W.M., Smedley, P.L., 1997. Isotopic evidence for palaeowaters in the British Isles. Applied Geochemistry, 12(6): 813-829. DOI:https://doi.org/10.1016/S0883-2927(97)00038-3

Datta, B., Vennalakanti, H., Dhar, A., 2009. Modeling and control of saltwater intrusion in a coastal aquifer of Andhra Pradesh, India. Journal of Hydro-Environment Research, 3(3): 148-159. DOI:10.1016/j.jher.2009.09.002

Day-Lewis, F., White, E., Johnson, C., Lane Jr, J., Belaval, M., 2006. Continuous resistivity profiling to delineate submarine groundwater discharge—Examples and limitations. The Leading Edge, 25(6): 724-728.

De Franco, R. et al., 2009. Monitoring the saltwater intrusion by time lapse electrical resistivity tomography: The Chioggia test site (Venice Lagoon, Italy). Journal of Applied Geophysics, 69(3-4): 117-130.

Diersch, H., 1998. FEFLOW reference manual: Interactive, graphics-based finite-element simulation system for modeling groundwater flow, contaminant mass and heat transport processes. Berlin: WASY Institute for Water Resources Planning and Systems Research Ltd.

Dimova, N.T., Burnett, W.C., Speer, K., 2011. A natural tracer investigation of the hydrological regime of Spring Creek Springs, the largest submarine spring system in Florida. Continental Shelf Research, 31(6): 731-738.

Dupuit, J.É.J., 1863. Études théoriques et pratiques sur le mouvement des eaux dans les canaux découverts et à travers les terrains perméables: avec des considérations relatives au régime des grandes eaux, au débouché à leur donner, et à la marche des alluvions dans les rivières à fond mobile. Dunod.

Eeman, S., Leijnse, A., Raats, P., Van der Zee, S., 2011. Analysis of the thickness of a fresh water lens and of the transition zone between this lens and upwelling saline water. Advances in Water Resources, 34(2): 291-302.

El-Bihery, M.A., 2009. Groundwater flow modeling of Quaternary aquifer Ras Sudr, Egypt. Environmental Geology, 58(5): 1095-1105. DOI:10.1007/s00254-008-1589-1

Elder, J.W., 1967. Steady free convection in a porous medium heated from below. Journal of Fluid Mechanics, 27(1): 29-48.

Essaid, H.I., 1990. A multilayered sharp interface model of coupled freshwater and saltwater flow in coastal systems: Model development and application. Water Resources Research, 26(7): 1431-1454. DOI:10.1029/WR026i007p01431

Fahs, M., Ataie-Ashtiani, B., Younes, A., Simmons, C.T., Ackerer, P., 2016. The Henry problem: New semianalytical solution for velocity-dependent dispersion. Water Resources Research, 52(9): 7382-7407. DOI:10.1002/2016WR019288

Farmer, C.L., 2002. Upscaling: a review. International Journal for Numerical Methods in Fluids, 40(1-2): 63-78. DOI:10.1002/fld.267

Faye, S. et al., 2005. Groundwater salinization in the Saloum (Senegal) delta aquifer: minor elements and isotopic indicators. Science of the Total Environment, 343(1-3): 243-259.

Fitterman, D.V., Deszcz-Pan, M., 1998. Helicopter EM mapping of saltwater intrusion in Everglades National Park, Florida. Exploration Geophysics, 29(1-2): 240-243.

Flathe, H., 1955. Possibilities and limitations in applying geoelectrical methods to hydrogeological problems in the coastal areas of North West Germany. Geophysical prospecting, 3(2): 95-109.

Forchheimer, P., 1886. Ueber die ergiebigkeit von brunnen-anlagen und sickerschlitzen. Z. Architekt. Ing. Ver. Hannover, 32: 539-563.

Fretwell, J.D., Stewart, M.T., 1981. Resistivity study of a coastal karst terrain, Florida. Groundwater, 19(2): 156-162.

Giambastiani, B.M.S., Antonellini, M., Oude Essink, G.H.P., Stuurman, R.J., 2007. Saltwater intrusion in the unconfined coastal aquifer of Ravenna (Italy): A numerical model. Journal of Hydrology, 340(1-2): 91-104. DOI:10.1016/j.jhydrol.2007.04.001

Giménez-Forcada, E., 2010. Dynamic of sea water interface using hydrochemical facies evolution diagram. Groundwater, 48(2): 212-216.

Ginsberg, A., Levanton, A., 1976. Determination of saltwater interface by electrical resistivity sounding. Hydrological science bulletin, 21(6): 561-568.

Goldman, M., Gilad, D., Ronen, A., Melloul, A., 1991. Mapping of seawater intrusion into the coastal aquifer of Israel by the time domain electromagnetic method. Geoexploration, 28(2): 153-174.

Gomis-Yagües, V., Boluda-Botella, N., Ruiz-Beviá, F., 2000. Gypsum precipitation/dissolution as an explanation of the decrease of sulphate concentration during seawater intrusion. Journal of Hydrology, 228(1-2): 48-55.

Gossel, W., Sefelnasr, A., Wycisk, P., 2010. Modelling of paleo-saltwater intrusion in the northern part of the Nubian Aquifer System, Northeast Africa. Hydrogeology Journal, 18(6): 1447-1463. DOI:10.1007/s10040-010-0597-x

Goswami, R.R., Clement, T.P., 2007. Laboratory-scale investigation of saltwater intrusion dynamics. Water Resources Research, 43(4). DOI:10.1029/2006wr005151

Graf, T., Therrien, R., 2005. Variable-density groundwater flow and solute transport in porous media containing nonuniform discrete fractures. Advances in Water Resources, 28(12): 1351-1367. DOI:10.1016/j.advwatres.2005.04.011

Grassi, S., Cortecci, G., 2005. Hydrogeology and geochemistry of the multilayered confined aquifer of the Pisa plain (Tuscany–central Italy). Applied Geochemistry, 20(1): 41-54.

Guo, Q., Li, H., Boufadel, M.C., Sharifi, Y., 2010. Hydrodynamics in a gravel beach and its impact on the Exxon Valdez oil. Journal of Geophysical Research: Oceans, 115(C12).

Guo, W., Langevin, C.D., 2002. User's guide to SEAWAT; a computer program for simulation of three-dimensional variable-density ground-water flow. 06-A7. DOI:10.3133/twri06A7

Harrar, W.G., Williams, A.T., Barker, J.A., Van Camp, M., 2001. Modelling scenarios for the emplacement of palaeowaters in aquifer systems, in Palaeowaters in coastal Europe: Evolution of groundwater since the late Pleistocene. Geological Society of London Special Publications 189: 213-229.

Held, R., Attinger, S., Kinzelbach, W., 2005. Homogenization and effective parameters for the Henry problem in heterogeneous formations. Water Resources Research, 41(11). DOI:10.1029/2004WR003674

Henderson, R.D. et al., 2010. Marine electrical resistivity imaging of submarine groundwater discharge: sensitivity analysis and application in Waquoit Bay, Massachusetts, USA. Hydrogeology Journal, 18(1): 173-185.

Henry, H.R., 1964. Effects of dispersion on salt encroachment in coastal aquifers. Water-Supply Paper 1613-C, 70.

Huppert, H.E., Woods, A.W., 2006. Gravity-driven flows in porous layers. Journal of Fluid Mechanics, 292: 55-69. DOI:10.1017/S0022112095001431

Isaacs, L., Hunt, B., 1986. A simple approximation for a moving interface in a coastal aquifer. Journal of Hydrology, 83(1-2): 29-43.

Johannsen, K., Kinzelbach, W., Oswald, S., Wittum, G., 2002. The saltpool benchmark problem–numerical simulation of saltwater upconing in a porous medium. Advances in Water Resources, 25(3): 335-348.

Kacimov, A., 2002. Analytical solutions in a hydraulic model of seepage with sharp interfaces. Journal of hydrology, 258(1-4): 179-186.

Kacimov, A., Obnosov, Y.V., 2001. Analytical solution for a sharp interface problem in sea water intrusion into a coastal aquifer, Proceedings of the Royal Society of London A: Mathematical, Physical and Engineering Sciences. The Royal Society, pp. 3023-3038.

Kacimov, A.R., Sherif, M.M., 2006. Sharp interface, one-dimensional seawater intrusion into a confined aquifer with controlled pumping: Analytical solution. Water Resources Research, 42(6). DOI:10.1029/2005wr004551

Kaleris, V., 2006. Submarine groundwater discharge: Effects of hydrogeology and of near shore surface water bodies. Journal of hydrology, 325(1-4): 96-117.

Kaleris, V., Lagas, G., Marczinek, S., Piotrowski, J., 2002. Modelling submarine groundwater discharge: an example from the western Baltic Sea. Journal of Hydrology, 265(1-4): 76-99.

Kerrou, J., Renard, P., 2010. A numerical analysis of dimensionality and heterogeneity effects on advective dispersive seawater intrusion processes. Hydrogeology Journal, 18(1): 55-72.

Kim, K.-Y. et al., 2006. Tidal effects on variations of fresh–saltwater interface and groundwater flow in a multilayered coastal aquifer on a volcanic island (Jeju Island, Korea). Journal of Hydrology, 330(3-4): 525-542.

Kinzelbach, W., Bauer, P., Siegfried, T., Brunner, P., 2003. Sustainable groundwater management--Problems and scientific tool. Episodes-Newsmagazine of the International Union of Geological Sciences, 26(4): 279-284.

Kiro, Y., Yechieli, Y., Lyakhovsky, V., Shalev, E., Starinsky, A., 2008. Time response of the water table and saltwater transition zone to a base level drop. Water Resources Research, 44(12). DOI:10.1029/2007WR006752

Kochina, P.I.A., 1962. Theory of ground water movement. Princeton, N.J., Princeton University Press, Princeton, N.J.

Konikow, L.F., Sanford, W., Campbell, P., 1997. Constant-concentration boundary condition: Lessons from the HYDROCOIN variable-density groundwater benchmark problem. Water Resources Research, 33(10): 2253-2261.

Kourakos, G., Mantoglou, A., 2009. Pumping optimization of coastal aquifers based on evolutionary algorithms and surrogate modular neural network models. Advances in Water Resources, 32(4): 507-521. DOI:10.1016/j.advwatres.2009.01.001

Krest, J.M., Harvey, J.W., 2003. Using natural distributions of short-lived radium isotopes to quantify groundwater discharge and recharge. Limnology and Oceanography, 48(1): 290-298.

Krupa, S.L., Belanger, T.V., Heck, H.H., Brock, J.T., Jones, B.J., 1998. Krupaseep—The next generation seepage meter. Journal of Coastal Research: 210-213.

Langevin, C.D., Shoemaker, W.B., Guo, W., 2003. MODFLOW-2000, the US Geological Survey Modular Ground-Water Model--Documentation of the SEAWAT-2000 Version with the Variable-Density Flow Process (VDF) and the Integrated MT3DMS Transport Process (IMT). 2331-1258.

Li, H., Boufadel, M.C., 2011. A tracer study in an Alaskan gravel beach and its implications on the persistence of the Exxon Valdez oil. Marine Pollution Bulletin, 62(6): 1261-1269. DOI:10.1016/j.marpolbul.2011.03.011

Li, L., Barry, D.A., Stagnitti, F., Parlange, J.Y., 1999. Submarine groundwater discharge and associated chemical input to a coastal sea. Water Resources Research, 35(11): 3253-3259. DOI:10.1029/1999wr900189

Lin, J., Snodsmith, J.B., Zheng, C., Wu, J., 2009. A modeling study of seawater intrusion in Alabama Gulf Coast, USA. Environmental Geology, 57(1): 119-130. DOI:10.1007/s00254-008-1288-y

Lu, C., Chen, Y., Zhang, C., Luo, J., 2013a. Steady-state freshwater-seawater mixing zone in stratified coastal aquifers, 505, 24-34 pp. DOI:10.1016/j.jhydrol.2013.09.017

Lu, C., Chen, Y., Zhang, C., Luo, J., 2013b. Steady-state freshwater–seawater mixing zone in stratified coastal aquifers. Journal of Hydrology, 505: 24-34. DOI:10.1016/j.jhydrol.2013.09.017

Lu, C., Werner, A.D., 2013. Timescales of seawater intrusion and retreat. Advances in Water Resources, 59: 39-51. DOI:10.1016/j.advwatres.2013.05.005

Lu, C., Werner, A.D., Simmons, C.T., Luo, J., 2015. A correction on coastal heads for groundwater flow models. Ground Water, 53(1): 164-70. DOI:10.1111/gwat.12172

Manheim, F.T., Krantz, D.E., Bratton, J.F., 2004. Studying ground water under Delmarva coastal bays using electrical resistivity. Groundwater, 42(7): 1052-1068.

Mao, X. et al., 2006. Tidal influence on behaviour of a coastal aquifer adjacent to a low-relief estuary. Journal of Hydrology, 327(1-2): 110-127. DOI:10.1016/j.jhydrol.2005.11.030

McClymonds, N., Franke, O.L., 1972. Water-transmitting properties of aquifers on Long Island, New York. US Government Printing Office.

Meisler, H., Leahy, P.P., Knobel, L.L., 1984. Effect of eustatic sea-level changes on saltwater-freshwater relations in the Northern Atlantic Coastal Plain. 2255.

Michael, H.A., 2005. Seasonal dynamics in costal aquifers: investigation of submarine groundwater discharge through field measurements and numerical models, Massachusetts Institute of Technology.

Michael, H.A., Mulligan, A.E., Harvey, C.F., 2005. Seasonal oscillations in water exchange between aquifers and the coastal ocean. Nature, 436(7054): 1145-8. DOI:10.1038/nature03935

Moore, W.S., 1996. Large groundwater inputs to coastal waters revealed by 226Ra enrichments. Nature, 380(6575): 612.

Moore, W.S., 2010. The effect of submarine groundwater discharge on the ocean. Annual review of marine science, 2: 59-88.

Moore, W.S. et al., 2002. Thermal evidence of water exchange through a coastal aquifer: Implications for nutrient fluxes. Geophysical Research Letters, 29(14): 49-1-49-4.

Moore, W.S., Shaw, T.J., 1998. Chemical signals from submarine fluid advection onto the continental shelf. Journal of Geophysical Research: Oceans, 103(C10): 21543-21552.

Moore, W.S., Wilson, A.M., 2005. Advective flow through the upper continental shelf driven by storms, buoyancy, and submarine groundwater discharge. Earth and Planetary Science Letters, 235(3-4): 564-576.

Mualem, Y., Bear, J., 1974. The shape of the interface in steady flow in a stratified aquifer. Water Resources Research, 10(6): 1207-1215.

Naji, A., Cheng, A.H.-D., Ouazar, D., 1998. Analytical stochastic solutions of saltwater/freshwater interface in coastal aquifers. Stochastic Hydrology and Hydraulics, 12(6): 413-430. DOI:10.1007/s004770050028

National Groundwater Association, 2019. Groundwater Facts.

Nishikawa, T. et al., 2009. Stratigraphic controls on seawater intrusion and implications for groundwater management, Dominguez Gap area of Los Angeles, California, USA. Hydrogeology Journal, 17(7): 1699-1725. DOI:10.1007/s10040-009-0481-8

Oberdorfer, J.A., 2003. Hydrogeologic Modeling of Submarine Groundwater Discharge: Comparison to Other Quantitative Methods. Biogeochemistry, 66(1/2): 159-169.

Ogilvy, R. et al., 2009. Automated monitoring of coastal aquifers with electrical resistivity tomography. Near Surface Geophysics, 7(5-6): 367-376.

Oki, D.S., Souza, W.R., Bolke, E.L., Bauer, G.R., 1998. Numerical analysis of the hydrogeologic controls in a layered coastal aquifer system, Oahu, Hawaii, USA. Hydrogeology Journal, 6(2): 243-263.

Oswald, S., Kinzelbach, W., 2004. Three-dimensional physical benchmark experiments to test variable-density flow models. Journal of Hydrology, 290(1-2): 22-42.

Öztürk, Y.F., 1970. Seawater intrusion length in stratified estuaries. Water Research, 4(7): 477-484. DOI:https://doi.org/10.1016/0043-1354(70)90062-X

Paine, J.G., 2003. Determining salinization extent, identifying salinity sources, and estimating chloride mass using surface, borehole, and airborne electromagnetic induction methods. Water Resources Research, 39(3).

Park, C.-H., Aral, M.M., 2004. Multi-objective optimization of pumping rates and well placement in coastal aquifers. Journal of Hydrology, 290(1-2): 80-99.

Paulsen, R.J., Smith, C.F., O'Rourke, D., Wong, T.F., 2001. Development and evaluation of an ultrasonic ground water seepage meter. Groundwater, 39(6): 904-911.

Petalas, C.P., Diamantis, I.B., 1999. Origin and distribution of saline groundwaters in the upper Miocene aquifer system, coastal Rhodope area, northeastern Greece. Hydrogeology Journal, 7(3): 305-316. DOI:10.1007/s100400050204

Pool, M., Carrera, J., 2010. Dynamics of negative hydraulic barriers to prevent seawater intrusion. Hydrogeology Journal, 18(1): 95-105. DOI:10.1007/s10040-009-0516-1

Pool, M., Carrera, J., 2011. A correction factor to account for mixing in Ghyben-Herzberg and critical pumping rate approximations of seawater intrusion in coastal aquifers. Water Resources Research, 47(5). DOI:10.1029/2010wr010256

Pool, M., Post, V.E.A., Simmons, C.T., 2015. Effects of tidal fluctuations and spatial heterogeneity on mixing and spreading in spatially heterogeneous coastal aquifers. Water Resources Research, 51(3): 1570-1585. DOI:doi:10.1002/2014WR016068

Post, V., 2005. Fresh and saline groundwater interaction in coastal aquifers: is our technology ready for the problems ahead? Hydrogeology Journal, 13(1): 120-123.

Post, V., Kooi, H., Simmons, C., 2007. Using hydraulic head measurements in variable-density ground water flow analyses. Groundwater, 45(6): 664-671.

Poulsen, S.E., Rasmussen, K.R., Christensen, N.B., Christensen, S., 2010. Evaluating the salinity distribution of a shallow coastal aquifer by vertical multielectrode profiling (Denmark). Hydrogeology journal, 18(1): 161-171.

Price, R.M., Swart, P.K., Fourqurean, J.W., 2006. Coastal groundwater discharge–an additional source of phosphorus for the oligotrophic wetlands of the Everglades. Hydrobiologia, 569(1): 23-36.

Rathore, S.S., Tang, Y., Lu, C., Luo, J., 2019. A Simplified Equation of Approximate Interface Profile in Stratified Coastal Aquifers. Journal of Hydrology: 124249. DOI:doi:10.1016/j.jhydrol.2019.124249

Rathore, S.S., Zhao, Y., Lu, C., Luo, J., 2018a. Analytical analysis of the temporal asymmetry between seawater intrusion and retreat. Advances in Water Resources, 111: 121-131. DOI:https://doi.org/10.1016/j.advwatres.2017.11.001

Rathore, S.S., Zhao, Y., Lu, C., Luo, J., 2018b. Defining the effect of stratification in coastal aquifers using a new parameter. Water Resources Research, 54(9). DOI:doi:10.1029/2018WR023114

Reilly, T., Goodman, A., 1987. Analysis of saltwater upconing beneath a pumping well. Journal of Hydrology, 89(3-4): 169-204.

Renard, P., de Marsily, G., 1997. Calculating equivalent permeability: a review. Advances in Water Resources, 20(5): 253-278. DOI:https://doi.org/10.1016/S0309-1708(96)00050-4

Robinson, C., Li, L., Prommer, H., 2007. Tide-induced recirculation across the aquifer-ocean interface. Water Resources Research, 43(7). DOI:10.1029/2006wr005679

Robinson, C.E. et al., 2018. Groundwater dynamics in subterranean estuaries of coastal unconfined aquifers: Controls on submarine groundwater discharge and chemical inputs to the ocean. Advances in Water Resources, 115: 315-331. DOI:https://doi.org/10.1016/j.advwatres.2017.10.041

Rumer, R.R., Shiau, J., 1968. Salt water interface in a layered coastal aquifer. Water Resources Research, 4(6): 1235-1247.

Sacks, L.A., Tihansky, A.B., 1996. Geochemical and isotopic composition of ground water, with emphasis on sources of sulfate, in the Upper Floridan Aquifer and Intermediate Aquifer System in Southwest Florida. US Department of the Interior, US Geological Survey.

Saeed, M.M., Bruen, M., Asghar, M., 2002. A review of modeling approaches to simulate saline-upconing under skimming wells. Hydrology Research, 33(2-3): 165-188.

Sanchez-Vila, X., Guadagnini, A., Carrera, J., 2006. Representative hydraulic conductivities in saturated groundwater flow. Reviews of Geophysics, 44(3). DOI:10.1029/2005rg000169

Shi, W. et al., 2018. Assessment of the impact of sea-level rise on steady-state seawater intrusion in a layered coastal aquifer. Journal of Hydrology, 563: 851-862. DOI:https://doi.org/10.1016/j.jhydrol.2018.06.046

Shibuo, Y., Jarsjö, J., Destouni, G., 2006. Bathymetry-topography effects on saltwater–fresh groundwater interactions around the shrinking Aral Sea. Water Resources Research, 42(11). DOI:10.1029/2005wr004207

Shishaye, H., 2015. Technical Note: Groundwater flow modeling in coastal aquifers – the influence of submarine groundwater discharge on the position of the saltwater–freshwater interface. Hydrology and Earth System Sciences Discussions, 12: 3753-3785. DOI:10.5194/hessd-12-3753-2015

Sholkovitz, E., Herbold, C., Charette, M., 2003. An automated dye-dilution based seepage meter for the time-series measurement of submarine groundwater discharge. Limnology and Oceanography: Methods, 1(1): 16-28.

Siemon, B., Christiansen, A.V., Auken, E., 2009. A review of helicopter-borne electromagnetic methods for groundwater exploration. Near Surface Geophysics, 7(5-6): 629-646.

Silliman, S.E., Booth, D.F., 1993. Analysis of time-series measurements of sediment temperature for identification of gaining vs. losing portions of Juday Creek, Indiana. Journal of Hydrology, 146: 131-148.

Simmons, C.T., Fenstemaker, T.R., Sharp Jr, J.M., 2001. Variable-density groundwater flow and solute transport in heterogeneous porous media: approaches, resolutions and future challenges. Journal of Contaminant Hydrology, 52(1-4): 245-275.

Simmons, C.T., Narayan, K.A., Wooding, R.A., 1999. On a test case for density-dependent groundwater flow and solute transport models: The Salt Lake Problem. Water Resources Research, 35(12): 3607-3620.

Simmons Jr, G.M., 1992. Importance of submarine groundwater discharge (Sgwd) and seawater cycling to material flux across sediment water interfaces in marine environments.

Simpson, M.J., Clement, T.P., 2003. Theoretical analysis of the worthiness of Henry and Elder

problems as benchmarks of density-dependent groundwater

flow models. Advances in Water Resources, 26: 17–31.

Simpson, M.J., Clement, T.P., 2004. Improving the worthiness of the Henry problem as a benchmark for density-dependent groundwater flow models. Water Resources Research, 40(1): n/a-n/a. DOI:10.1029/2003wr002199

Smart, P., Dawans, J., Whitaker, F., 1988. Carbonate dissolution in a modern mixing zone. Nature, 335(6193): 811.

Smith, A.J., 2004a. Mixed convection and density-dependent seawater circulation in coastal aquifers. Water Resources Research, 40(8): n/a-n/a. DOI:10.1029/2003WR002977

Smith, A.J., 2004b. Mixed convection and density-dependent seawater circulation in coastal aquifers. Water Resources Research, 40(8).

Stewart, M.T., 1982. Evaluation of electromagnetic methods for rapid mapping of salt-water interfaces in coastal aquifers. Groundwater, 20(5): 538-545.

Strack, O.D., 1989. Groundwater mechanics. Prentice Hall.

Strack, O.D.L., 1976. A single-potential solution for regional interface problems in coastal aquifers. Water Resources Research, 12(6): 1165-1174. DOI:10.1029/WR012i006p01165

Strack, O.D.L., 2016. Salt water interface in a layered coastal aquifer: The only published analytic solution is in error. Water Resources Research, 52(2): 1502-1506. DOI:doi:10.1002/2015WR018127

Strack, O.D.L., 2017. Vertically integrated flow in stratified aquifers. Journal of Hydrology, 548: 794-800. DOI:https://doi.org/10.1016/j.jhydrol.2017.01.039

Strack, O.D.L., Ausk, B.K., 2015. A formulation for vertically integrated groundwater flow in a stratified coastal aquifer. Water Resources Research, 51(8): 6756-6775. DOI:10.1002/2015wr016887

Strack, O.D.L. et al., 2016. Reduction of saltwater intrusion by modifying hydraulic conductivity. Water Resources Research, 52(9): 6978-6988. DOI:10.1002/2016WR019037

Swartz, J., 1937. Resistivity-studies of some salt-water boundaries in the Hawaiian Islands. Eos, Transactions American Geophysical Union, 18(2): 387-393.

Taniguchi, M., Fukuo, Y., 1993. Continuous measurements of ground-water seepage using an automatic seepage meter. Groundwater, 31(4): 675-679.

Thompson, A., 2007. Happy birthday EngineerIT! EngineerIT(JULY): 1.

Thompson, C., Smith, L., Maji, R., 2007. Hydrogeological modeling of submarine groundwater discharge on the continental shelf of Louisiana. Journal of Geophysical Research: Oceans, 112(C3). DOI:10.1029/2006jc003557

Toller, E.A.L., Strack, O.D.L., 2019. Interface Flow With Vertically Varying Hydraulic Conductivity. Water Resources Research, 55(11): 8514-8525. DOI:10.1029/2019wr024927

Valocchi, A.J., Street, R.L., Roberts, P.V., 1981. Transport of ion-exchanging solutes in groundwater: Chromatographic theory and field simulation. Water Resources Research, 17(5): 1517-1527.

Van Dam, J., Meulenkamp, J., 1967. Some results of the geo-electrical resistivity method in ground water investigations in the Netherlands. Geophysical Prospecting, 15(1): 92-115.

Vandenbohede, A., Lebbe, L., 2006. Occurrence of salt water above fresh water in dynamic equilibrium in a coastal groundwater flow system near De Panne, Belgium. Hydrogeology Journal, 14(4): 462-472. DOI:10.1007/s10040-005-0446-5

Vandenbohede, A., Lebbe, L., 2011. Heat transport in a coastal groundwater flow system near De Panne, Belgium. Hydrogeology Journal, 19(6): 1225-1238. DOI:10.1007/s10040-011-0756-8

Vandenbohede, A. et al., 2010. Hydrogeological study for improved nature restoration in dune ecosystems-Kleyne Vlakte case study, Belgium. Journal of Environmental Management, 91(11): 2385-2395. DOI:10.1016/j.jenvman.2010.06.023

Vandenbohede, A., Lebbe, L., Gysens, S., Delecluyse, K., DeWolf, P., 2008a. Salt water infiltration in two artificial sea inlets in the Belgian dune area. Journal of Hydrology, 360(1-4): 77-86. DOI:10.1016/j.jhydrol.2008.07.018

Vandenbohede, A., Luyten, K., Lebbe, L., 2008b. Effects of global change on heterogeneous coastal aquifers: A case study in Belgium. Journal of Coastal Research, 24(2 SUPPL. B): 160-170. DOI:10.2112/05-0447.1

Vandenbohede, A., Van Houtte, E., Lebbe, L., 2008c. Groundwater flow in the vicinity of two artificial recharge ponds in the Belgian coastal dunes. Hydrogeology Journal, 16(8): 1669-1681. DOI:10.1007/s10040-008-0326-x

Vappicha, V.N., Nagaraja, S.H., 1976. An approximate solution for the transient interface in a coastal aquifer. Journal of Hydrology, 31(1): 161-173. DOI:http://dx.doi.org/10.1016/0022-1694(76)90027-5

Vengosh, A., Spivack, A.J., Artzi, Y., Ayalon, A., 1999. Geochemical and boron, strontium, and oxygen isotopic constraints on the origin of the salinity in groundwater from the Mediterranean Coast of Israel. Water Resources Research, 35(6): 1877-1894. DOI:10.1029/1999wr900024

Verruijt, A., 1970. Theory of Groundwater Flow. Theory of Groundwater Flow.

Voss, C.I., Provost, A.M., 2002. SUTRA: A model for 2D or 3D saturated-unsaturated, variable-density ground-water flow with solute or energy transport. 2002-4231. DOI:10.3133/wri024231

Voss, C.I., Souza, W.R., 1987. Variable density flow and solute transport simulation of regional aquifers containing a narrow freshwater-saltwater transition zone. Water Resources Research, 23(10): 1851-1866. DOI:10.1029/WR023i010p01851

Watson, T.A., Werner, A.D., Simmons, C.T., 2010. Transience of seawater intrusion in response to sea level rise. Water Resources Research, 46(12): n/a-n/a. DOI:10.1029/2010WR009564

Wen, X.-H., Gómez-Hernández, J.J., 1996. Upscaling hydraulic conductivities in heterogeneous media: An overview. Journal of Hydrology, 183(1): ix-xxxii. DOI:https://doi.org/10.1016/S0022-1694(96)80030-8

Werner, A.D., 2010. A review of seawater intrusion and its management in Australia. Hydrogeology journal, 18(1): 281-285.

Werner, A.D. et al., 2011. Current Practice and Future Challenges in Coastal Aquifer Management: Flux-Based and Trigger-Level Approaches with Application to an Australian Case Study. Water Resources Management, 25(7): 1831-1853. DOI:10.1007/s11269-011-9777-2

Werner, A.D. et al., 2013. Seawater intrusion processes, investigation and management: Recent advances and future challenges. Advances in Water Resources, 51: 3-26. DOI:10.1016/j.advwatres.2012.03.004

Werner, A.D., Gallagher, M.R., 2006. Characterisation of sea-water intrusion in the Pioneer Valley, Australia using hydrochemistry and three-dimensional numerical modelling. Hydrogeology Journal, 14(8): 1452-1469. DOI:10.1007/s10040-006-0059-7

Werner, A.D., Simmons, C.T., 2009. Impact of Sea-Level Rise on Sea Water Intrusion in Coastal Aquifers. Ground Water, 47(2): 197-204. DOI:10.1111/j.1745-6584.2008.00535.x

Werner, A.D. et al., 2012. Vulnerability Indicators of Sea Water Intrusion. Ground Water, 50(1): 48-58. DOI:10.1111/j.1745-6584.2011.00817.x

WHO, W.H.O., 2011. Guidelines for Drinking-water Quality 4th Ed.[J].

Wigley, T., Plummer, L., 1976. Mixing of carbonate waters. Geochimica et Cosmochimica Acta, 40(9): 989-995.

Wirojanagud, P., Charbeneau, R.J., 1985. Saltwater upconing in unconfined aquifers. Journal of Hydraulic Engineering, 111(3): 417-434.

Xia, Y., Li, H., Boufadel, M.C., Sharifi, Y., 2010. Hydrodynamic factors affecting the persistence of the Exxon Valdez oil in a shallow bedrock beach. Water Resources Research, 46(10).

Yechieli, Y., Shalev, E., Wollman, S., Kiro, Y., Kafri, U., 2010. Response of the Mediterranean and Dead Sea coastal aquifers to sea level variations. Water Resources Research, 46(12). DOI:10.1029/2009wr008708